The endo-lysosomal system of *Trypanosoma brucei*: insights from a protist cell model

Das Endo-lysosomale System von *Trypanosoma brucei*: Erkenntnisse aus einem Protisten-Zellmodell

Doctoral thesis for a doctoral degree
at the Graduate School of Life Sciences,
Julius-Maximilians-Universität Würzburg,
Section Infection and Immunity

submitted by

Alyssa Bergmann Borges

from

Bicas, Brazil

Würzburg, 2023

Submitted on: ……..……..

Office stamp

Members of the Thesis Committee

Chairperson: Prof. Dr. Keram Pfeiffer

Primary Supervisor: Prof. Dr. Markus Engstler

Supervisor (Second): Dr. Brooke Morriswood

Supervisor (Third): Prof. Dr. Philip Kollmannsberger

Supervisor (Fourth): Prof. Dr. Derek Nolan

“Education is the most powerful weapon which you can use to change the world.”

Nelson Mandela

Summary

Most of the studies in cell biology primarily focus on models from the opisthokont group of eukaryotes. However, opisthokonts do not encompass the full diversity of eukaryotes. Thus, it is necessary to broaden the research focus to other organisms to gain a comprehensive understanding of basic cellular processes shared across the tree of life. In this sense, *Trypanosoma brucei*, a unicellular eukaryote, emerges as a viable alternative. The collaborative efforts in genome sequencing and protein tagging over the past two decades have significantly expanded our knowledge on this organism and have provided valuable tools to facilitate a more detailed analysis of this parasite. Nevertheless, numerous questions still remain.

The survival of *T. brucei* within the mammalian host is intricately linked to the endo-lysosomal system, which plays a critical role in surface glycoprotein recycling, antibody clearance, and plasma membrane homeostasis. However, the dynamics of the duplication of the endo-lysosomal system during *T. brucei* proliferation and its potential relationship with plasma membrane growth remain poorly understood. Thus, as the primary objective, this thesis explores the endo-lysosomal system of *T. brucei* in the context of the cell cycle, providing insights on cell surface growth, endosome duplication, and clathrin recruitment. In addition, the study revisits ferritin endocytosis to provide quantitative data on the involvement of TbRab proteins (TbRab5A, TbRab7, and TbRab11) and the different endosomal subpopulations (early, late, and recycling endosomes, respectively) in the transport of this fluid-phase marker. Notably, while these subpopulations function as distinct compartments, different TbRabs can be found within the same region or structure, suggesting a potential physical connection between the endosomal subpopulations. The potential physical connection of endosomes is further explored within the context of the cell cycle and, finally, the duplication and morphological plasticity of the lysosome are also investigated. Overall, these findings provide insights into the dynamics of plasma membrane growth and the coordinated duplication of the endo-lysosomal system during *T.*

brucei proliferation. The early duplication of endosomes suggests their potential involvement in plasma membrane growth, while the late duplication of the lysosome indicates a reduced role in this process. The recruitment of clathrin and TbRab GTPases to the site of endosome formation supports the assumption that the newly formed endosomal system is active during cell division and, consequently, indicates its potential role in plasma membrane homeostasis.

Furthermore, considering the vast diversity within the *Trypanosoma* genus, which includes ~500 described species, the macroevolution of the group was investigated using the combined information of the 18S rRNA gene sequence and structure. The sequence-structure analysis of *T. brucei* and other 42 trypanosome species was conducted in the context of the diversity of Trypanosomatida, the order in which trypanosomes are placed. An additional analysis focused on *Trypanosoma* highlighted key aspects of the group's macroevolution. To explore these aspects further, additional trypanosome species were included, and the changes in the *Trypanosoma* tree topology were analyzed. The sequence-structure phylogeny confirmed the independent evolutionary history of the human pathogens *T. brucei* and *Trypanosoma cruzi*, while also providing insights into the evolution of the Aquatic clade, paraphyly of groups, and species classification into subgenera.

Zusammenfassung

Die meisten Studien in der Zellbiologie konzentrieren sich in erster Linie auf Modelle aus der Opisthokont-Gruppe der Eukaryonten. Die Opisthokonten umfassen jedoch nicht die gesamte Vielfalt der Eukaryonten. Daher ist es notwendig, den Forschungsschwerpunkt auf andere Organismen auszuweiten, um ein umfassendes Verständnis grundlegender zellulärer Prozesse zu erlangen, die im gesamten Lebensbaum vorkommen. In diesem Sinne stellt *Trypanosoma brucei*, ein einzelliger Eukaryote, eine brauchbare Alternative dar. Die gemeinsamen Anstrengungen bei der Genomsequenzierung und der Markierung von Proteinen in den letzten zwei Jahrzehnten haben unser Wissen über diesen Organismus erheblich erweitert und wertvolle Instrumente für eine detailliertere Analyse dieses Parasiten bereitgestellt. Dennoch bleiben noch zahlreiche Fragen offen.

Das Überleben von *T. brucei* im Säugetierwirt ist eng mit dem endo-lysosomalen System verknüpft, das eine entscheidende Rolle beim Recycling von Oberflächenglykoproteinen, der Antikörper-Clearance und der Homöostase der Plasmamembran spielt. Die Dynamik der Verdoppelung des endo-lysosomalen Systems während der Vermehrung von *T. brucei* und seine mögliche Beziehung zum Wachstum der Plasmamembran sind jedoch noch wenig bekannt. In dieser Arbeit wird daher das endo-lysosomale System von *T. brucei* im Kontext des Zellzyklus untersucht, um Erkenntnisse über das Wachstum der Zelloberfläche, die Verdopplung der Endosomen und die Clathrin-Rekrutierung zu gewinnen. Darüber hinaus wird in der Studie die Ferritin-Endozytose erneut untersucht, um quantitative Daten über die Beteiligung der TbRab-Proteine (TbRab5A, TbRab7 und TbRab11) und der verschiedenen endosomalen Subpopulationen (frühe, späte bzw. Recycling-Endosomen) am Transport dieses Flüssigphasenmarkers zu erhalten. Bemerkenswert ist, dass diese Subpopulationen zwar als unterschiedliche Kompartimente fungieren, aber verschiedene TbRabs in derselben Region oder Struktur gefunden werden können, was auf eine mögliche physische Verbindung zwischen den endosomalen Subpopulationen hindeutet. Die potenzielle physikalische Verbindung von

Endosomen wird im Zusammenhang mit dem Zellzyklus weiter erforscht, und schließlich werden auch die Verdopplung und die morphologische Plastizität des Lysosoms untersucht. Insgesamt bieten diese Ergebnisse Einblicke in die Dynamik des Plasmamembranwachstums und die koordinierte Verdopplung des endo-lysosomalen Systems während der Proliferation von *T. brucei*. Die frühe Verdoppelung der Endosomen deutet auf ihre mögliche Beteiligung am Plasmamembranwachstum hin, während die späte Verdoppelung der Lysosomen auf eine geringere Rolle in diesem Prozess hindeutet. Die Rekrutierung von Clathrin- und TbRab-GTPasen an der Stelle der Endosomenbildung unterstützt die Annahme, dass das neu gebildete endosomale System während der Zellteilung aktiv ist, und deutet folglich auf seine potenzielle Rolle bei der Homöostase der Plasmamembran hin.

In Anbetracht der enormen Vielfalt innerhalb der Gattung *Trypanosoma*, die etwa 500 beschriebene Arten umfasst, wurde die Makroevolution der Gruppe anhand der kombinierten Informationen der 18S rRNA-Gensequenz und Struktur untersucht. Die Sequenz-Struktur-Analyse von *T. brucei* und anderen 42 Trypanosomen-Arten wurde im Zusammenhang mit der Vielfalt der Trypanosomatida, der Ordnung, in die Trypanosomen eingeordnet werden, durchgeführt. Eine zusätzliche Analyse, die sich auf *Trypanosoma* konzentrierte, hob Schlüsselaspekte der Makroevolution dieser Gruppe hervor. Um diese Aspekte weiter zu erforschen, wurden zusätzliche Trypanosomenarten einbezogen und die Veränderungen in der Topologie des *Trypanosoma*-Baums analysiert. Die Sequenz-Struktur-Phylogenie bestätigte die unabhängige Evolutionsgeschichte der humanen Krankheitserreger *T. brucei* und *Trypanosoma cruzi*, während sie gleichzeitig Einblicke in die Evolution der aquatischen Klade, die Paraphylie von Gruppen und die Klassifizierung der Arten in Untergattungen lieferte.

[Translated with DeepL]

List of Contents

General Introduction

Cell biology research in eukaryotic cells is extensively focused on models belonging to a group named Opisthokonta, which harbors a variety of organisms, such as mammals, yeast, and *Drosophila* (Burki et al., 2020). Because our understanding of essential cellular processes is more detailed in opisthokonts than in trypanosomes, this thesis will commence by presenting an overview of the main aspects of the endo-lysosomal system and the cell cycle progression in opisthokonts before focusing on *T. brucei*, the specific organism of interest.

The endo-lysosomal system of opisthokonts[1]

The endo-lysosomal system is a key component for cellular homeostasis acting in various physiological processes, such as nutrient uptake, membrane remodeling, and cell signaling (Ballabio and Bonifacino, 2020; Barral et al., 2022). Endosomes serve as platforms for sorting of endocytosed cargo that can be either recycled (Gruenberg et al., 1989; Kok et al., 1992; Mao et al., 2021; Steinman et al., 1976) or ultimately degraded in the lysosome (Geuze et al., 1983; Pantazopoulou et al., 2023; Straus, 1964). In addition, endosomes have an essential role in lysosomal maintenance by delivering newly synthesized lysosomal membrane proteins and enzymes (Geuze et al., 1988, 1985; Puertollano et al., 2001).

The endocytic pathways in opisthokonts can be clathrin-independent, such as caveolae-mediated (Palade, 1955; Song et al., 2021; Yamada, 1955) and raft-dependent endocytosis (Wan et al., 2020), or mediated by clathrin (Roth and Porter, 1964). In fact, the latter is considered the major and the best understood endocytic pathway (Figure 1) (reviewed in Kaksonen and Roux, 2018; Prichard et al., 2022; Rennick et al., 2021). The recruitment of clathrin to the plasma membrane is orchestrated by several proteins, such

[1] This subsection contains text fragments of Link et al. (2021) – published review in which I share the first authorship.

as F-BAR domain only protein 1 and 2 complex (FCHO1/2), adaptor protein 2 (AP-2), and epidermal growth factor receptor substrate 15 (EPS15) (Cocucci et al., 2012; Ma et al., 2016; Matsui and Kirchhausen, 1990; Shih et al., 1995). After recruitment, clathrin-coated pits (CCPs) are formed, which bud as clathrin-coated vesicles (CCVs) (Roth and Porter, 1964). Membrane scission requires the polymerization of an actin cytoskeleton (Fujimoto et al., 2000; Gottlieb et al., 1993; Lamaze et al., 1997; Li et al., 2015), which involves several other molecules such as dynamin, type I myosins, actin-related protein 2/3 complex (Arp2/3), Las17, Sla1, Sla2, and Ent1 (Cheng et al., 2012; Feliciano and Di Pietro, 2012; Galletta et al., 2008; Lizarrondo et al., 2021; Mettlen et al., 2009). Once the CCVs have pinched off from the plasma membrane they are uncoated in a process involving dephosphorylation and ATP hydrolysis with the help of auxilin and heat shock protein Hsc70 (Prasad et al., 1993; Ungewickell et al., 1995). Uncoated vesicles can fuse with endosomes, which are subdivided into populations named early, late, and recycling endosomes (Geuze et al., 1983; Kamentseva et al., 2020; Roth and Porter, 1964; Straus, 1964; Wall et al., 1980). These subpopulations are decorated with small Rab GTPases, among which Rab5, Rab7, and Rab11 are major players and widely used as markers for the early, late, and recycling compartments, respectively. The Rab GTPases regulate intracellular membrane trafficking based on their GTP/GDP cycle. When in their inactive state (GDP-bound), Rabs are localized in the cytosol, but upon activation (GTP-bound conformation) they bind to specific membrane compartments (reviewed in Cullen and Steinberg, 2018; Jin et al., 2021; Wandinger-Ness and Zerial, 2014).

The first endosomal subpopulation that endocytosed cargo reaches is the early endosome, a compartment with documented homotypic fusion capacity (Gruenberg et al., 1989). Inside this organelle, cargo is sorted for recycling or degradation. The fate of the cargo is proposed to be determined by the endosomal sorting complex required for transport (ESCRT), which is a group of protein complexes that selects ubiquitinated cargo for the degradation pathway (Katzmann et al., 2001; Raiborg et al., 2002). Cargo not

selected for degradation has been proposed to move directly to recycling, following a sort of negative selection inside the early endosome (Klumperman and Raposo, 2014).

When destined for recycling, cargo moves to the recycling endosome. Vesicles that bud from this compartment are directed to the plasma membrane through interaction with motor proteins (Ji et al., 2019). Early endosomes have contact sites with the recycling compartment allowing a fast route back to the cell surface (Klumperman and Raposo, 2014). In addition, cargo recycling from late endosomes has been proposed to happen either via direct delivery of exosomes to the plasma membrane (Edgar, 2016; Harding et al., 1983; Johnstone et al., 1987; Pan et al., 1985) or via cargo retrieval in the *trans*-Golgi network (Seaman et al., 1997).

Cargo destined for degradation is accumulated by the ESCRT into luminal invaginations of the early endosome membrane, which pinch off into its luminal space forming intraluminal vesicles (ILVs) (Klumperman and Raposo, 2014). The ILVs accumulate in vacuolar regions, which ultimately detach and become free multivesicular bodies (MVBs), also called endosomal carrier vesicles (ECVs). The MVBs have been proposed to be transported on microtubules to deliver the cargo to late endosomes (Saito et al., 1997). However, other studies have suggested a maturation process in which the MVBs progressively differentiate from early to late endosomes (Poteryaev et al., 2010; Rink et al., 2005; Stoorvogel et al., 1991).

From late endosomes, cargo is finally delivered to the lysosome (Bucci et al., 2000; Karim et al., 2018). In mammalian cells, lysosomes were observed juxtaposed to the nuclear region or close to the plasma membrane (Encarnação et al., 2016; Korolchuk et al., 2011). Along with the diverse positioning, the lysosomes can vary in size, pH, and enzyme composition (Barral et al., 2022). Cargo delivery from late endosomes to the lysosome is proposed to happen either via fusion, during which a hybrid organelle is formed, named the endolysosome (Bucci et al., 2000; Futter et al., 1996; Karim et al., 2018), or via a process known as kiss-and-run, which is a temporary fusion used to release cargo from the late endosomes to the lysosome (Bright et al., 2005). The hybrid endolysosome matures into

the classical lysosome, in which hydrolases break down the enclosed material (Podinovskaia et al., 2021; van der Beek et al., 2021).

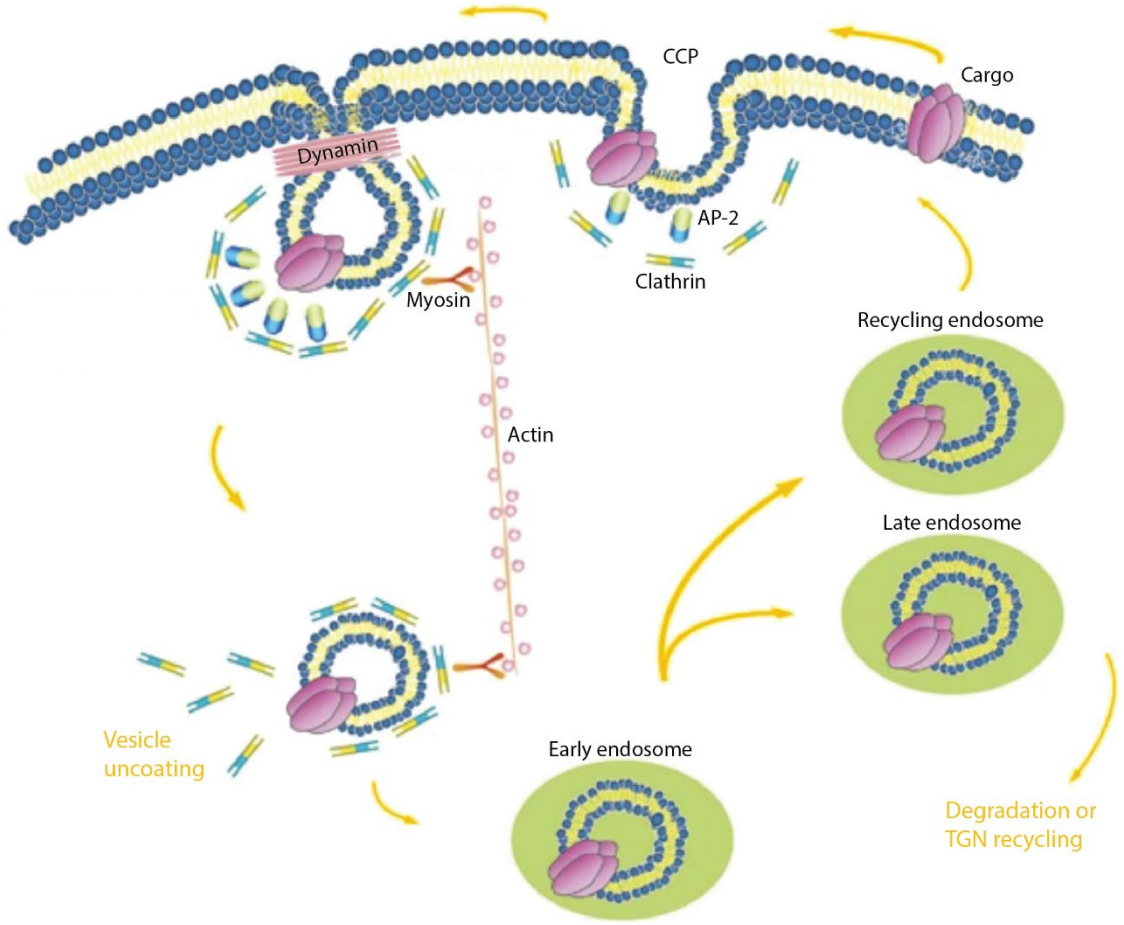

Figure 1. Overview of clathrin-mediated endocytosis pathways in opisthokonts. Cargo binds to the plasma membrane and clathrin is recruited by accessory molecules, such as AP-2, to the location. A local deformation of the membrane forms a clathrin-coated pit (CCP). The CCP invaginates further and pinches off with the help of dynamin and actin, yielding clathrin-coated vesicles that are transported with the help of motor proteins (myosin and actin). After vesicle uncoating, cargo is moved to the early endosome from which it is sorted to the late or the recycling endosome. From late endosomes, cargo can be degraded or sent for recycling in the *trans*-Golgi network (TGN). From the recycling endosome, cargo returns to the plasma membrane. Image adapted from Schubert et al. (2012).

The cell cycle in opisthokonts

The cell cycle comprises a series of events that take place in a cell as it grows and divides to produce two daughter cells. It is a highly coordinated and controlled process that ensures accurate duplication and segregation of genetic material and cellular components (Alberts et al., 2002; Carlton et al., 2020; Moore et al., 2021). Traditionally, these events

are grouped into four sequential phases named G1, S, G2, and M, of which the first three are collectively named interphase. The G stands for “gap”, in which cell growth and monitoring of internal and external environments occurs (Alberts et al., 2002). The gap phases are essential for the cell to ensure proper conditions before committing to the critical phases of DNA replication (S phase) and then segregation (M phase; mitosis). When there is a lack of favorable conditions, a cell can delay its progress through G1 and even enter a specialized resting state (G0), which is of variable duration. From G0, cells may re-enter G1 or remain permanently in this stage until they die (Alberts et al., 2002; Granot and Snyder, 1991; Small and Osley, 2023). However, the arrest/delay of G1 is only possible before cells reach a “commitment point”, named “start” in yeast and “restriction point” in mammals. After this point, cells will enter the S phase independently of the conditions (Adikes et al., 2020; Alberts et al., 2002; Moser et al., 2018).

Both chromosome segregation and cell division occur during mitosis (M phase), which can be further subdivided into a series of steps according to the alignment of chromosomes and the cytoskeleton, named prophase, prometaphase, metaphase, anaphase, and telophase (Alberts et al., 2002; Carlton et al., 2020; Walczak et al., 2010). In prophase, the duplicated chromosomes are condensed, the centrosomes begin to separate, and the nuclear envelope starts disassembling. During prometaphase, the chromosomes connect to the microtubules of the mitotic spindle and can proceed for alignment at the spindle equator, marking the metaphase state. In anaphase, the chromosomes progressively move toward the poles of the spindle. In this way, each sister chromatid is placed on opposite sides of the division plane. During telophase, the nuclear envelope begins to reassemble, and the chromosomes start to decondense – reforming two intact nuclei (Figure 2). Some opisthokont cells, such as the yeast *Schizosaccharomyces pombe*, undergo closed mitosis, in which the nuclear envelope is not entirely disassembled (Dey et al., 2020).

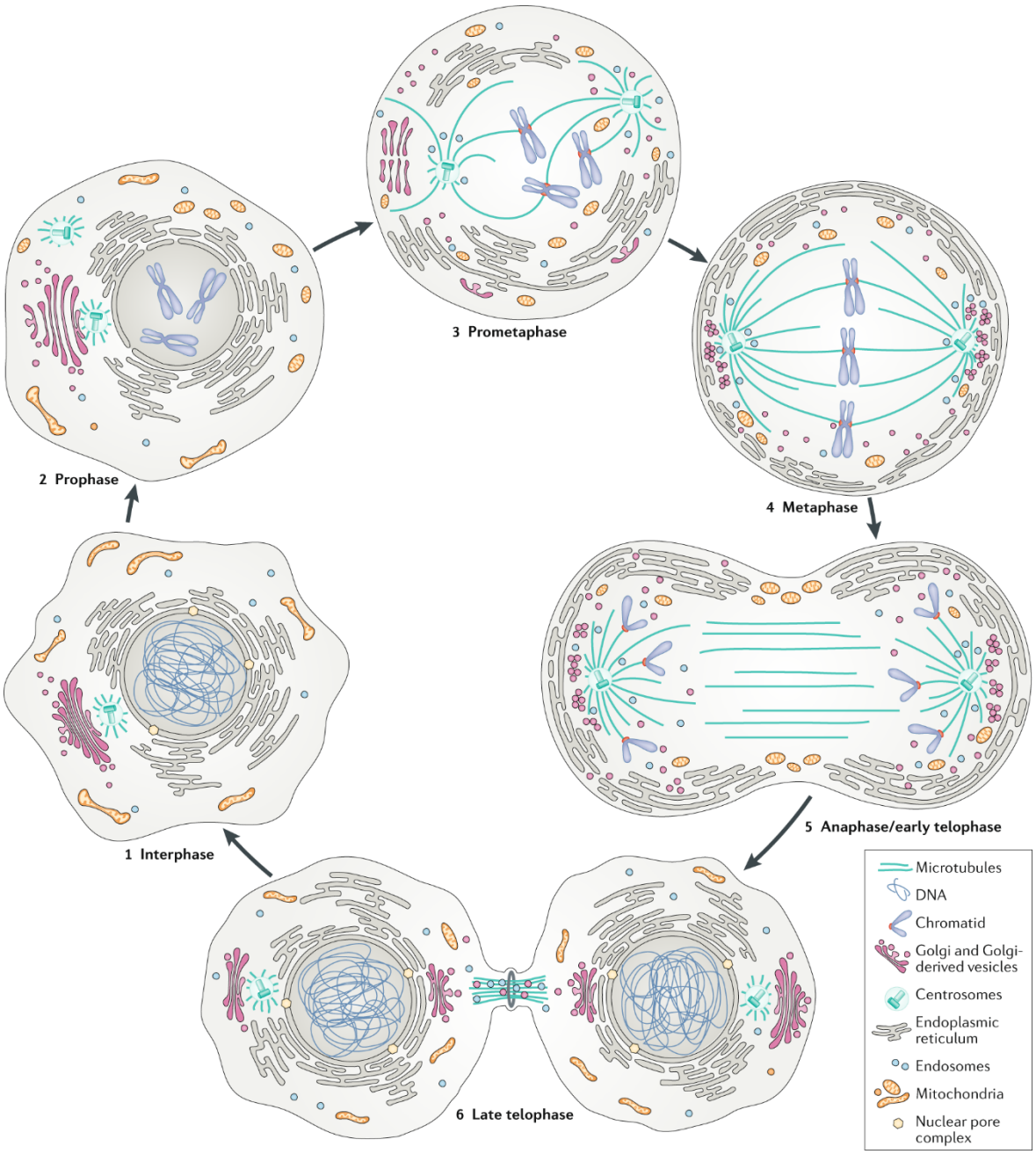

Figure 2. Schematic overview of the sequential mitotic stages of a mammalian cell. Cells progress from interphase (1) to the mitotic phase of the cell cycle. Prophase (2): microtubules rearrange in centrosomes to form a bipolar spindle, and DNA condenses in chromosomes. Prometaphase (3): chromosomes connect with microtubules of the mitotic spindle. Metaphase (4): chromosomes align at the spindle equator. Anaphase/early telophase (5): chromosomes are pulled to the opposite poles of the mitotic spindle, separating the sister chromatids, and the cleavage furrow starts its ingression. Late telophase (6): reassembly of the nuclear envelope, decondensation of DNA, and cytokinesis. After cytokinesis, cells initially remain connected through the midbody, which is disassembled by the endosomal sorting complex required for transport (ESCRT). Image taken from Carlton et al. (2020).

At the end of mitosis, the cytoplasm of the two daughter cells is divided in a process called cytokinesis (Esau and Gill, 1965; Rappaport, 1986). The cytoplasm partitioning is governed by the cleavage furrow, which consists of a contractile actomyosin ring connected

to the plasma membrane (Bi et al., 1998; Lippincott and Li, 1998). The ring formation involves the participation of several molecules, such as Rho proteins and their regulators, and the kinases Aurora B and Polo. The ingression of the cleavage furrow is carried out by the actomyosin cytoskeleton, decreasing the volume of the contractile ring, and pinching the plasma membrane inwards (reviewed in Frappaolo et al., 2022; Fraschini, 2020). After cytokinesis, the two daughters may remain connected by a thin bridge named the midbody. This structure seems to be a key regulator of cytokinesis and appears to play a role in cell polarization after division (Halcrow et al., 2022; Presle et al., 2021; Terada et al., 1998). The midbody abscission involves the ESCRT (Bajorek et al., 2009; Gulluni et al., 2021). According to the characteristics of the daughter cells, cytokinesis can be symmetric or asymmetric. The first generates two equal daughter cells and is important for tissue homeostasis. The latter gives rise to daughter cells with different morphology and function generating cellular diversity that is important, for example, for stem cells (Karim et al., 2018; Wheeler, 1891; Whitman, 1878).

It has been suggested that the cleavage furrow ingression, and consequently cell division, must be coordinated with local membrane deposition (reviewed in Carlton et al., 2020; Fraschini, 2020). In addition, the cell volume grows exponentially during interphase and displays a rapid and pronounced (10-30 %) increase during mitosis (Boucrot and Kirchhausen, 2008; Zlotek-Zlotkiewicz et al., 2015). Thus, to sustain all these volumetric changes, plasma membrane growth is of paramount importance. The incorporation of new membrane can happen via plasma membrane remodeling or vesicle trafficking (Albertson et al., 2008; Boucrot and Kirchhausen, 2007; Wang et al., 2016), but the internal sources of the new membrane are still a matter of debate (reviewed in Carlton et al., 2020).

Evidence has suggested that membrane recycling is essential for plasma membrane growth during mitosis and that impairments in clathrin-mediated endocytosis decrease the cell surface area (Boucrot and Kirchhausen, 2007). However, other studies indicated a temporary shutdown of endocytosis during mitosis (Fielding et al., 2012; Warren et al., 1984). Thus, the “emerging consensus is that some degree of endocytosis persists

throughout division, and specific endocytic cargoes that are important to the cell [cycle progression], such as growth factor receptors, may be prioritized to allow their partitioning during division" (Carlton et al., 2020, p. 5). Lysosome activity during mitosis is still controversial, with some findings suggesting that lysosome autophagic functions must be repressed (Odle et al., 2020), while others argue the need for lysosomal activity to ensure correct chromosome inheritance (Almacellas et al., 2021). In this sense, it is interesting to note that a potential "additional layer of complexity is added [for organelle inheritance] if the function of an organelle must be maintained for division to occur" (Carlton et al., 2020, p. 1).

Compared to mitotic events, knowledge of organelle partitioning is still evolving. It has been proposed that some organelles pass through a coordinated segregation/inheritance, such as the Golgi apparatus and the vacuoles of yeast, which may be influenced by kinases (e.g., Aurora B), phosphatases, myosin, and phospholipids (Carlton et al., 2020; Chung et al., 2016; Ouellet and Barral, 2012; Weisman, 2006). Some organelles, such as the endo-lysosomal system, have been associated with a stochastic distribution into the daughter cells. However, clusters of Rab5 and Rab11 were spotted around the mitotic spindle and have been suggested to contribute to chromosome segregation (Capalbo et al., 2011; Hehnly and Doxsey, 2014; Serio et al., 2011). Because of this, the distribution of endosomes into the daughter cells has been suggested to be influenced/coordinated by the mitotic spindle instead of being merely stochastic (Carlton et al., 2020). Regarding the lysosome, data from mammalian neural stem cells show an asymmetric inheritance of the lysosome (Bohl et al., 2022; Loeffler et al., 2019), which could result from coordinated events (Loeffler et al., 2022; Moore et al., 2021).

Trypanosoma brucei as a cell biology model

Although opisthokonts are the most studied organisms in cell biology, this group is far from representative of the vast diversity of eukaryotic cells (Figure 3). The precise

positioning of the root in the eukaryote tree of life is still a matter of debate (Burki et al., 2020), but a comprehensive phylogenomic analysis recently proposed the tree root between Opisthokonta and all other eukaryotes (Cerón-Romero et al., 2022). Such a root positioning is controversial for suggesting an independent evolutionary history of opisthokonts. However, it highlights that these organisms may harbor deep divergences from other eukaryotic cells. Thus, our comprehension of the evolution of the eukaryotic cell, cellular organization/organelle complexity, and the key aspects that govern a cell's life, such as the cell cycle, are still incomplete. To overcome this, it is important to expand our focus to include other eukaryotic taxa. In this context, trypanosomes present an interesting group due to the existence of established laboratory cell lines and the availability of molecular tools that enable cell engineering.

Trypanosoma is a monophyletic genus (Kostygov et al., 2021) placed in the eukaryote group Discoba (Burki et al., 2020) (Figure 3). This genus comprises ~500 species of parasites found in all vertebrate classes (Kostygov et al., 2021). Such a species richness is usually studied within an evolutionary context, by employing the widely used genetic markers glyceraldehyde 3-phosphate dehydrogenase (GAPDH) and 18S rRNA, more specifically the v7/v8 hypervariable region (Fermino et al., 2019, 2015; Hamilton and Stevens, 2017; Lemos et al., 2015; Maia da Silva et al., 2004). Recently, the v7/v8 region of trypanosomes was shown to be a synonym of the v4 region according to the European Database on small ribosomal RNA (see Rackevei et al., 2022).

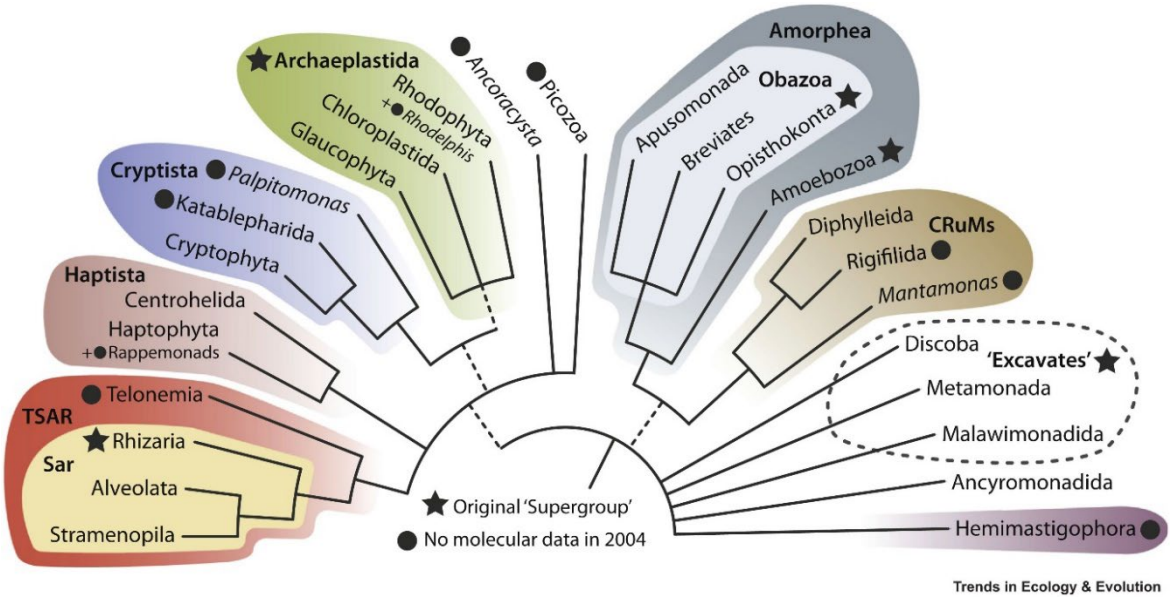

Figure 3. Eukaryote tree of life. The tree is a representation of the consensus on eukaryote supergroups based on phylogenomics. The inclusion of new data (represented by circles) changed the original configuration of eukaryote supergroups (indicated by stars), which are currently superseded by the monophyletic supergroups TSAR, Haptista, Cryptista, Archaeplastida, Amorphea, CruMs, and Hemimastigophora (indicated by the different colors). The former supergroup known as Excavata is now considered artificial and it is subdivided into three clades (Discoba, Metamonoda, and Malawimonadida). *Ancoracysta*, *Picozoa*, malawimonads, and ancyromonads have low number of species, so they are considered "orphan taxa". The root of the eukaryote tree is still uncertain. Image taken from Burki et al. (2020).

In the context of cell biology, the human pathogens *T. brucei* and *T. cruzi* are the most studied trypanosome species. In fact, the availability of genomes and the launch of initiatives such as TriTrypDB (Aslett et al., 2010) and TrypTag (Dean et al., 2017) have made important contributions to consolidate *T. brucei* as a viable model organism. In this way, this parasite can be used to investigate a plethora of cellular processes, such as cell motility (Alizadehrad et al., 2015), mitochondrial genome replication (Hoffmann et al., 2018), and phospholipid biosynthesis (reviewed in Borges et al., 2021; Serricchio and Bütikofer, 2011). The complex polarized cell architecture of *T. brucei* along with unique features, such as the presence of a single mitochondria and the concentration of all endo- and exocytic processes in one portion of the plasma membrane (Figure 4), make them an interesting organism to be explored.

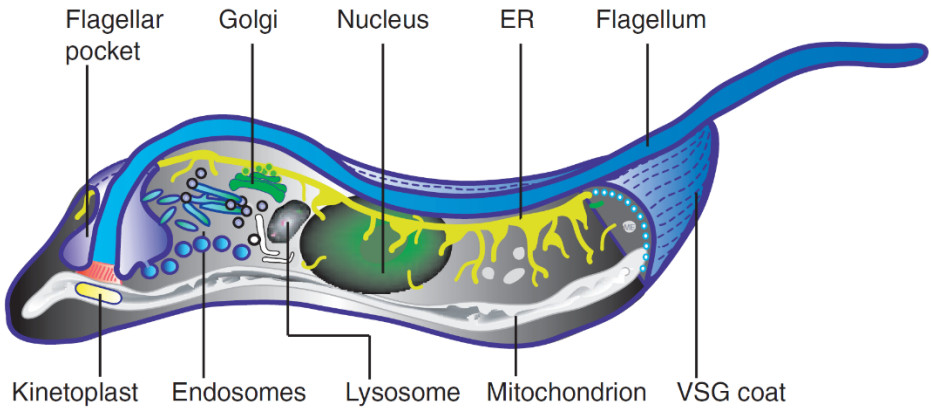

Figure 4. The architecture of the bloodstream form of *Trypanosoma brucei*. Schematic representation of the *T. brucei* cell and its major organelles. Image adapted from Overath and Engstler (2004).

The life cycle of *T. brucei*[2]

Trypanosoma brucei is an extracellular pathogen that causes chronic and eventually fatal infections in humans and livestock (WHO, 2023). In 1985, David Bruce reported the discovery of the parasite and proved that the disease was transmitted by the tsetse fly and not caused by it, as believed at that time (Bruce, 1895). As a dixenous parasite, *T. brucei* alternates between mammalian hosts and tsetse flies during its life cycle (Schuster et al., 2021, 2017; Szöőr et al., 2020; Vickerman, 1985). The switch between such distinct microenvironments challenges the parasite with different temperatures, pH, nutrient availability, and host defense mechanisms (Schuster et al., 2017; Seed and Sechelski, 1989; Seed and Wenck, 2003). As a way to overcome these bottlenecks, *T. brucei* differentiates into distinct life cycle stages, which are adapted for survival inside each host's environment. An example of such adaptation is the versatile composition of the cell surface, which is the interface for interactions with the host and differs from one life cycle stage to another (Figure 5) (reviewed in Borges et al., 2021).

[2] This subsection contains fragments of Borges et al. (2021) – published review in which I share the first authorship

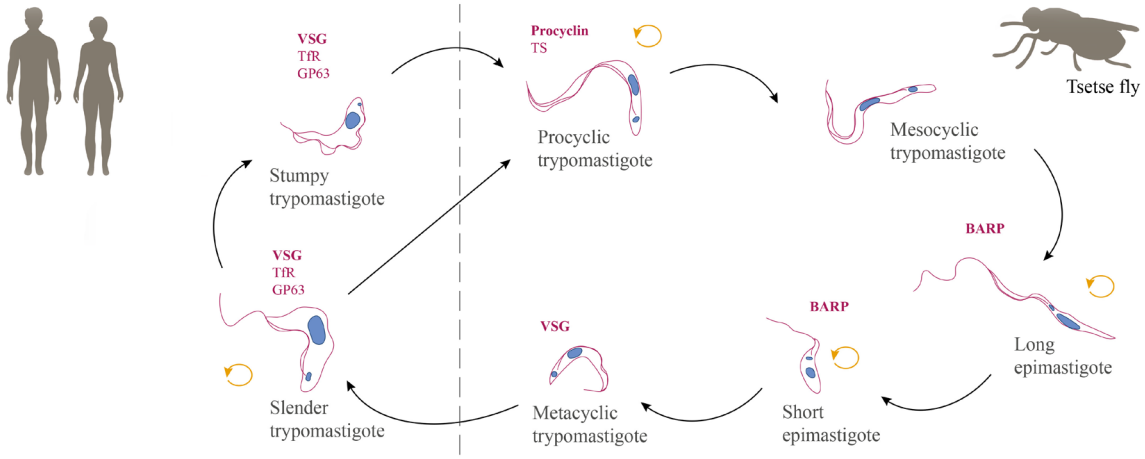

Figure 5. Schematic overview of the life cycle of *Trypanosoma brucei*. The replicative stages are highlighted by a circular arrow (orange), and the cell surface composition is indicated: variant surface glycoprotein (VSG), transferrin receptor (TfR), GP63, procyclin, *trans*-sialidase (TS), and brucei alanine rich protein (BARP). The predominant cell surface molecule of each stage is written in bold. Image adapted from Borges et al. (2021).

Infection of the tsetse starts when the fly ingests blood from an infected mammalian host containing the bloodstream forms of *T. brucei* (Nolan et al., 2000; Robertson, 1912; Robertson and Bradford, 1912; Schuster et al., 2021). Once inside the fly, trypanosomes pass through the crop to the tsetse midgut and differentiate into procyclic forms (Vickerman, 1969). Procyclic trypanosomes cross the peritrophic matrix at the site of its synthesis (proventriculus) (Lehane et al., 1996; Rogerson et al., 2018; Rose et al., 2020, 2014). Inside the endotrophic space, procyclic trypanosomes can differentiate into mesocyclic trypanosomes, which then invade the proventriculus (Vickerman, 1985) and develop into long epimastigotes (Rose et al., 2020; Sharma et al., 2008; Van Den Abbeele et al., 1999; Vickerman, 1985). Epimastigotes undergo an asymmetric division to create a long and a short daughter cell and migrate to the salivary glands. In the salivary gland, the long daughter cell is assumed to die and the short daughter cell attaches to the gland epithelium via its flagellum (Vickerman, 1969). Attached epimastigotes divide symmetrically, increasing the number of attached epimastigote cells. Alternatively, attached epimastigotes can also undergo an asymmetric division resulting in the formation of the free-swimming metacyclic stage, which is the mammalian infective form (Schuster et al., 2017; Szöőr et al., 2020; Vickerman, 1985).

During feeding, infected tsetse flies transmit the metacyclic *T. brucei* to the mammalian host. Inside this host, *T. brucei* differentiates into the bloodstream form of the parasite and lives exclusively in extracellular fluids where it exhibits a glycocalyx predominantly composed of variant surface glycoproteins (VSGs) (Cross, 1975; Jackson et al., 1985; Vickerman, 1985). The bloodstream forms can be classified into two morphologically distinct forms: the long slender and the short stumpy trypomastigotes (Robertson, 1912; Schuster et al., 2021; Seed and Sechelski, 1989; Seed and Wenck, 2003). The slender trypomastigotes are proliferative, while the stumpy form is cell cycle arrested. The differentiation into stumpy forms can be either stimulated in a quorum sensing fashion via accumulation of the stumpy induction factor (SIF) (Rojas and Matthews, 2019; Vassella et al., 1997) or in a SIF-independent pathway controlled by the transcriptional status of the VSG expression site (Batram et al., 2014; Zimmermann et al., 2017). Stumpy forms are proposed to be an adaptation that limits parasite burden and increases host survival, as these cells have a lifespan of only 48-72 hours (Seed and Sechelski, 1989; Seed and Wenck, 2003). Interestingly, the stumpy trypomastigotes were seen as the only life cycle stage capable of infecting tsetse flies (reviewed in Rico et al., 2013; Szöőr et al., 2020). However, recent findings have shown that slender trypomastigotes can also infect and complete the life cycle in flies (Schuster et al., 2021).

Survival inside the vertebrate host[3]

The mammalian host reacts to *T. brucei* infections by activating both cellular and humoral immunity (reviewed in Onyilagha and Uzonna, 2019), of which the latter represents the main line of defense against the parasite due to its extracellular lifestyle (Machado et al., 2021; Magez et al., 2020; Stijlemans et al., 2017). By employing a sophisticated

[3] This subsection contains fragments of Borges et al. (2021) – published review in which I share the first authorship

mechanism of antigenic variation and antibody clearance, *T. brucei* evades the host's immune system, leading to a long-term infection.

The antigenic variation is promoted by the VSG coat formed by 1×10^7 VSG monomers anchored to the cell surface via glycosylphosphatidylinositol (GPI) anchors (Bartossek et al., 2017; Cross, 1975; Ferguson, 1997; Ferguson et al., 1988; Jackson et al., 1985). VSG molecules are distributed on the cell surface by lateral diffusion (Bülow et al., 1988; Hartel et al., 2016), and full coverage is aided by conformational changes in VSG molecules (Bartossek et al., 2017). In this way, the flexible and dense VSG coat shields invariant surface proteins of the parasite from immune recognition while presenting itself as a target for the immune response. From a large repertoire (>1000) of VSG coding genes (Cross et al., 2014), the parasite expresses only one VSG isoform at a time on its cell surface. The periodic switches in VSG expression, which form the basis for antigenic variation (Mugnier et al., 2016), help the parasite population evade clearance, leading to fluctuations in parasitemia over the course of infection. These parasitemia waves are considered a hallmark of *T. brucei* infection in mammals (Faria, 2021).

In addition to the population survival strategy, single cells can use their directional swimming and the high mobility of the GPI anchor in their favor when opsonized by the host's antibodies. The directional movement of trypomastigotes generates hydrodynamic flow forces on the cell surface that drag VSG-antibody complexes to the posterior region of the cell, where they can be internalized and transported to the lysosome for degradation in about 2 minutes (Engstler et al., 2007). Thus, the endo-lysosomal system of *T. brucei* bloodstream forms, which is vital for nutrient uptake and immune evasion, plays a central role in the parasites' survival in its vertebrate host.

The endo-lysosomal system of *T. brucei*[4]

The endo-lysosomal system of *T. brucei* is found in the posterior part of the cell (Figure 6), extending from the vicinities of the flagellar pocket, the exclusive site for endo- and exocytosis, to the nucleus (Engstler et al., 2004; Gull, 2003; Overath et al., 1997; Vickerman, 1969).

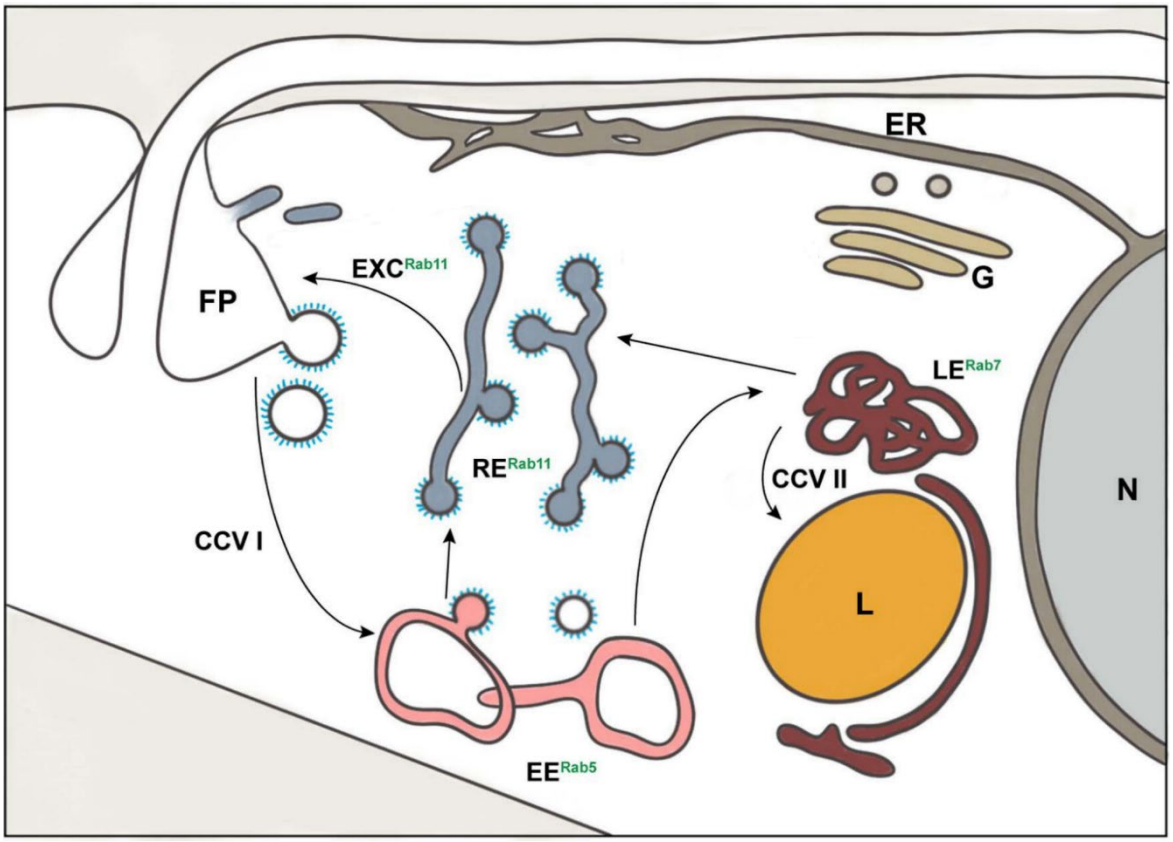

Figure 6. Schematic representation of the endo-lysosomal system of *Trypanosoma brucei*. The endocytic pathways are shown (arrows), and the organelles indicated: class I clathrin-coated vesicles (CCV I), class II clathrin-coated vesicles (CCV II), early endosomes (EE), endoplasmic reticulum (ER), exocytic carrier (EXC), flagellar pocket (FP), Golgi apparatus (G), lysosome (L), late endosomes (LE), nucleus (N), and recycling endosomes (RE). The endocytic compartment is marked by the presence of small GTPases of the Rab family: Rab5 (EE), Rab7 (LE), and Rab11 (RE). Figure modified from Link et al. (2021).

In *T. brucei*, all endocytosis is clathrin-mediated. Clathrin can be recruited to any part of the flagellar pocket membrane except for the microtubule quartet region (Gadelha et al., 2009). Clathrin recruitment involves TbEpsinR and TbCALM (Gabernet-Castello et

[4] This subsection contains fragments of Link et al. (2021) – published review in which I share the first authorship

al., 2009; Manna et al., 2015). Although AP-2, one of the major clathrin recruiters in opisthokonts, has not been identified in the genome of *T. brucei* (Manna et al., 2013; Morgan et al., 2002), the parasite possesses several other clathrin-associating proteins (TbCAP). Of these, eight seem exclusive to trypanosomatids (TbCAP116, TbCAP118, TbCAP125, TbCAP161, TbCAP186, TbCAP292, TbCAP334, and TbTOR-like 1), and four (TbCAP100, TbCAP116, TbCAP161, and TbCAP334) are associated with clathrin recruitment/assembly (Adung'a et al., 2013). Upon clathrin recruitment, the flagellar pocket membrane forms clathrin-coated pits (Allen et al., 2003; Engstler et al., 2004; Grünfelder et al., 2003; Morgan et al., 2001). These pits rapidly pinch off as class I CCVs, which have a diameter of 135 nm (Grünfelder et al., 2003; Overath and Engstler, 2004). The cytoskeleton component TbMyo1 is distributed in the posterior part of the cell and it was suggested to be involved in the trafficking of clathrin-coated vesicles (Spitznagel et al., 2010). The polarization of this mechanoenzyme is related to actin, and its depletion leads to endocytosis impairment (García-Salcedo et al., 2004; Spitznagel et al., 2010).

From CCVs, cargo passes to the endosomes, which have been described as compartments of elongated, circular, and irregular shape (Engstler et al., 2004; Grünfelder et al., 2003, 2002). These compartments are decorated with homologs of the main endosome markers TbRab5A (early endosome), TbRab7 (late endosome), and TbRab11 (recycling endosome) (Engstler et al., 2004; Field et al., 1998; Jeffries et al., 2001; Pal et al., 2002). All endocytosed cargo, membrane-bound and fluid-phase, enter the early endosomes (Engstler et al., 2004; Grünfelder et al., 2003). Studies focused on VSG showed that endocytosed VSG starts to colocalize with early endosomes after 2.2 seconds and finally fills up to 85 % of the compartment volume (Engstler et al., 2004). From this compartment, 53 % of the VSG pool moves to recycling endosomes and returns to the surface, a route known as the fast route, which is completed within approximately 10 seconds (Engstler et al., 2004). Alternatively, 47 % of VSGs are recycled through the slow route, which takes approximately 50 seconds to complete (Engstler et al., 2004). Here, VSG passes first from the early endosomes to the late endosomes and then returns to the

surface via the recycling endosome. VSG was never detected inside the lysosome (Engstler et al., 2004).

Fluid-phase cargo moves from early endosomes to late endosomes and, then, arrives in the lysosome (Engstler et al., 2004). This transport was proposed to occur via class II CCVs, which bud from the endosomes and are always depleted in VSG but filled with fluid-phase cargo (Engstler et al., 2004), and seem to be influenced by TbRab7, of which depletion impairs endocytosed cargo delivery to the lysosome (Silverman et al., 2013, 2011). A detailed study of the kinetics of endocytosis in *T. brucei* showed that the fluid-phase marker dextran and biotinylated VSG (VSG_{biotin}) were endocytosed at the same time but gradually segregated, reaching a maximum of spatial separation after approximately 1 minute. At steady state, 37 % of the intracellular VSG_{biotin} did not lie on the endocytic route of internalized dextran, suggesting that the separation of VSG from the fluid-phase marker occurred concurrently with the biphasic filling of the recycling endosome (Engstler et al., 2004). Bovine serum albumin (BSA), a physiological cargo, was reported to overlap with dextran inside *T. brucei* bloodstream forms (Schichler et al., 2022, preprint), suggesting a similar endocytic pathway. The use of electron microscopy to visualize the pathway of ferritin, another physiological cargo, never spotted it inside structures with morphological resemblance of recycling endosomes (Engstler et al., 2004; Langreth and Balber, 1975). Considering all these observations, recycling endosomes seem not involved in the fluid-phase cargo pathway. However, electron microscopy evidence showed horseradish peroxidase inside exocytic carriers (Engstler et al., 2004). Thus, TbRab11 has been proposed to be involved in both fluid-phase and receptor-mediated cargo recycling to the cell surface. Consistent with these results, depletion of TbRab11 was shown to reduce ~80 % of transferrin recycling (Hall et al., 2005). Nevertheless, it is important to note that endosomal compartments marked by TbRab11 seem to have, to a certain extent, an interface with early endosomes (Chung et al., 2004; Engstler et al., 2004; Jeffries et al., 2001), which could influence the distribution of fluid-phase cargo inside TbRab11-positive structures.

Orthologs of the ESCRT machinery (TbVps4, TbVps23, TbVps24, and TbVps28) were found in *T. brucei* late endosomes (Gilden et al., 2017; Leung et al., 2008; Silverman et al., 2013; Umaer and Bangs, 2020). Although the ESCRT is connected to cargo sorting inside ILVs, leading to the formation of MVBs in mammalian cells (see General Introduction "The endo-lysosomal system of opisthokonts"), *T. brucei* lacks a well-defined MVB (Silverman et al., 2013). Considering that fluid-phase cargo was shown to be sorted into class II CCVs from endosomal compartments (Engstler et al., 2004; Grünfelder et al., 2003), it is possible to envisage a distinct mechanism for the ESCRT-like machinery of *T. brucei*. The ESCRT components TbVps4, TbVps23, and TbVps24 were shown to be involved in the transport of the lysosomal markers p67 and TbCathepsin L (TbCatL) (Silverman et al., 2013, 2011; Umaer and Bangs, 2020). In addition, TbVps23 and TbVps4 were also involved in endocytosed cargo delivery to the lysosome (Silverman et al., 2013, 2011).

The cell cycle of *T. brucei*

The proliferation of *T. brucei* bloodstream form cells involves remodeling and extension of the microtubule cytoskeleton (Robinson, 1995; Wheeler et al., 2013), volume growth, and organelle replication (Gluenz et al., 2011; Hughes, et al., 2017; Siegel et al., 2008). At the end of the process, the duplicated content is divided by cytokinesis into two non-equivalent daughter cells (reviewed in Wheeler et al., 2019).

Trypanosomes possess one kinetoplast (K), which is "a large mass of mitochondrial DNA" (Adl et al., 2019, p. 85), and one nucleus (N), a morphology commonly referred to as 1K1N. As one of the first events of the cell cycle, the basal body is duplicated and the new flagellum emerges. The new flagellum grows continuously, tracking the old flagellum throughout the cell cycle (Hughes et al., 2013; Lacomble et al., 2010; Sherwin and Gull, 1989). Thus, the 1K1N morphology defines either cells that have not started the proliferation or cells in the very early stages of the cell cycle. Following these events, the kinetoplast starts its replication by progressively elongating, curving, and forming a bilobe ($1K^{d}1N$).

During these initial events, the nucleus enters its S phase and shows a slight volume increase (Hughes et al., 2017). Other modifications are: Golgi and endoplasmic reticulum exit site (ERES) replication, replication of the flagellar pocket and its associated structures (collar, centrin arm, hook complex), and flagellum outgrowth (reviewed in Morriswood and Engstler, 2018). After duplication, the kinetoplasts eventually segregate, forming cells with two kinetoplasts and one nucleus (2K1N) (Gluenz et al., 2011). During kinetoplast segregation, the new flagellum migrates toward the posterior pole of the cell (Absalon et al., 2007; Hughes et al., 2017). The next event is the nuclear segregation which yields 2K2N cells. These cells will be divided (cytokinesis) with the ingression of the cleavage furrow, typically starting from the anterior pole of the division fold (Hughes et al., 2017; Sherwin and Gull, 1989; Wheeler et al., 2013). An overview of the cell cycle is depicted in Figure 7.

The low conservation between the molecules orchestrating the cell cycle in *T. brucei* and opisthokont models makes characterizing the signaling networks challenging (Wheeler et al., 2019). However, substantial progress in this regard was made in the past decade with the characterization of the trypanosome-specific interactors, such as the cytokinesis initiation factors CIF1/TOEFAZ1, CIF2, CIF3, and CIF4 (Hilton et al., 2018; Hu et al., 2019; Sinclair-Davis et al., 2017; Zhou et al., 2016, 2014). Another important aspect to be aware of is that some signaling cascades can be stage-specific, as observed for FRW1, a cleavage furrow localizing protein required for furrow initiation in the bloodstream form but not in procyclic cells (Zhang et al., 2019).

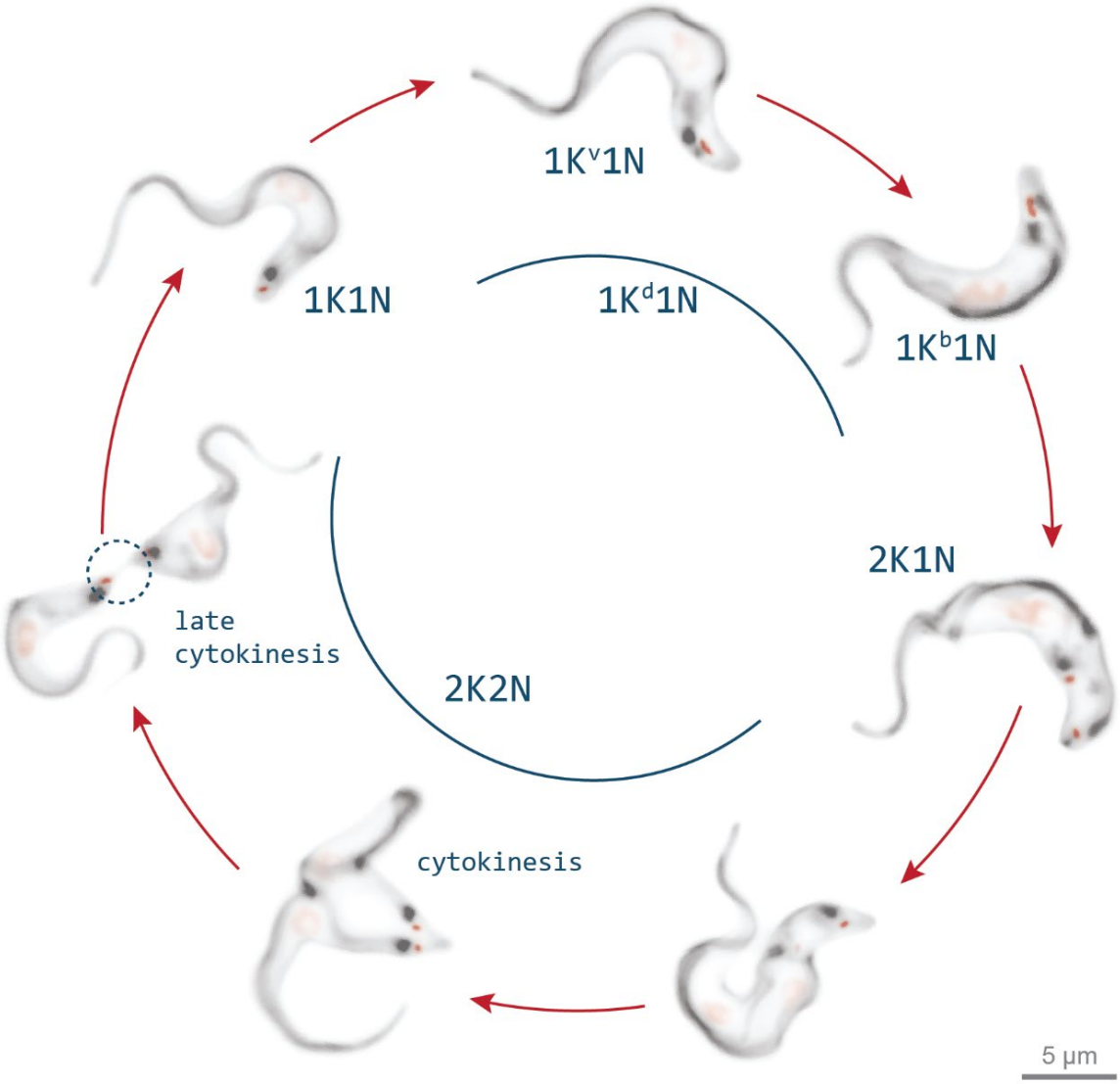

Figure 7. Overview of the cell cycle of *Trypanosoma brucei* emphasizing the morphology of the nucleus (N) and the kinetoplast (K). *T. brucei* cells with one nucleus and one kinetoplast (1K1N) start the cell cycle with the duplication of the kinetoplast ($1K^d1N$) that will curve ($1K^v1N$) and form a bilobe ($1K^b1N$) prior to segregation. Cells with two kinetoplasts (2K1N) undergo nuclear segregation, yielding cells with two nuclei and two kinetoplasts (2K2N). These cells enter cytokinesis following a directional segregation along the long-axis of the cell. During the late stages of cytokinesis, cells are connected by a cytoplasmic bridge (dashed circle). The arrows indicate the direction of the cell cycle. The cell surface was stained with Atto-NHS dye (shown in gray) and the nucleus and the kinetoplast with DAPI (shown in red).

Chapter 1

The duplication of the endo-lysosomal system of *Trypanosoma brucei*

1. Introduction

Cell division in eukaryotes can be proliferative, named mitosis, and non-proliferative, called meiosis (Paweletz, 2001; Sato et al., 2021; Schulz-Schaeffer, 1980). Cells undergoing mitosis can pass through symmetric division, generating two identical daughter cells with the same function, or asymmetric division, resulting in daughters with different functions and/or morphology (Majumdar and Liu, 2020; Ruijtenberg and van den Heuvel, 2016; Wheeler et al., 2019). During symmetric division, cells must duplicate the genetic material and the cellular organelles in order to ensure their proper inheritance by the daughter cells (Champion et al., 2017; Jongsma et al., 2015; Mascanzoni et al., 2019). Organelle inheritance is believed to be either coordinated or stochastic, depending on the organelle number, size, and function in the cell. Single-copy organelles must be duplicated to ensure equal inheritance, while smaller organelles are believed to be inherited via stochastic distribution (Carlton et al., 2020). To accommodate all of the changes during mitosis, the cell volume grows and is sustained by plasma membrane remodeling and reshaping (Boucrot and Kirchhausen, 2007; Carlton et al., 2020). To keep cell surface homeostasis, eukaryotic cells, especially when unprotected by a cell wall, round up and unfold membrane projections to maintain the surface area-to-volume ratio (Boucrot and Kirchhausen, 2007; de França et al., 1993; Figard and Sokac, 2014). Despite the obvious role of the Golgi apparatus in the biosynthesis of the plasma membrane (Agliarulo and Parashuraman, 2022), evidence suggests that this organelle is not the leading actor enabling plasma membrane growth (Boucrot and Kirchhausen, 2007). In fact, homeostasis of the cell surface is associated with the endosomal system, which acts in membrane shaping, delivery, and removal. The endosomes can promote the incorporation of new membranes in the cell surface via exocytosis or endocytic recycling (Carlton et al., 2020; Morris and Homann, 2001; Sabharanjak et al., 2002). However, whether endocytosis continues during cell division has been a matter of debate. Evidence from African green monkey kidney cells suggests that clathrin-mediated endocytosis happens throughout the

entire cell cycle (Boucrot and Kirchhausen, 2007), while observations in HeLa cells show endocytosis impairment during early mitosis (Fielding et al., 2012). Nevertheless, it is believed that some degree of endocytosis persists throughout the cell division (Carlton et al., 2020).

Trypanosoma brucei is a unicellular eukaryotic pathogen found in the blood and fluids of infected humans, livestock, and game animals (Crilly and Mugnier, 2021; WHO, 2023). Inside the host, *T. brucei* slender trypomastigotes proliferate and can differentiate (Matthews and Gull, 1994; Robertson, 1912; Schuster et al., 2021). The parasite proliferation happens via non-equivalent mitosis, resulting in two similar daughters that are remodeled after mitosis (reviewed in R. J. Wheeler et al., 2019). During the cell cycle, *T. brucei* organelles, such as the kinetoplast, nucleus, Golgi apparatus, mitochondria, and glycosomes, grow in volume and/or number. Organelle inheritance is believed to be associated with the flagellum attachment zone, but a stochastic segregation has also been suggested for smaller and numerous cellular components, such as glycosomes and acidocalcisomes. All of these changes are accompanied by the progressive increase in cell volume (Hughes et al., 2017; Wheeler et al., 2019).

The cell volume growth implies an enlargement in the cell surface area, which must be carefully balanced by the parasite. The cell surface of *T. brucei* is decorated with VSG molecules anchored to the plasma membrane via glycosylphosphatidylinositol (GPI) anchors (Bartossek et al., 2017; Cross, 1975; Ferguson, 1997; Ferguson et al., 1988; Jackson et al., 1985). The antigenic variation promoted by the VSGs protects the parasite population against clearance by the host's immune system (Cross, 1975; Magez et al., 2020; Mugnier et al., 2016, 2015; Stijlemans et al., 2017). In addition, the mobility of the GPI anchor allows the parasite to internalize VSGs opsonized by the host's antibodies and degrade them in about 2 minutes (Engstler et al., 2007). Thus, *T. brucei* endurance inside the host is intrinsically connected to its endo-lysosomal system that influences the homeostasis of the parasite's cell surface.

All endocytosis in *T. brucei* is clathrin-mediated (Allen et al., 2003; Engstler et al., 2004; Grünfelder et al., 2003; Morgan et al., 2002, 2001) and involves cargo transport into distinct endosomal subpopulations. These subpopulations are named early, late, and recycling endosomes and are identified with Rab GTPases, TbRab5A, TbRab7, and TbRab11, respectively (Engstler et al., 2004; Grünfelder et al., 2003; Overath and Engstler, 2004). The first endosome to receive endocytosed cargo is the early endosome, which sorts the cargo for recycling or degradation. Recycling cargo then passes into late endosomes or goes directly to the recycling compartment, from where it will return to the cell surface via exocytic carriers that deliver the cargo to the flagellar pocket. On the other hand, cargo intended for degradation is proposed to pass to late endosomes and, from there, to the lysosome. Class II CCVs that bud from endosomal cisternae filled with fluid-phase cargo have been proposed to be responsible for this transport (Engstler et al., 2004; Grünfelder et al., 2003).

Despite the importance of the endo-lysosomal system for *T. brucei* survival, the dynamics of its duplication during *T. brucei* proliferation remains poorly understood. In addition, the relationship between this system and membrane homeostasis during the parasite cell cycle remains enigmatic. To contribute to such an overlooked topic of *T. brucei* cell biology, this chapter investigates the duplication of the endo-lysosomal system during the *T. brucei* cell cycle as a basis to understand membrane homeostasis during the proliferation of the parasite.

2. Material and Methods

2.1 Materials

2.1.1 Trypanosome cell lines

Table 1. Cell lines of *Trypanosoma brucei brucei* used in this study.

Cell line*	Description	Selection antibiotics	Reference
MITat1.2 1390 (referred in this thesis as *T. brucei* 1390)	Monomorphic wild-type cell line (expressing VSG221) transfected with pLew13 & pLew90 plasmids.	5 µg/mL Hygromycin 2.5 µg/mL G418	Wirtz et al. (1999)
EP1::GFP	MITat1.2 1390 transfected with a pKD4 based plasmid containing the procyclin isoform EP1 tagged with GFP that integrates upstream of the VSG in the active expression site. Used to visualize the endosomes.	5 µg/mL Hygromycin 30 µg/mL G418	Günzel (2010)
YFP::CLC	MITat1.2 1390 transfected with p2627(p) plasmid. The cell line expresses an eYFP N-terminus tagged clathrin light chain. Used to visualize clathrin.	5 µg/mL Hygromycin 30 µg/mL G418 0.3 µg/mL Puromycin	Heddergott (2006)

*The cell lines were not generated in this study. For more information on the plasmids and transfection check the references.

2.1.2 Fluorescent dyes

Table 2. Sulfo-NHS dyes used for the surface staining of trypanosomes.

Sulfo-NHS dye	Fabricant	Working concentration	Excitation	Emission
Atto 488	Atto-Tec GmbH, Germany	200 µM	488 nm	520 nm
Atto 542	Atto-Tec GmbH, Germany	100 µM	542 nm	562 nm

2.1.3 Mounting Media

Table 3. Mounting media used for microscopy specimen preparations.

Mounting Media	Fabricant
VECTASHIELD® Antifade Mounting Medium with DAPI	Vector Laboratories (USA)
ProLong™ Diamond Antifade Mountant with DAPI	Thermo Fisher Scientific (USA)
ProLong™ Diamond Antifade Mountant	Thermo Fisher Scientific (USA)

2.1.4 Antibodies

Table 4. **Pairwise list of primary and secondary antibodies used for immunofluorescence assays**. Distinct dilutions were tested for each combination; only the optimal dilutions are presented.

Primary antibody	Dilution	Secondary antibody[c]	Dilution
Rabbit anti-p67[a]	1:500	Goat anti-rabbit conjugated with Alexa Fluor 488 or Alexa Fluor Plus 488	1:3000
Mouse anti-p67[a]	1:500	Goat anti-mouse conjugated with Alexa Fluor 488	1:3000
Rabbit anti-TbCatL[a]	1:500	Goat anti-rabbit conjugated with Alexa Fluor 488	1:3000
Rabbit anti-TbRab11[b]	1:500	Goat anti-rabbit conjugated with Alexa Fluor 488	1:1000
Rabbit anti-TbRab11[b]	1:500	Goat anti-rabbit conjugated with Alexa Fluor 594	1:1000
Guinea pig anti-TbRab7[b]	1:250	Goat anti-guinea pig conjugated with Alexa Fluor 488	1:1000
Rat anti-TbRab5A (crude serum)[b]	1:250	Goat anti-rat conjugated with Alexa Fluor 488	1:500

[a]Courtesy of J. Bangs; [b]Available in AG Engstler (F. Link) (for more information see Link et al., 2023, preprint); [c]Invitrogen (Thermo Fisher Scientific).

Table 5. **Pairwise list of primary and secondary antibodies used for immunofluorescence assays on electron microscopy sections**. Distinct dilutions were tested for each combination; only the optimal dilutions are presented.

Primary antibody	Dilution	Secondary antibody[d]	Dilution
Rabbit anti-TbCatL[a]	1:250	Goat anti-rabbit conjugated with Alexa Fluor 488	1:150
Rabbit anti-VSG 221[b]	1:100	Goat anti-rabbit conjugated with Alexa Fluor 594	1:150
Chicken anti-GFP[c]	1:250	Donkey anti-chicken conjugated with Alexa Fluor 488	1:150
Chicken anti-GFP[c]	1:250	Goat anti-chicken conjugated with Alexa Fluor Plus 488	1:250

[a]Courtesy of J. Bangs; [b]Available in AG Engstler (N. Jones); [c]Abcam; [d]Invitrogen (Thermo Fisher Scientific, USA).

Table 6. **Pairwise list of primary and secondary antibodies used for immunogold assays on electron microscopy sections**. Distinct dilutions were tested for each combination; only the optimal dilutions are presented.

Primary antibody	Dilution	Secondary antibody	Dilution
Rabbit anti-TbCatL[a]	1:250	Goat anti-rabbit conjugated with colloidal gold: 12 nm[d] or 6 nm[e]	1:10
Rabbit anti-VSG 221[b]	1:250	Goat anti-rabbit conjugated with colloidal gold: 12 nm[d] or 6 nm[e]	1:10
Rabbit anti-Rab11[c]	1:250	Goat anti-rabbit conjugated with colloidal gold: 12 nm[d] or 6 nm[e]	1:10
Rabbit anti-p67[a]	1:250	Goat anti-rabbit conjugated with colloidal gold: 12 nm[d] or 6 nm[e]	1:10

[a]Courtesy of J. Bangs; [b]Available in AG Engstler (N. Jones); [c]Available in AG Engstler (F. Link) (for more information see Link et al., 2023, preprint); [d]Dianova (DE); [e]Jackson ImmunoResearch (USA).

2.1.5 Equipment and devices

Table 7. List of equipment and devices used in this study.

Equipment/Device	Manufacturer
Neubauer chamber	Marienfeld (DE)
CO_2 Incubators	Binder (DE)
Centrifuge Spectrafuge™ Mini	Labnet International Inc. (USA)
Centrifuge Z 216 MK	Hermle Labortechnik GmbH (DE)
Centrifuge Z 383 K	Hermle Labortechnik GmbH (DE)
EM AFS2 automated freeze substitution machine	Leica Microsytems (DE)
EM HPF100 high-pressure freezing system	Leica Microsytems (DE)
UC7 ultramicrotome	Leica Microsytems (DE)
Diamond knives Ultra and Jumbo	DIATOME (Switzerland)
DMI6000B widefield microscope	Leica (DE)
EL6000 Mercury short-arc reflector lamp	OSRAM (DE)
CCD sensor ICX285 A	Sony (Japan)
Elyra S.1 structured illumination microscope	Carl Zeiss Microscopy (DE)
sCMOS camera pco.edge 5.5	Excelitas PCO (DE)
JSM-7500F electron microscope	JEOL (Japan)
JEOL JEM-1400 Flash electron microscope	JEOL (Japan)
JEOL JEM-2100 electron microscope	JEOL (Japan)

2.1.6 Buffers and solutions

The chemicals used to prepare buffers and solutions were obtained from Sigma-Aldrich (St. Louis, USA), AppliChem (Darmstadt, DE) or Carl Roth (Karlsruhe, DE).

HMI-9 medium: For 1 L of HMI-9 medium, 17.66 g Iscove's modified Dulbecco's medium (IMDM), 3 g sodium bicarbonate, 136 mg hypoxanthine, 28.2 mg bathocuproine sulfonate, 14 µL β-mercaptoethanol, 39 mg thymidine, 100,000 U penicillin, 100 mg streptomycin, 182 mg cysteine and 10 % (v/v) fetal calf serum (FCS) were used. Components of the medium were dissolved in filtered ddH_2O and the pH adjusted to 7.5. The medium was then sterilized by filtration (pore size 0.2 µm), followed by addition of 10 % of heat-inactivated FCS.

Trypanosome dilution buffer (TDB), pH 7.6: 20 mM Na_2HPO_4, 2 mM NaH_2PO_4 (pH 7.7), 5 mM KCl, 80 mM NaCl, 1 mM $MgSO_4$ (pH 7.7), and 20 mM glucose in ddH_2O (filter sterilized).

2x Trypanosome freezing mix (for bloodstream forms): mix 20 % (v/v) glycerol in HMI-9 medium (filter sterilized).

Phosphate buffered saline (PBS): 10 mM Na_2HPO_4, 1.7 mM KH_2PO_4, 137 mM NaCl, 2.7 mM KCl, pH 7.4.

1 % Bovine serum albumin (BSA) diluted in PBS (1 % BSA/PBS): 1 % (w/v) BSA freshly diluted in PBS (filtered with pore size 0.2 µm).

8 % Formaldehyde (FA): 16 % (v/v) FA (EM grade) diluted in PBS.

Freezing substitution mix: 0.1 % $KMnO_4$ diluted in anhydrous acetone.

LB1: 1 % (w/v) BSA diluted in 0.1 % Tween 20/PBS.

LB2: 0.1 % (v/v) BSA diluted in 0.1 % Tween 20/PBS, starting from LB1.

2.2 Methods

2.2.1 *In vitro* culture of trypanosomes

Cultures of monomorphic bloodstream forms of *T. brucei* 1390 (Wirtz et al., 1999) were maintained in a humidified environment at 37 °C with 5 % CO_2. The density was kept at a maximum of 1 x 10^6 cells/mL with regular passages in fresh HMI-9 medium with the selection antibiotics (Table 1). Genetically engineered cell lines derived from this one had similar maintenance, with changes in the selection antibiotics (Table 1).

For cryopreservation of trypanosomes, ~4 x10^6 cells were harvested by centrifugation (1400 x *g*, 10 min, 4 °C), resuspended in 500 µL ice-cold HMI-9 medium, and mixed with 500 µL of ice-cold 2x freezing mix. Stabilates were kept at -80 °C for at least 24 h and transferred to -150 °C for long-term storage.

For the establishment of a new culture, stabilates were thawed in a water bath at 37 °C, washed with 10 mL of HMI-9 medium, and pelleted (1400 x *g*, 10 min, 37 °C). After discarding the supernatant, cells were resuspended in 10 mL of fresh pre-warmed HMI-9 medium and kept in a humidified environment at 37 °C with 5 % CO_2 for 1 h. After this time, 10 µL of culture was added to a Neubauer counting chamber to determine cell density. Then, the culture was diluted to a density of ~5 x 10^4 cells/mL in fresh HMI-9 containing the necessary antibiotics and maintained as previously described.

2.2.2 Staining trypanosomes with sulfo-NHS dyes

For surface staining, a minimum of 2 x 10^7 cells cultivated in suspension were harvested (1400 x *g*, 10 min, 37 °C), washed once in warm TDB (37 °C), and stained with sulfo-NHS dyes (Table 2) (15 min, 37 °C, in the dark). After this time, cells were washed

twice in warm TDB and fixed in 2 % FA/0.05 % glutaraldehyde (GA) overnight (4 °C). After fixation, cells were washed twice in PBS, attached to coverslips treated with poly-L-lysine, and mounted on glass slides with VECTASHIELD® Antifade Mounting Medium with DAPI (Table 3). Coverslips were sealed with nail polish and stored at 4 °C until imaging.

2.2.3 Immunofluorescence assays

For immunofluorescence, 1 x 10^7 trypanosomes were harvested (1400 x *g*, 10 min, 37 °C) and washed once in 1 mL of ice-cold TDB (2000 x *g*, 90 s). After aspiration of the supernatant (leaving ~100 µL), cells were resuspended in 400 µL of ice-cold TDB, and fixed with 4 % FA (overnight at 4 °C, or 1 h at room temperature – RT).

Fixed cells were used for immunofluorescence assays performed either in suspension or attached to Ø 12 mm coverslips coated with poly-L-lysine. Cells were washed two times in PBS and blocked in 1 % BSA/PBS for a minimum of 10 min at RT. A permeabilization step with 0.25 % Triton X-100 diluted in PBS (5 min, RT) was necessary only for cells attached to coverslips. Samples were incubated for 1 h at RT with primary antibody diluted in 1 % BSA/PBS, followed by three washing steps of 5 min using either PBS or 1 % BSA/PBS. The incubation with the secondary antibody diluted in 1 % BSA/PBS was performed in the dark, proceeded by three washing steps of 5 min using either PBS or 1 % BSA/PBS also in the dark. Cells were mounted on microscope glass slides using the commercial mounting media ProLong™ Diamond Antifade Mountant with or without DAPI, and VECTASHIELD® Antifade Mounting Medium with DAPI (Table 3). Specimens for structured illumination microscopy (SIM) were prepared on #1.5 coverslips (~170 µm thickness). The samples mounted with ProLong™ Diamond Antifade Mountant were left at RT overnight and subsequently stored at 4 °C until imaging, while the samples prepared with VECTASHIELD® Antifade Mounting Medium were sealed with nail polish and stored at 4 °C. A list of the antibodies used in this study can be found in Table 4. Negative and

secondary-only controls were prepared by substituting both or only primary antibodies by 1 % BSA/PBS.

2.2.4 Preparing microscopy specimens: trypanosomes with a fluorescent tag

For the visualization of endosomal membranes and clathrin-coated vesicles, two cell lines derived from *T. brucei* 1390 were used: EP1::GFP and YFP::CLC (Table 1). These cell lines were generated by M. Günzel and N. Heddergott and are available in the collection of the Engstler group.

For microscopy, 1 x 10^7 trypanosomes were harvested (1400 x *g*, 10 min, 37 °C), washed once in 1 mL of ice-cold TDB (2000 x *g*, 90 s), and the supernatant was discarded (leaving ~100 µL). Cells were resuspended in 400 µL of ice-cold TDB, fixed with 4 % FA (overnight at 4 °C, or 1 h at room temperature – RT), attached to poly-L-lysine coverslips and mounted on microscope glass slides using commercial mounting media (Table 3). Samples mounted with ProLong™ Diamond Antifade Mountant were kept at RT overnight and then moved to 4 °C until imaging. Samples prepared with VECTASHIELD® Antifade Mounting Medium were sealed with nail polish and stored at 4 °C.

2.2.5 Cargo uptake assays

Bloodstream forms of *T. brucei* growing in culture were harvested (1400 x *g*, 10 min, 37 °C) and incubated with ~250 µg/mL of ferritin conjugated with the NHS-dye Atto 647 (15 min, 37 °C, in the dark). Negative controls were incubated with TDB. Endocytosis was stopped with the addition of ice-cold TDB to the cells. Samples were centrifuged (2000 x *g*, 90 s), washed in 1 mL ice-cold TDB, and fixed with 4 % FA overnight (4 °C). Fixed cells were attached to coverslips and used for immunofluorescence assays with anti-TbRab5A, anti-TbRab7, and anti-TbRab11 (as previously described). Coverslips were mounted on slides with a drop of ProLong™ Diamond Antifade Mountant.

2.2.6 Cell cycle analysis

To analyze the cell cycle of bloodstream forms of *T. brucei* 1390, 2 x 10^7 cells were harvested, stained with sulfo-NHS-dyes, fixed with 2 % FA/0.05 % GA, and placed onto coverslips treated with poly-L-lysine (see Material and Methods 2.2.3). Coverslips were mounted on slides with ~2 µL of VECTASHIELD® Antifade Mounting Medium with DAPI, sealed with nail polish, and imaged using a DMI6000 B widefield microscope (100x Objective, NA = 1.4). Three technical replicates were prepared, and 400 cells were classified according to the cell cycle stage per replicate.

2.2.7 Influence of centrifugal forces on the cell cycle analysis

Cells in late cytokinesis are linked by a cytoplasmic bridge that could be potentially broken by centrifugal forces. Thus, a set of three experiments were performed to analyze the impacts of the centrifugation steps in the cell cycle analysis. Each experiment was designed to analyze the impacts of harvesting, washing, and fixation steps in the encounter of late cytokinesis stages. To do this, each set of experiments comprised three groups, the control and the two tested conditions, with a minimum of 10 technical replicates. A differential counting of "late cytokinesis" and “single cells” was performed using Neubauer chambers. A total of 150 "stages" per replicate were analyzed (meaning that each stage, either single cells or late cytokinesis, summed up as 1 for the total number).

For harvesting experiments, the control group consisted of cells directly counted from the culture. One testing group was centrifuged at 1400 x *g* for 10 min, and the other at 750 x *g* for 10 min, both using a swing-out rotor centrifuge. The total volume of centrifugation was 10 mL, consisting of 1 mL of culture plus 9 mL of warm TDB. For washing experiments, cells were harvested (10 mL of total volume centrifuged at 1400 x *g*, 10 min, consisting of 2 mL of culture and 8 mL of warm TDB), and the supernatant was discarded (leaving ~500 µL). Cells were resuspended in 500 µL of TDB and transferred to a 1.5 mL microcentrifuge tube. The control group was counted directly after resuspension.

In contrast, the testing groups were centrifuged: in a picofuge (2000 x *g*, 90 s) or in a microcentrifuge (750 x *g*, 2 min). After centrifugation, the supernatant was discarded (leaving ~100 µL), and cells were resuspended in 1 mL of TDB and counted. For the fixation experiment, 2 x 10^7 cells were harvested (1400 x *g*, 10 min) and washed (2000 x *g*, 90 s) as previously described. After washing, cells were resuspended in 500 µL and fixed with 4 % formaldehyde overnight at 4 °C. Following this step, 250 µL of fixed cells were placed in 1.5 mL microfuge tubes (to have about 1 x 10^6 cells per tube), the volume was completed with 750 µL of PBS, and the content was mixed by inversion. For the control group, cells were loaded in the Neubauer chamber and counted. The other two groups followed a washing step with centrifugation performed either with a picofuge (2000 x *g*, 90 s) or a microcentrifuge (500 x *g*, 5 min). After centrifugation, the supernatant was discarded (leaving ~100 µL), and cells were resuspended with 1 mL of PBS and counted.

2.2.8 Fixing samples for electron microscopy: high-pressure freezing

For high-pressure freezing of *T. brucei* bloodstream forms, 3 x 10^7 cells cultivated in suspension were harvested in a swing-out rotor centrifuge (750 x *g*, 3 min, RT). After pelleting the cells, the supernatant was aspirated (leaving 4 mL in the tube), 4 mL of warm FCS was added to the tube, and cells were resuspended by gentle pipetting up-and-down. Cells were once again pelleted (750 x *g*, 3 min, RT), the supernatant was discarded (leaving up to 200 µL), and cells were resuspended in the remaining volume by swirling the tube and pipetting up-and-down twice. The entire content was transferred into a 200-µL PCR tube, spun down (2000 x *g*, 10 s), and the supernatant was quickly discarded. Finally, 1.5 µL of the cell pellet was carefully added to the specimen carrier (avoiding bubbles), the lid of the carrier was closed, and the specimen sandwich was immediately submitted to high-pressure freezing using a Leica EM HPF100. Samples were transferred to liquid nitrogen until freeze substitution.

2.2.9 Freeze substitution and embedding

For freeze substitution, samples were transferred from liquid nitrogen into an automated freeze substitution machine EM AFS2 containing the freezing substitution mix cooled down to -90 °C. The samples were incubated at these conditions for 65 h in total, with one change with fresh freezing substitution mix happening during the first 24 h of incubation. The temperature was gradually increased to -45 °C over the course of 11 h before the samples were washed with acetone until the solution became clear. To exchange the acetone with ethanol, the samples were subjected to ethanol/acetone gradient washes: once with 1/3 ethanol (30 min incubation at -45 °C), once with 2/3 ethanol (30 min incubation at -45 °C), and twice with 100 % ethanol (1 h incubation at -45 °C per wash). Then, the temperature was increased to 4 °C over the course of 16 h and the samples were washed twice with 100 % ethanol (1 h incubation at 4 °C per wash) and transferred to 50 % LR-White resin in ethanol (3-4 h incubation at 4 °C). The 50 % LR-White resin was changed once, and the samples were removed from the freezing platelets, collected in small glass vials (sealed to avoid evaporation), and incubated overnight at 4 °C. Samples were washed three times with 100 % LR-White at 4 °C with progressive incubation times: first 1h, then 3-4 h, and finally overnight. A final incubation with 100 % LR-White at 4 °C (3-4 h) was done, and the samples were transferred to gelatin capsules which were tightly locked to avoid the presence of oxygen. Samples were polymerized by heat (52 °C) for at least 72 h.

2.2.10 Ultramicrotomy

Before sectioning, the gelatin capsule was removed from one of the tips with a razor blade. To localize the samples and check for integrity, initial sections were obtained and stained with methylene blue. After finding the region of interest, the block was trimmed into a trapezoid block and sectioned using a Leica UC7 ultramicrotome with diamond knives Ultra and Jumbo. For studies using correlative light and electron microscopy (CLEM), 100

nm thick sections were collected onto a glass slide, while for transmission electron microscopy (TEM), 60 nm sections were placed on nickel TEM grids.

2.2.11 Immunofluorescence on sections

The glass slides containing the sections were incubated in PBS for 15 min (RT). In a humidity chamber, the sections were covered with 0.02 M glycine (diluted in PBS) and incubated for 15 min (RT). After discarding the solution, the sections were covered with 1 % (w/v) BSA (diluted in PBS) and incubated for 15 min (RT). After blocking, sections were covered with the primary antibody diluted in 0.1 % BSA/PBS and incubated at RT for 2 h. The glass slides were washed four times in PBS; each wash had a 5 min incubation time. Then, the sections were covered with the secondary antibody diluted in 0.1 % BSA/PBS and incubated for 30 min in the dark (RT). The samples were washed four times in PBS (each wash had a 5 min incubation time in the dark), dried, and mounted with ProLong™ Diamond Antifade Mountant with DAPI. For imaging by SIM, #1.5 coverslips (~170 µm thickness) were used. Slides were kept at RT overnight for curation of the mounting medium and then transferred to 4 °C until imaging. For antibody dilutions, see Table 5.

2.2.12 Contrasting sections for scanning electron microscopy

After the completion of fluorescence microscopy image acquisition, the samples were immersed in ddH_2O to loosen the coverslip. Following that, the sections were covered with 2 % uranyl acetate in ddH_2O, incubated for 10 min, and washed in ddH_2O. Then, the sections were covered with 50 % Reynold's lead citrate in ddH_2O, incubated for 5 min, and washed once more in ddH_2O. After drying, the sections had the glass slide cut around them using a diamond pen. The glass pieces containing the sections were mounted to SEM specimen holders containing a carbon sticker on top. Then, the glass pieces were surrounded with silver paint and were carbon coated (5 nm). The specimens were kept at RT in a vacuum-sealed stub box until imaging.

2.2.13 Immunogold labeling

Grids containing 60 nm sections were placed in PBS for 10 min (RT), followed by a 10 min incubation in LB1. Then, grids were placed onto the primary antibody (1:250, diluted in PBS) and incubated for 1 h (RT) in a humidity chamber. This step was followed by 4 washes (10 min incubation each) with LB2. Then, grids were incubated with the secondary antibody (1:10, diluted in LB2) for 2 h (RT) in the humidified chamber. After this, grids were washed twice in LB2 (10 min incubation each), twice in PBS (5 min incubation each), and were then placed in 1.25 % GA (freshly diluted in PBS) and incubated for 2 min. Finally, grids were washed three times with ddH_2O (5 min incubation each), dried, and stored in a grid box (RT) until contrasting. The following primary antibodies were used: rabbit anti-Rab11, rabbit anti-VSG 221, rabbit anti-TbCatL, and rabbit anti-p67. The secondary antibodies were conjugated with 6 nm and 12 nm gold (Table 6).

2.2.14 Contrasting sections for transmission electron microscopy

Grids were placed onto 2 % uranyl acetate in ddH_2O, incubated for 5 min (RT), and washed in ddH_2O. Then, grids were incubated with 50 % Reynold's lead citrate in ddH_2O for 90 seconds (RT), washed in ddH_2O, dried, and stored in a grid box (RT) until imaging.

2.2.15 Widefield fluorescence microscopy

Samples were screened using a DMI6000B widefield microscope equipped with an HCX PL APO CS objective (100x, NA = 1.4) and Type F Immersion Oil (refractive index = 1.518). The illumination of an EL6000 Mercury short-arc reflector lamp was selected by bandpass filter cubes for the proper excitation light. Differential interference contrast (DIC) was used to visualize cell morphology and choose fields of view for image acquisition. 3D recording of each field of view was obtained using 40 to 120 Z-slices (step size = 0.21 µm) using a black-and-white CCD sensor ICX285 A (pixel size = 6.45 µm). Information on the

nominal power density at the objective focal plane, excitation, and emitted light for each filter cube is listed in Table 8.

Table 8. Light source parameters used for image acquisition of immunofluorescence assays.

Filter cube	Power density (W/cm^2)[a]	Excitation (nm)	Emission (nm)
Y5	0.651 ± 0.080	590-650	662-738
Y3	0.749 ± 0.086	530-560	572-648
GFP	0.557 ± 0.069	450-490	500-550
A4	0.278 ± 0.076	340-380	450-490

[a]The power densities were measured at the objective focal plane by Timothy Krüger using an HCX PL APO CS objective (100x, NA = 1.4, Leica Microsystems, DE) on 19.10.2021.

2.2.16 Structured illumination microscopy

Samples were screened using a Zeiss Elyra S.1 SIM equipped with a Plan-Apochromat objective (63x, NA = 1.4) and immersion oil Immersol™ 518 F (refractive index = 1.518). The laser lines 405 nm, 488 nm, 561 nm, and 642 nm were used for specimen illumination with bandpass and long pass emission filters. 3D recording of each field of view was obtained using 5-13 Z-slices using a sCMOS camera pco.edge 5.5 (pixel size = 6.5 µm).

2.2.17 Scanning electron microscopy

To investigate the ultrastructure of samples destined to correlative light and electron microscopy (CLEM), specimens mounted on glass slides and attached to stubs were analyzed via scanning electron microscopy (SEM) using a JSM-7500F electron microscope (JEOL, Japan) equipped with a detector for backscattered electrons at low acceleration voltages (LABE). The acceleration voltage used was 5 kV. The areas of interest were chosen based on the fluorescence microscopy results, and a few overview pictures were taken (6k magnification) before proceeding to imaging with higher magnifications (25k, 30k,

or 35k). The images were collected in overlapping regions to enable the preparation of the SEM mosaic (see Material and Methods 2.2.22).

2.2.18 Transmission electron microscopy

Samples destined for transmission electron microscopy (TEM) were analyzed with JEOL JEM-1400 Flash (JEOL, Japan) and JEOL JEM-2100 (JEOL, Japan) microscopes operating at 120 kV and 200 kV, respectively. The obtained images varied from 15k to 40k magnification.

2.2.19 Image deconvolution

The hyperstacks were deconvolved using the software Huygens Essential version 21.04.0p6 (Scientific Volume Imaging B.V., Hilversum, Netherlands). The sampling intervals (X = 92.143 nm, Y = 92.143 nm, Z = 205.128 nm), the optical parameters (NA = 1.4), and refractive indices were defined according to the microscopic parameters and embedding medium used (immersion oil = 1.515, embedding medium = 1.45 for VECTASHIELD® Antifade Mounting Medium with DAPI and 1.47 for ProLong™ Diamond Antifade Mountant with DAPI or without DAPI). The advanced microscopic configurations were also set accordingly (objective quality = good, coverslip position = 3.077, imaging direction = upward). The wavelengths for fluorescence channels were defined for each experiment according to the fluorophores used (Table 9), and the multiphoton excitation was kept as default. The deconvolution algorithm of choice was classic maximum likelihood estimation (CMLE), and the point spread function (PSF) was calculated by the software (theoretical). The maximum number of iterations was set to 50, and the system-optimized iteration mode was used. The signal-to-noise ratio (SNR) was estimated by the software, probed for possible distortions, and set for the channel accordingly. All other deconvolution parameters were kept as default. Deconvolved images were saved as 16-bit .tif files.

Table 9. Fluorophore wavelengths defined during setup of deconvolution analysis.

Fluorophores	Excitation (nm)	Emission (nm)
Alexa Fluor 647	650	665
Alexa Fluor 568	578	603
Alexa Fluor 488/Alexa Fluor Plus 488	496	519
Atto 647	647	667
Atto 390	390	476
DAPI	350	470
eYFP	500	535
GFP	488	510

2.2.20 Quantitative colocalization analysis

On images obtained with widefield fluorescence microscopy, single cells were selected based on DAPI and DIC channels (blind for the signal of interest). Deconvoluted images were inspected, and the slices containing in-focus information were kept. After the preparations of projections (Sum Slices), the posterior region of the cell was selected as the region of interest (ROI), and a convoluted background subtraction (method = median) was applied to the projections whenever necessary (Brocher, 2023). The intensity-based correlation analysis of two channels was performed based on Zhang and Cordelières (2016). The cytofluorograms were used to determine the adequate correlation coefficients to be estimated (Pearson correlation or Spearman's rank correlation). On super-resolved images obtained with SIM, single cells were selected according to the presence of the signal of interest. After the initial cell selection, the ROI was used to prepare projections (Sum Slices) of each channel that had the background subtracted. The signal overlap was measured with Mander's colocalization coefficient using a manual threshold (Zhang and Cordelières, 2016).

The open-source software Fiji/ImageJ (National Institutes of Health, USA) was used for image analysis (Schindelin et al., 2012). The coefficients obtained with Pearson/Spearman correlation and Mander's overlap were analyzed with R version 4.1.2

(R Core Team, 2021) in the environment RStudio 2021.09.1.372 (RStudio Team, 2020). The packages used were ggplot2 (Wickham et al., 2023a), ggVennDiagram (Gao et al., 2021), openxlsx (Schauberger et al., 2023), psych (Revelle, 2022), and RColorBrewer (Neuwirth, 2022). All ImageJ macros and R scripts are available at https://github.com/alyssaborges/PhD-Thesis_2023.

2.2.21 Area measurements and statistical analysis

For area measurements, cells were fluorescently labeled and imaged in widefield microscopy. For the analysis of the area of the cell, contrast enhancement was applied in individually selected cells, followed by thresholding using the method Li (Li and Lee, 1993). For area measurements of the endosomes (using EP1::GFP cell line) and clathrin vesicles (using YFP::CLC cell line), single cells were selected after deconvolution and inspected for the signal of interest. Slices containing in-focus information were kept, and maximum intensity projections were prepared. The method Otsu was used to obtain binary masks of these projections (Otsu, 1979). For all measurements, the scale was calibrated (1 µm = 10.8527 pixels), and the area was obtained with the particle analyzer.

The information on the total area grouped by the cell cycle stage was checked for normality via visual inspection of QQ plots, and a comparison of the mean was performed using one-way ANOVA and Tukey's range test as a post hoc.

The open-source software Fiji/ImageJ (National Institutes of Health, USA) was used for image analysis (Schindelin et al., 2012), and statistics were performed using R version 4.1.2 (R Core Team, 2021) in the environment RStudio 2021.09.1.372 (RStudio Team, 2020). The packages used were ggplot2 (Wickham et al., 2023a), ggpubr (Kassambara, 2023a), openxlsx (Schauberger et al., 2023), psych (Revelle, 2022), rstatix (Kassambara, 2023b), and tidyr (Wickham et al., 2023b). All ImageJ macros and R scripts are available at https://github.com/alyssaborges/PhD-Thesis_2023.

2.2.22 Correlation of light and electron microscopy

The imaging of sections with the SIM microscope was done by obtaining z-stacks for proper processing and generation of the super-resolved images. For the correlation, the brightest z-layer of each channel was chosen and saved as portable network graphics (PNG). The SEM mosaic of the region of interest in high magnification (≥ 25k) was prepared via manual alignment of the overlapping images and exported as PNG. The open-source software Fiji/ImageJ (Schindelin et al., 2012) and the plug-in TrakEM2 (Cardona et al., 2012) were used for these steps.

The correlation was performed with the open-source vector graphics editor Inkscape (version 1.0; http://www.inkscape.org). For one section, the SEM mosaic image and one SIM image per color channel were placed onto the Inkscape canvas. For an unbiased correlation, all the channels were perfectly aligned, and the channel(s) containing the fiducials (DNA staining for nucleus and kinetoplast, and VSG for cell surface) were placed on top. In this way, the channel of interest was hidden underneath the fiducials. Then, the opacity was also reduced so that the SEM image and the fiducials were easily visible but not the signal of interest. All SIM images were grouped into one object, and the aspect ratio was locked before starting the image registration (i.e., rotating and resizing the SIM images to align accurately with the corresponding regions in the SEM mosaic). Once the correlation result was considered optimal, the grouping was released, the opacity was returned to 100 %, and all correlated images were exported as PNG, and overlaid using Fiji/ImageJ (Schindelin et al., 2012).

3. Results

3.1 Centrifugal forces affect the ratios of *T. brucei* cell cycle stages

The cell surface homeostasis during the proliferation of *T. brucei* is poorly studied. Considering the high rates of VSG endocytosis and recycling showed by the parasite, this work investigates whether the duplication of the endo-lysosomal system could be related to plasma membrane homeostasis. For a detailed analysis of events related to the *T. brucei* cell cycle, single cells must be grouped into sequential cell cycle stages according to their organelle morphology. One of the most straightforward ways of achieving this consists in observing the division stage of the nucleus and the kinetoplast of fixed cells (Gluenz et al., 2011; Hughes et al., 2017; Lacomble et al., 2010; Wheeler et al., 2013). Thus, as a first step of this work, fluorescence microscopy was used to analyze and classify *T. brucei* bloodstream forms into their different cell cycle stages.

Generally, *T. brucei* cell cycle stages are named 1K1N (one kinetoplast and one nucleus), $1K^{d}1N$ (one kinetoplast in the process of division and one nucleus), 2K1N (two kinetoplasts and one nucleus), and 2K2N (two kinetoplasts and two nuclei) (Gluenz et al., 2011; Siegel et al., 2008; Woodward and Gull, 1990). The $1K^{d}1N$ stage can be further subdivided into $1K^{v}1N$ (one dividing kinetoplast with a V-shape form and one nucleus) and $1K^{b}1N$ (one dividing kinetoplast with a bone-shape morphology and one nucleus), representing two sequential stages of the kinetoplast division (Gluenz et al., 2011). Similarly, 2K2N cells can also be subdivided into three successive phases: 2K2N (when the cleavage furrow has not started), 2K2N in cytokinesis, and 2K2N in late cytokinesis (a pre-abscission stage in which the cells are linked by a cytoplasmic bridge) (Hughes et al., 2017).

For the cell cycle analysis of bloodstream forms of *T. brucei* 1390, cells were stained with sulfo-NHS dyes, fixed, and imaged using a widefield fluorescence microscope. A total of 400 cells of each replicate were examined and manually categorized according to their respective cell cycle stage.

In an exponentially growing population *in vitro*, 50 % of cells observed were 1K1N, 30 % 1K^{d}1N, 12 % 2K1N, and 8 % 2K2N. Interestingly, virtually no cells were found in the 2K2N late cytokinesis stage (Figure 1 A). Due to this, further experiments were conducted to investigate whether the fixation protocol could interfere with the cell cycle analysis by breaking the cytoplasmic bridges linking the 2K2N cells in late cytokinesis. In support of this hypothesis, the highest number of cells in late cytokinesis was observed in samples examined directly from culture (Figure 1 B; Figure S1.1). In these samples, on average, 13.8 % of the cells were in late cytokinesis. After harvesting, this proportion dropped to 1.2 % (when centrifuging at 1400 x *g*, 10 min) and 1.5 % (when centrifuging at 750 x *g*, 10 min). After harvesting (1400 x *g*, 10 min), the subsequent washing procedures only slightly affected the late cytokinesis stage, with the incidence falling to 1 % (2000 x *g*, 90 s) and 1.1 % (750 x *g*, 2 min). Harvested (1400 x *g*, 10 min) and washed (2000 x *g*, 90 s) cells were fixed, and washed once more, and the occurrence of the late cytokinesis stages decreased to 0.5 % (2000 x *g*, 90 s) and 0.2 % (500 x *g*, 5 min) (Figure 1 B). Thus, the centrifugal forces imposed on trypanosomes, especially during harvesting from culture, affected the accuracy of cell cycle analysis. The breakage of the cytoplasmic bridges potentially caused a decrease in the number of 2K2N cells while inflating the number of 1K1N cells. Because cell harvesting via centrifugation is a common and necessary step for any cell biology method, it is essential to acknowledge that cell cycle analyses of trypanosomes grown *in vitro* are subjected to this potential bias. This becomes particularly important when applying the ergodic analysis to estimate the time of progression through the cell cycle (Wheeler, 2015).

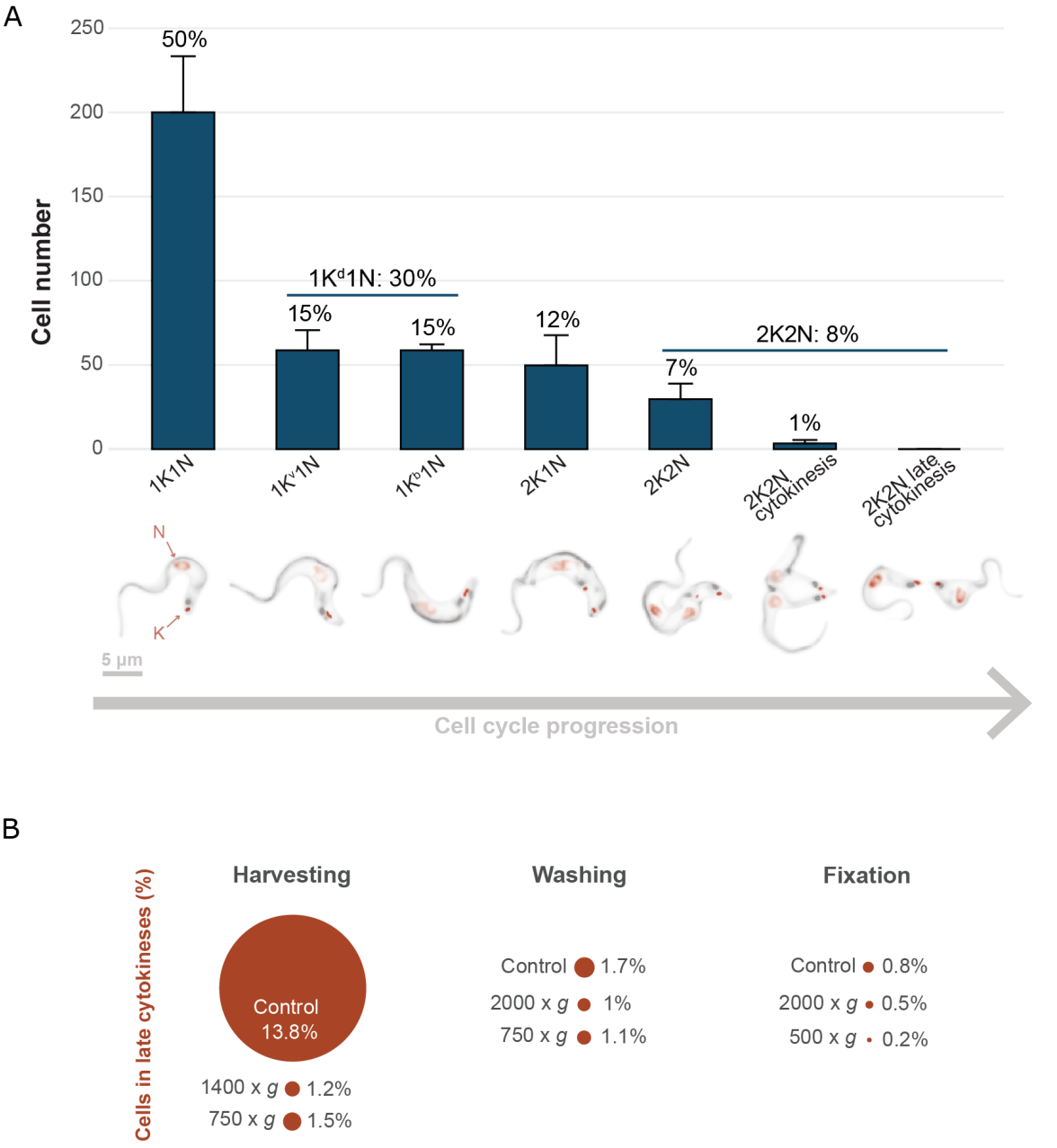

Figure 1. The cell cycle analysis of fixed *Trypanosoma brucei* bloodstream forms is impacted by centrifugal forces. (A) The cell cycle analysis of fixed *T. brucei* bloodstream forms. Half of the population were in the 1K1N stage, while virtually no cells were observed in late cytokinesis. Trypanosomes were harvested from culture, stained with a sulfo-NHS dye, and mounted on coverslips with mounting media containing DAPI for visualization of the nucleus (N) and the kinetoplast (K). The bar plot is presented in the same order of the cell cycle progression, and the percentage of cells in each cell cycle stage is displayed (N = 400, 3 replicates). Exemplary images of each one of the seven cell cycle stages named in the bar plot are presented underneath in the same order. (B) The centrifugal forces imposed on trypanosomes during harvesting, washing, and fixation decrease the number of cells in late cytokinesis in the population. Venn diagrams illustrate the ratio of cells in late cytokinesis (in comparison to the total number of cells) found for each tested condition. The circle size is proportional to the average percentage of late cytokinesis stages. The differential counting of cell stages (single cells *vs.* late cytokinesis stages) was performed using a Neubauer chamber, and a total of 150 stages were counted per assay. A minimum of 10 replicates were performed. The control groups of harvesting, washing, and fixation represent, respectively: cells counted directly from culture; cells harvested (1400 x *g*) and counted; cells harvested (1400 x *g*, 10 min), washed (2000 x *g*, 90 s), fixed and counted without washing to remove the fixative. The tested accelerations are presented below the control for each group.

3.2 The cell surface area of replicating *T. brucei* cells continuously grows during the cell cycle

Having established the proportions of the different cell cycle stages in cultures of *T. brucei* bloodstream forms, the next step was to investigate the changes in the parasite's cell surface area while the cell prepares to divide into two daughter cells. To achieve this, surface area measurements were taken from 322 fixed cells lying perfectly aligned with the x-y plane (i.e., with the complete cell body in focus using one z slice).

The cell surface area of bloodstream forms increased according to the progression of the cell cycle (Figure 2 A), showing significant differences between all cell cycle stages (Figure 2 B). On average, 1K1N cells (N = 129) had 49.8 ± 4.8 μm^2, which increased to 57.0 ± 4.3 μm^2 in $1K^d1N$ (N = 89), to 65.9 ± 6.3 μm^2 in 2K1N (N = 61), and achieved the maximum of 71.1 ± 8.0 μm^2 during 2K2N phase (N = 43) (Figure 2 B). This suggests a continuous increase in the cell surface throughout the cell cycle, which agrees with volumetric measurements obtained via FIB-SEM (Hughes et al., 2017).

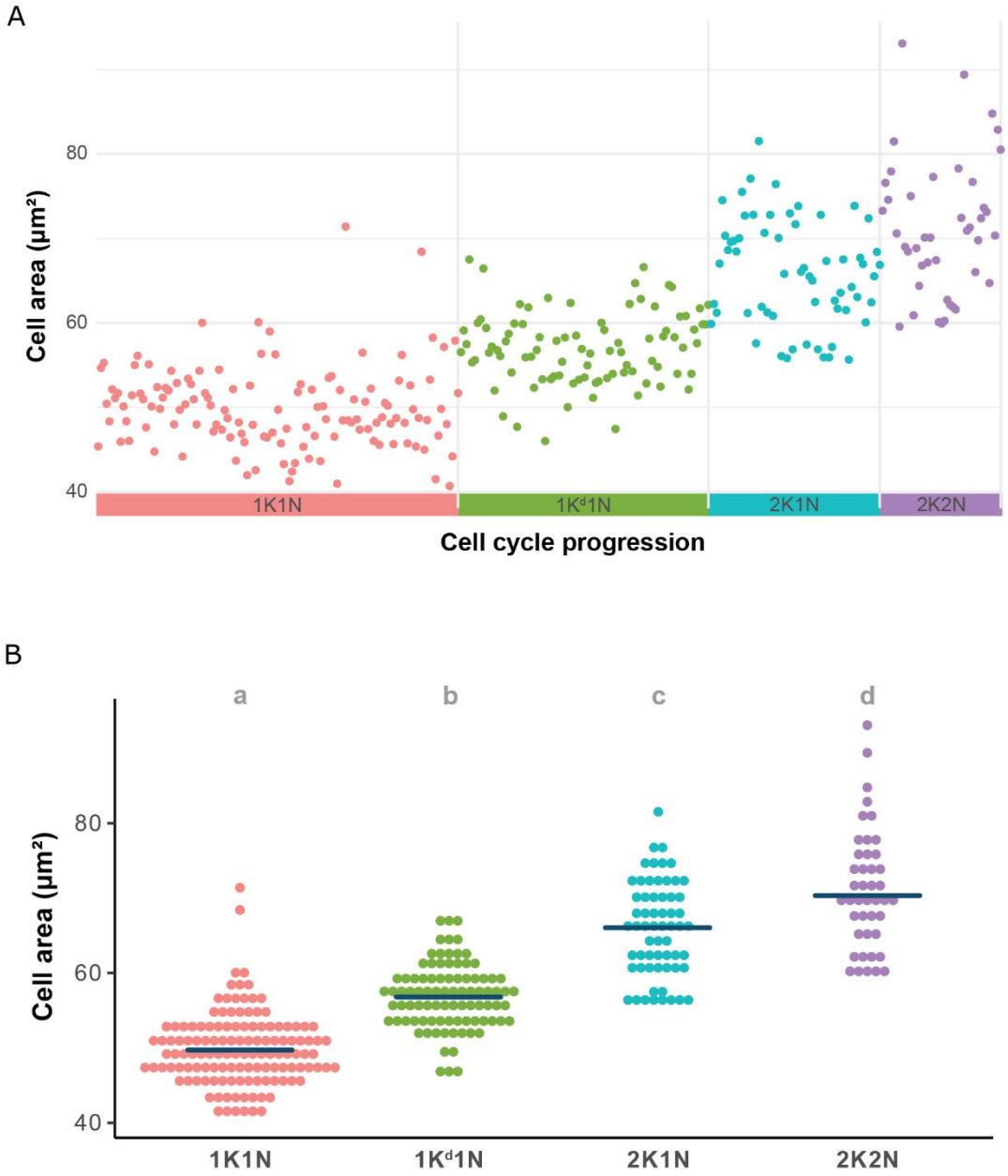

Figure 2. The cell surface area of replicating *Trypanosoma brucei* cells continuously grows during the cell cycle. (A) The cell surface area of *T. brucei* bloodstream forms increases according to the progression of the cell cycle. Trypanosomes were harvested from *in vitro* culture, stained with a sulfo-NHS dye, chemically fixed, and mounted on coverslips with mounting medium containing DAPI. The scatter plot shows the cell surface area measurements (μm^2) of single cells classified according to their cell cycle stage (1K1N = pink; $1K^d1N$ = green; 2K1N = blue; 2K2N = lilac). Each dot represents measurements from one cell. Data is randomly distributed inside each progressive cell cycle stage. (B) The cell surface area of *T. brucei* significantly increases at each stage of the cell cycle. The dot plot shows the area (μm^2) of *T. brucei* cells grouped according to distinct cell cycle stages (1K1N = pink, $1K^d1N$ = green, 2K1N = blue, 2K2N = lilac). Each dot represents measurements from one cell, and dark blue bars represent the median (1K1N = 49.7 μm^2; $1K^d1N$ = 56.8 μm^2; 2K1N = 66.1 μm^2; 2K2N = 70.3 μm^2). Differences in the cell surface area among the cell cycle stages were evaluated using a one-way ANOVA with Tukey's range test as the *post hoc* analysis. Groups with different letters (a/b/c/d) are significantly different from each other. The area measurements were taken from 322 cells in 3 independent experiments.

3.3 The endosomes duplicate early during the *T. brucei* cell cycle

During the cell cycle, the surface area of *T. brucei* increases, achieving its maximum in the 2K2N stage (see Figure 2 B). For such an enlargement, it is necessary to increase the plasma membrane area and, consequently, the number of VSG molecules covering the cell surface. Such increased demand for VSG likely has two impacts: a boost in VSG production and a higher load on the endosomal system. The effect on the endosomes, not classically part of the biosynthetic/secretory pathway, can be assumed due to the high rates of VSG endocytosis and recycling observed in trypanosomes (Engstler et al., 2004; Grünfelder et al., 2003; Link et al., 2021). In addition, plasma membrane growth is impacted by the relative rates of endo- and exocytosis (Boucrot and Kirchhausen, 2007; Haucke and Kozlov, 2018; McCusker and Kellogg, 2012). Thus, to probe whether changes in the cell surface area are connected to the endosomes, the duplication of these organelles was investigated.

Bloodstream forms of *T. brucei* expressing the procyclin isoform EP1 tagged with GFP (EP1::GFP) (Günzel, 2010) were used for the visualization of the endosomes. Because EP1 is a procyclin, it is not trafficked to the cell surface of bloodstream forms (reviewed in Borges et al., 2021) making this a suitable marker of the parasite's endosomes (Engstler and Boshart, 2004). EP1::GFP was previously shown to overlap with biotinylated VSG, and the fluid-phase marker dextran in the bloodstream forms of *T. brucei* (Engstler and Boshart, 2004; Günzel, 2010). A total of 212 fixed cells were measured and manually grouped according to the cell cycle stage they were in.

The endosomal compartments were localized in the posterior region of the cell in all cell cycle stages analyzed and extended from the kinetoplast to the nucleus (Figure 3 A). During kinetoplast division ($1K^d1N$), and especially in cells with marked bilobed kinetoplasts, it was possible to see a new punctate signal appearing close to the kinetoplast disk positioned nearer to the posterior pole of the cell (Figure 3 A, arrowhead). Progressively, this point-like signal increased in size and extended toward the nucleus.

After the nuclear division (2K2N cells), the two endosomal systems occupied two distinct cytoplasmic regions: one belonging to the old-flagellum daughter and another corresponding to the new-flagellum daughter (Figure 3 A). On average, the endosomal area of 1K1N cells (N = 87) was 1.20 ± 0.48 μm^2 and slightly bigger in $1K^d1N$ cells (N = 71) 1.37 ± 0.53 μm^2. After kinetoplast duplication, the area of the endosomes increased to 1.90 ± 0.65 μm^2 in 2K1N (N = 28) and 2.08 ± 0.66 μm^2 in 2K2N cells (N = 26) (Figure 3 B). Although the endosome started growing in $1K^d1N$ (with the appearance of the new dot-like signal), a pronounced growth (~58 % increase) was observed only in 2K1N cells. The latter showed an endosomal area significantly different from 1K1N and $1K^d1N$ cells but not from the 2K2N stage (Figure 3 C). Thus, the results indicate that the new endosome of *T. brucei* is formed early during the cell cycle. Although the appearance of a dot-like signal close to one of the kinetoplast disks suggests a *de novo* formation, additional experiments using different methods would be required to corroborate this, such as time-lapse microscopy. Of note, the new endosome was formed close to the posterior extremity of the cell, which corresponds to the cytoplasmic region of the new-flagellum daughter.

The majority of endosomal growth is observed after the kinetoplast division. After its formation in the $1K^d1N$ stage, the endosome significantly increases in size (2K1N), and continues expanding to nearly double its initial size in the last stage of the cell division cycle (2K2N). The endosomal expansion accompanies the growth of the cell surface area, starting in $1K^d1N$ and continuing to the last stage of the cell cycle. However, the dynamics underlying their expansion differ. While the endosome undergoes a pronounced increase in 2K1N, the cell surface area shows a progressive increase at each cell cycle stage. Thus, the duplication of the endosomal system seems to be a crucial step related to plasma membrane growth.

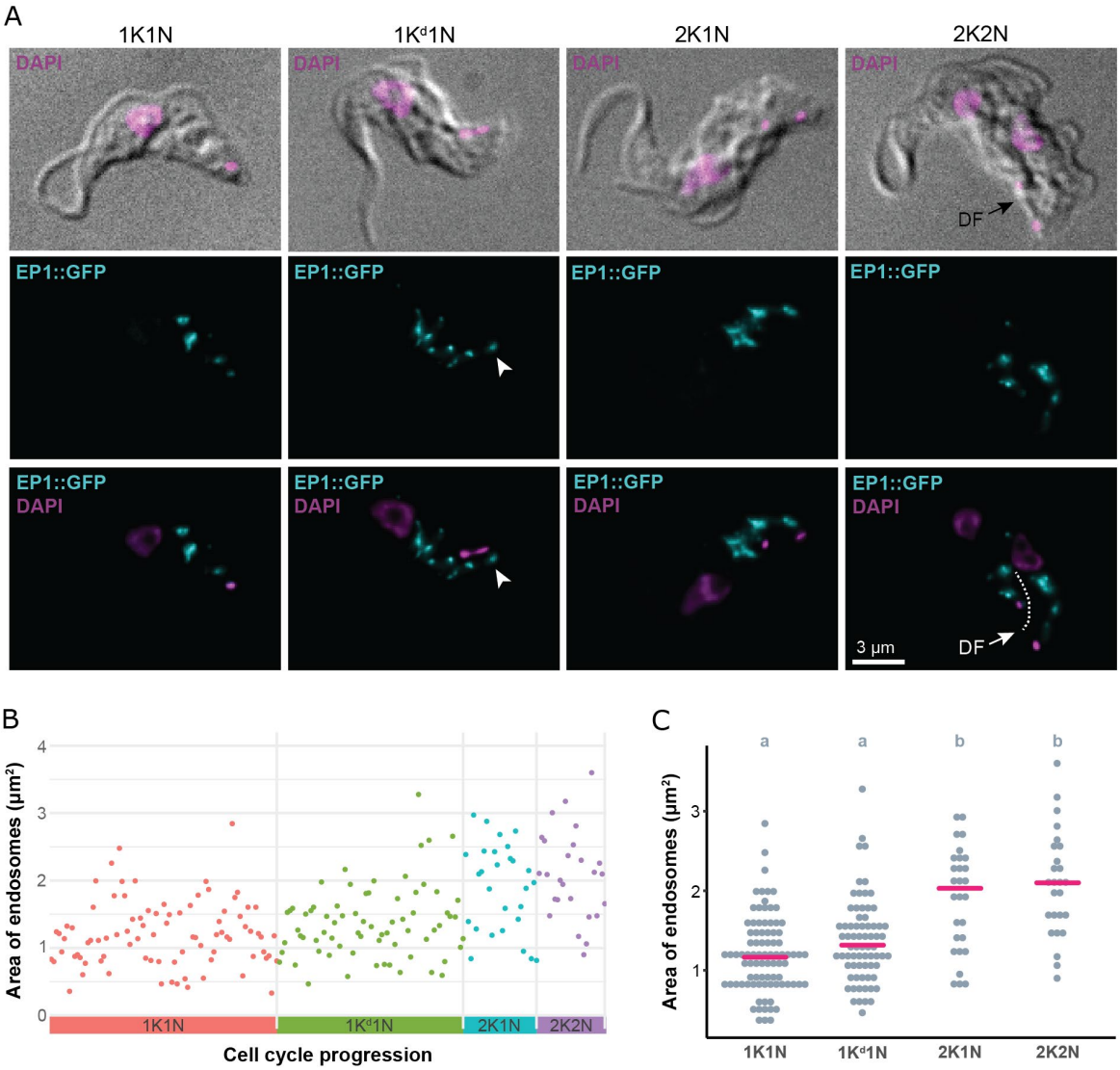

Figure 3. The endosomes duplicate early during the *Trypanosoma brucei* cell cycle. (A) The endosomes, marked by EP1::GFP (cyan), span from the kinetoplast to the nucleus in all cell cycle stages. In 1K^{d}1N cells, a new punctate signal (arrowhead) appears close to the kinetoplast disk nearer to the cell's posterior end, suggesting a *de novo* formation during kinetoplast division. The newly formed endosomal system continues to increase, extending toward the nucleus. During cytokinesis (indicated by the division fold: arrow, DF), both endosomal systems are arranged in the cytoplasmic regions of the old-flagellum daughter and the new-flagellum daughter. (B) The area of *T. brucei* endosomes enlarges after kinetoplast duplication. The scatter plot depicts the area (µm^2) of EP1::GFP signal used as the endosomal marker. Data were obtained from single cells and classified according to their cell cycle stage (1K1N = pink; 1K^{d}1N = green; 2K1N = blue; 2K2N = lilac). Each dot represents measurements from one cell. Data is randomly distributed inside each progressive cell cycle stage. (C) The area of the endosomes significantly increases after kinetoplast division. The dot plot shows the area (µm^2) of EP1::GFP signal used as the endosomal marker. Data were classified according to the cell cycle stage. Each dot represents measurements from one cell, and pink bars represent the median (1K1N = 1.16 µm^2; 1K^{d}1N = 1.32 µm^2; 2K1N = 2.03 µm^2; 2K2N = 2.09 µm^2). Differences in the area of the endosome-associated signal (EP1::GFP) among the cell cycle stages were evaluated using a one-way ANOVA with Tukey's range test as the *post hoc* analysis. Groups with different letters (a/b) are significantly different from each other. The total area measurements were obtained from 212 cells (1K1N = 87; 1K^{d}1N = 71; 2K1N = 28; 2K2N = 26) in 2 independent experiments.

3.4 Clathrin vesicles are recruited to both flagellar pockets during the cell cycle

The early duplication of the endosomes in the cytoplasmic region of the new-flagellum daughter during the kinetoplast division and its expansion in 2K1N cells seemed to coincide with alterations in the cell surface area. It is possible that the plasma membrane increase results from an imbalance between endo- and exocytosis. By maintaining the endocytosis rate while increasing exocytosis, the cell enables plasma membrane growth via the “excess” of fused membrane. Considering that all endocytosis of *T. brucei* is clathrin-mediated (Engstler et al., 2004; Grünfelder et al., 2003; Link et al., 2021; Morgan et al., 2001), the recruitment of clathrin molecules was investigated to check for endocytic activity during the division of *T. brucei*. To assess this, the area of the clathrin-associated signal was measured in 92 fixed cells expressing a YFP tagged clathrin light chain. After the analysis, cells were manually grouped according to the cell cycle stage.

Clathrin was found between the nucleus and the kinetoplast of all cell cycle stages (Figure 4 A). Clathrin recruitment showed a marginal increase during the cell cycle, going from 1.1 ± 0.3 μm^2 in 1K1N cells (N = 51) to 1.2 ± 0.4 μm^2 in $1K^d1N$ (N = 26) and 1.5 ± 0.4 μm^2 in 2K1N (N = 9). Intriguingly, 2K2N cells (N = 6) showed a smaller clathrin area of 1.3 ± 0.4 μm^2 (Figure 4 B). The largest clathrin-associated signal area was observed in 2K1N cells, which exhibited a significant difference to the area found in 1K1N cells (Figure 4 C).

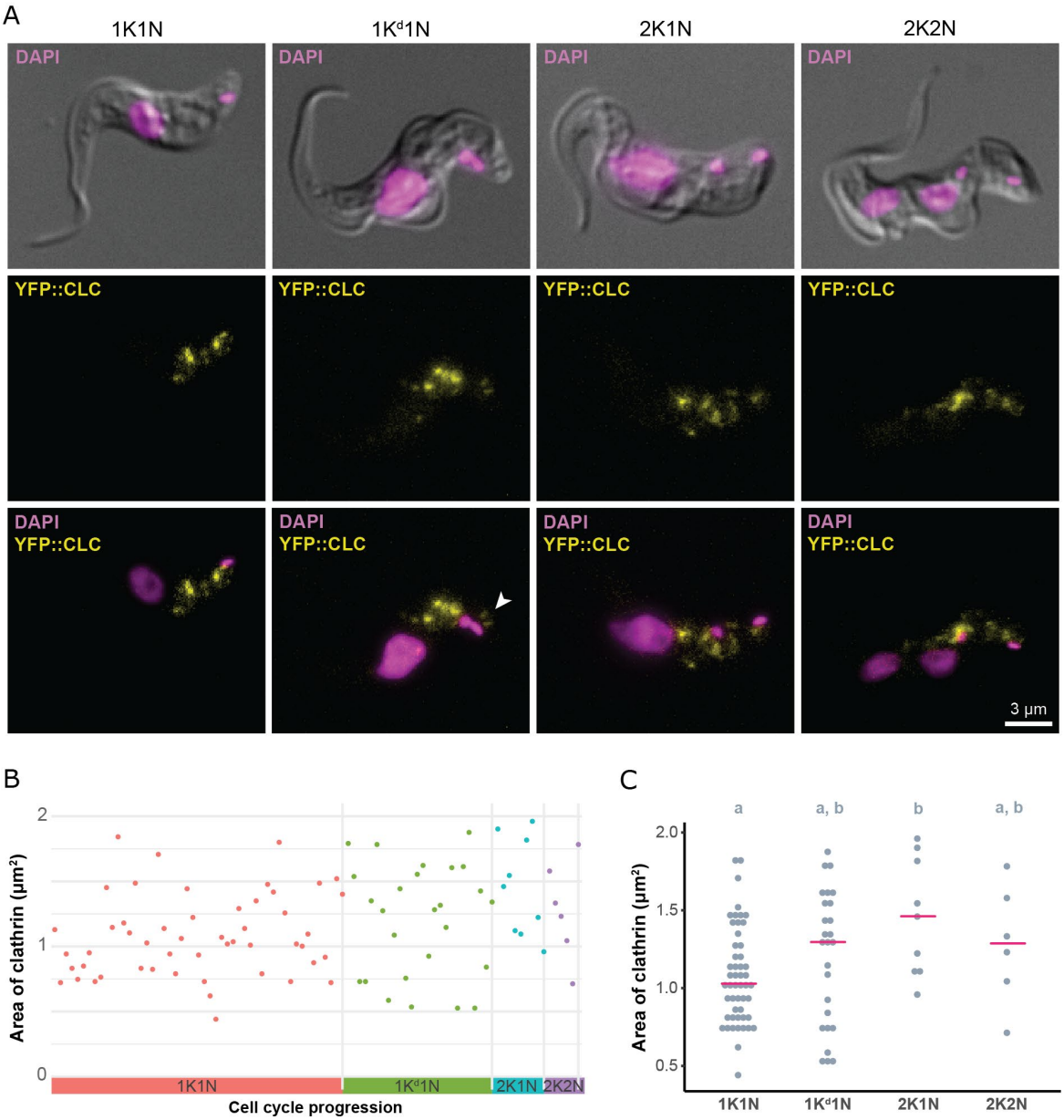

Figure 4. Clathrin recruitment increases after kinetoplast duplication. (A) Clathrin (YFP::CLC) was observed in the posterior region of *T. brucei* cells – between the nucleus and the kinetoplast – in all cell cycle stages. In 1K^{d}1N cells, clathrin was also observed in proximity to the kinetoplast disks close to the posterior end of the body (arrowhead). This signal persisted in 2K1N and 2K2N cells. (B) The area of clathrin marginally increased during the cell cycle. The scatter plot depicts the area (µm^2) of the clathrin-associated signal (YFP::CLC) obtained from single cells and classified according to the cell cycle stage of the respective cell (1K1N = pink; 1K^{d}1N = green; 2K1N = blue; 2K2N = lilac). Each dot represents measurements from one cell. Data is randomly distributed inside each progressive cell cycle stage. (C) The highest clathrin recruitment is observed in 2K1N cells. The dot plot shows the area (µm^2) of the clathrin-associated signal (YFP::CLC) classified according to each cell cycle stage. Each dot represents measurements from one cell, and pink bars represent the median (1K1N = 1.03 µm^2; 1K^{d}1N = 1.30 µm^2; 2K1N = 1.46 µm^2; 2K2N = 1.28 µm^2). Differences in the area of the clathrin-associated signal (YFP::CLC) among the cell cycle stages were evaluated using a one-way ANOVA with Tukey's range test as the *post hoc* analysis. Groups with different letters (a/b) are significantly different from each other. The total area measurements were obtained from 92 cells (1K1N = 51; 1K^{d}1N = 26; 2K1N = 9; 2K2N = 6) in 2 independent experiments.

Fluorescence microscopy showed the clathrin signal spanning from the kinetoplast to the nucleus in all cell cycle stages. To visualize clathrin recruitment in more detail, transmission electron microscopy was performed in high-pressure frozen cells. The recruitment of clathrin to the flagellar pocket was evidenced by the formation of membrane invaginations (CCPs) (Figure 5 A). The pits eventually pinch off yielding CCVs (Grünfelder et al., 2003; Link et al., 2021; Morgan et al., 2001), which were observed in the vicinities of the flagellar pocket (Figure 5 A-C) and endosomes (Figure 5 A, D). The CCVs pinching from the flagellar pocket are known as class I CCVs, while those budding from the endosomes are named class II CCVs (Engstler et al., 2004).

In $1K^{d}1N$ cells, especially the ones showing an advanced stage of kinetoplast duplication ($1K^{b}1N$), the presence of clathrin molecules next to both kinetoplast disks was noted (see Figure 4 A). This observation suggested that both flagellar pockets carry out endocytosis in dividing *T. brucei* cells. To examine this possible activity, correlative light and electron microscopy of high-pressure frozen cells was performed. The method allowed the visualization of CCPs and CCVs in the proximity of the flagellar pockets (Figure 6 A, Ai, B, Bi). In cells with two flagellar pockets, CCVs could be observed in the proximity of both (Figure 6 B, Bi), suggesting endocytic activity in both pockets during *T. brucei* division.

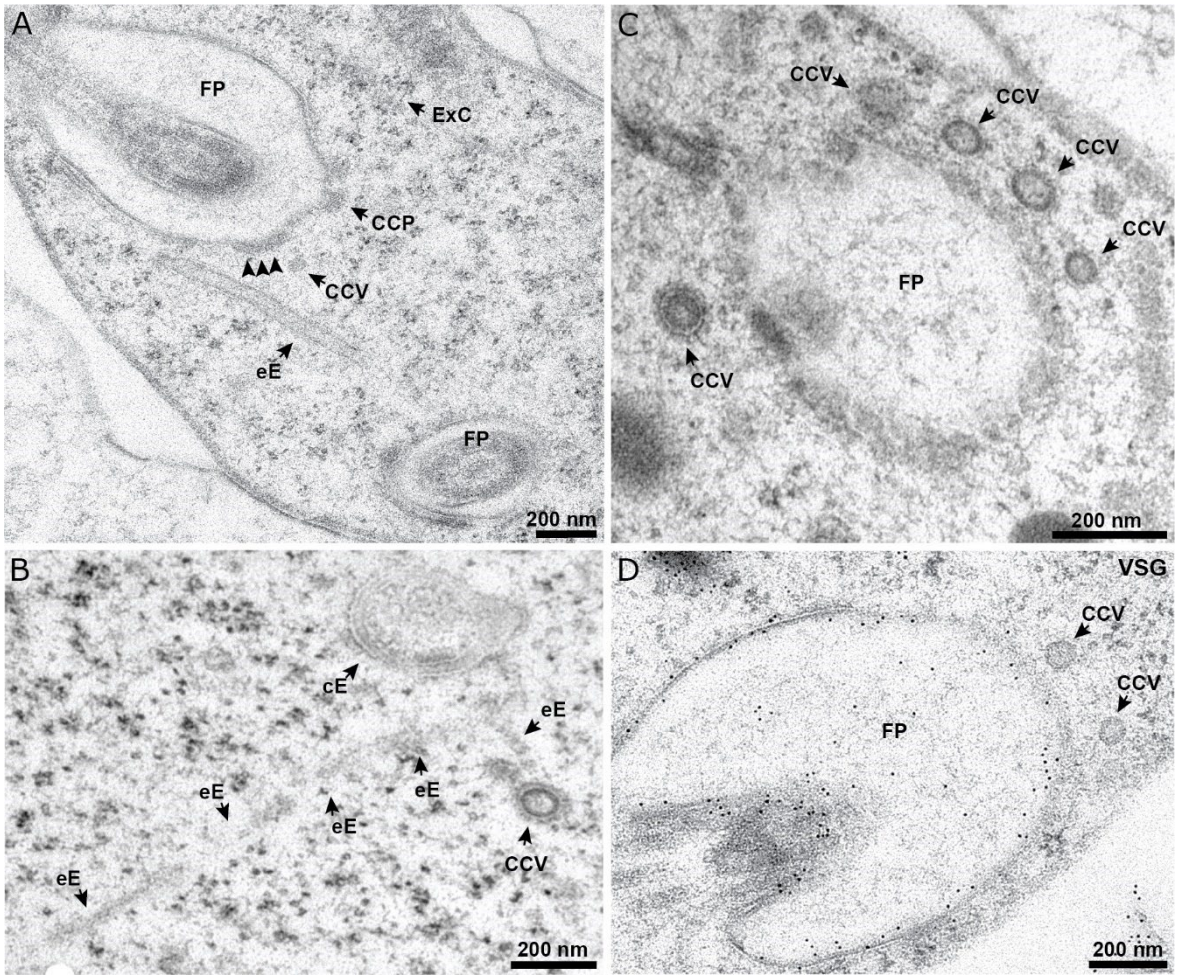

Figure 5. Transmission electron microscopy displaying clathrin recruitment. (A) Clathrin is recruited to the flagellar pocket leading to the formation of clathrin-coated pits and vesicles. Arrowheads point to a region with clathrin recruitment in the flagellar pocket membrane. In the vicinities, a clathrin-coated vesicle is also observed, as well as an elongated endosomal cisterna. (B) Clathrin-coated vesicles surrounding a flagellar pocket. (C) Clathrin-coated vesicles close to the flagellar pocket transporting non-VSG cargo. Immunogold labeled VSG (6-nm gold), which is observed in the flagellar pocket membrane but not inside the clathrin-coated vesicles nearby, suggesting that these vesicles are actively transporting other types of cargo. (D) A clathrin-coated vesicle is observed in the vicinity of elongated and circular endosomal cisternae. CCP: clathrin-coated pit; CCV: clathrin-coated vesicle; cE: circular endosome; eE: elongated endosome; FP: flagellar pocket.

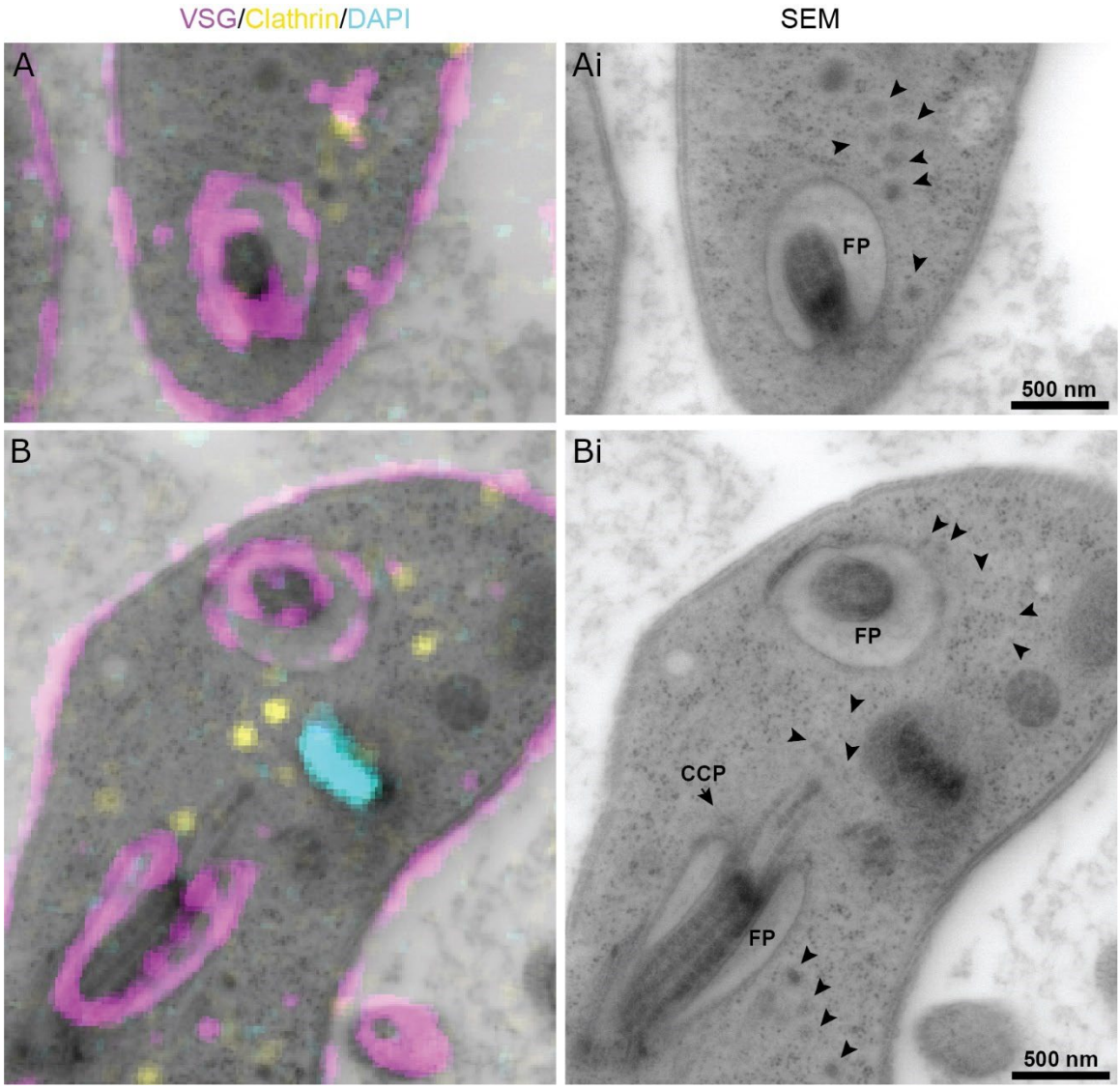

Figure 6. Correlative light and electron microscopy shows the formation of clathrin-coated pits and vesicles. High-pressure frozen *T. brucei* cells were embedded in LR-White and sectioned (100 nm). Sections were used for immunofluorescence assays and imaged via structured illumination microscopy. After imaging, sections were contrasted for electron microscopy and imaged in a scanning electron microscope. The fluorescence images and electron microscopy mosaics were manually correlated, using DAPI (nucleic acids) and VSG (cell surface) as fiducials. (A, Ai) Clathrin-coated vesicles (arrowheads) in the proximity of the flagellar pocket. (B, Bi) Cell with endocytic activities in both flagellar pockets during division. The formation of a clathrin-coated pit and the presence of clathrin-coated vesicles (arrowheads) in the proximity of both flagellar pockets are evidenced. CCP: clathrin-coated pit; FP: flagellar pocket.

Overall, clathrin recruitment showed a marginal increase during the cell cycle with evidence of recruitment to both flagellar pockets. The moderate increase in clathrin recruitment seemed to coincide with the duplication of the flagellar pocket and the endosomes, starting in the $1K^{d}1N$ stage and achieving its highest value in 2K1N cells. This suggests the endocytic activity of the newly formed endosomal system, which could be necessary for the maintenance of VSG coat integrity during growth of the cell surface.

Nevertheless, it is important to note that the changes in clathrin recruitment were discrete, pointing to a balanced ratio of endocytosis during the cell cycle. This supports the idea of plasma membrane growth via imbalance in endo- and exocytosis.

3.5 The subpopulations of *T. brucei* endosomes function as distinct compartments

The duplication and expansion of the endosomes, the marginal increase in clathrin recruitment, and the suggested endocytic activity of both flagellar pockets during *T. brucei* division, advocate coordination between endocytosis and cell surface expansion. Because VSG recycling is critical for trypanosomes and its endosomal transport is well-described (Engstler et al., 2004; Grünfelder et al., 2003; Link et al., 2021), immunogold assays on ultrathin sections of high-pressure frozen cells were used to visualize the VSG and the endosomal system components. Besides the plasma membrane and the flagellar pocket, VSG-gold (6 and 12 nm) was visualized inside vesicles near the flagellar pocket and endosomal cisternae (Figure 7 A-C). These cisternae showed diverse morphologies, including circular, elongated, and irregular shapes (Figure 7 B-E). In addition, exocytic carriers filled with VSG were also observed (Figure 7 D).

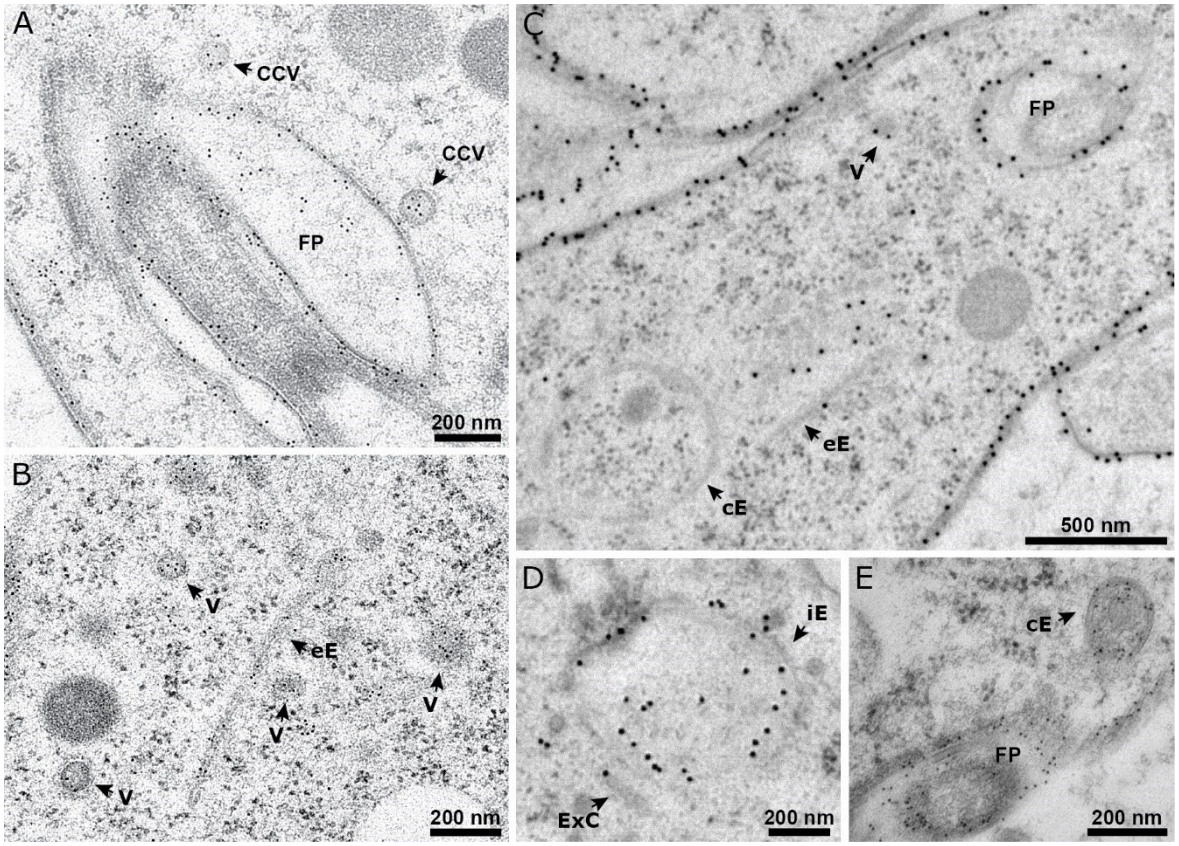

Figure 7. Transmission electron microscopy emphasizing VSG recycling pathway. (A) VSG inside clathrin-coated vesicles near the flagellar pocket. (B) Elongated endosomal compartment surrounded with vesicles filled with VSG. (C) VSG on the trypanosome cell surface, and in the flagellar pocket, endocytic vesicles, and elongated endosomal cisternae. (D) VSG inside an irregularly shaped endosome and an exocytic carrier. (E) VSG in the flagellar pocket and circular endosomal compartment. (A-B): VSG labeled with 6 nm gold; (C-E): VSG labeled with 12 nm gold. CCV: clathrin-coated vesicle; cE: circular endosomal cisternae; eE: elongated endosomal cisternae; iE: irregular-shaped endosomal cisternae; ExC: exocytic carrier; FP: flagellar pocket; V: vesicle.

Such a morphological variety of the endosomes has been recorded in the literature and is generally attributed to distinct endosomal subpopulations. These subpopulations are known to be decorated with Rab GTPases named TbRab5A (early endosomes), TbRab7 (late endosomes), and TbRab11 (recycling endosomes) (Engstler et al., 2004; Hall et al., 2005, 2004a; Link et al., 2021; Silverman et al., 2011). The marker TbRab5A was primarily observed on circular and elongated endosomal cisternae, TbRab7 on irregular structures (Engstler et al., 2004), and TbRab11 on elongated cisternae and disk-shaped carriers (Grünfelder et al., 2003). All three TbRab markers have been reported on vesicular structures (Engstler et al., 2004; Grünfelder et al., 2003). Although the role of the different

endosomal subpopulations in VSG recycling is well-documented (Engstler et al., 2004), in-depth colocalization studies with other physiological cargo are still sparse.

Ferritin is not synthesized by trypanosomes (Carbajo et al., 2021) but is internalized and likely digested in the lysosome (Engstler et al., 2004; Langreth and Balber, 1975). Therefore, uptake of ferritin can serve as a fluid-phase marker. The ferritin pathway in *T. brucei* has been described based on the morphological analysis of the endosomal system components using electron microscopy. In these studies, ferritin was observed in CCVs and in the lumen of endosome cisternae (Engstler et al., 2004; Langreth and Balber, 1975). Based on the morphology of these cisternae, the pathway was postulated as passage through early and late endosomes followed by degradation in the lysosome. Because ferritin was assumed to be degraded in the lysosome, it was not expected to be found in the recycling compartments. In fact, ferritin was never observed in the lumen of exocytic carriers (Engstler et al., 2004). Although well-documented through electron microscopy studies, the colocalization of ferritin and endosomal markers is still missing. Thus, in order to explore the role of the endosomal subpopulations in the transport of fluid-phase cargo, the ferritin pathway was revisited.

Bloodstream forms of *T. brucei* 1390 were incubated with ferritin labeled with Atto 647 for 15 min. Then, cells were fixed and used in triple-labeling immunofluorescence experiments with antibodies against TbRab5A, TbRab7, and TbRab11. A total of 100 cells were analyzed, and the intensity-based colocalization was determined. All internalized ferritin was in the posterior region of the cell, showing a strong correlation with TbRab5A ($r = 0.89$), moderate with TbRab7 ($r = 0.41$), and weak with TbRab11 ($r = 0.20$) (Figure 8 A-C). The weak colocalization with TbRab11 points to ferritin degradation by the parasite, while the overlap with TbRab5A and TbRab7 demonstrates their involvement in ferritin transport. The highest overlap observed with TbRab5A can either suggest a slower passage through the early endosomes or a possible cargo overload. The overload would impose challenges for lysosomal degradation and could lead to the accumulation of cargo

in the early endosomes. However, an investigation of the kinetics of ferritin endocytosis would be necessary to test the above mentioned hypotheses.

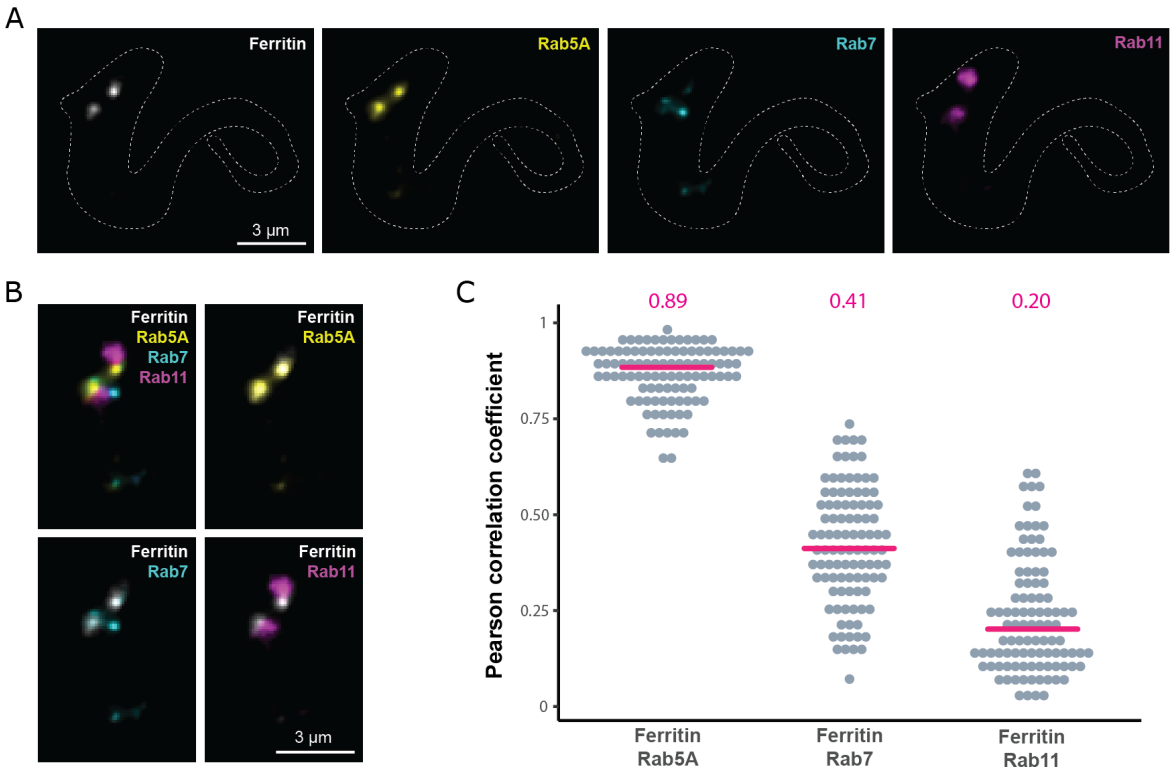

Figure 8. The TbRab markers define endosomal regions with distinct functions. (A) Ferritin and TbRab markers localize in the posterior region of fixed bloodstream forms of *T. brucei*. The subcellular localization of ferritin (white), TbRab5A (yellow), TbRab7 (cyan), and TbRab11 (magenta) is shown in an exemplary cell. The cell surface is marked with dashed lines. (B) The endosomal markers TbRab5A, TbRab7, and TbRab11 overlap with ferritin. The superimposed images suggest colocalization of the cargo and the distinct endosomal subpopulations. A small overlap between the TbRab markers can also be visualized. (C) Ferritin presents distinct spatial overlap with endosomal subpopulations. The dot plot shows the colocalization of ferritin and TbRab markers. Each dot represents data from one cell, and pink bars and numbers represent median values. The correlation coefficients indicate a strong colocalization between ferritin and TbRab5A, medium with TbRab7, and weak with TbRab11. The Pearson correlation coefficient was obtained from 100 cells analyzed in 3 independent experiments.

The weak colocalization of ferritin and the recycling compartment marked by TbRab11 was intriguing. Therefore, one additional test was performed to verify that the antibody against TbRab11 was indeed labeling an endosomal compartment. For this, *T. brucei* expressing the endosomal marker EP1::GFP were fixed and used in immunofluorescence experiments with TbRab11 labeling. The colocalization was checked in 221 fixed cells grouped according to their cell cycle stage (Figure 9 A). In all of them, the TbRab11 signal overlayed with the EP1::GFP signal which labels the endosome, whereas

not all EP1::GFP was coincident with TbRab11. Because the endosome is proposed to be subdivided into the subpopulations mentioned previously, this result was expected. A strong correlation ($\rho > 0.7$) between TbRab11 and EP1::GFP was observed across all cell cycle stages (Figure 9 B).

In conclusion, *T. brucei* endosome subpopulations labeled by TbRab5A, TbRab7, and TbRab11 function as distinct compartments during fluid-phase cargo uptake.

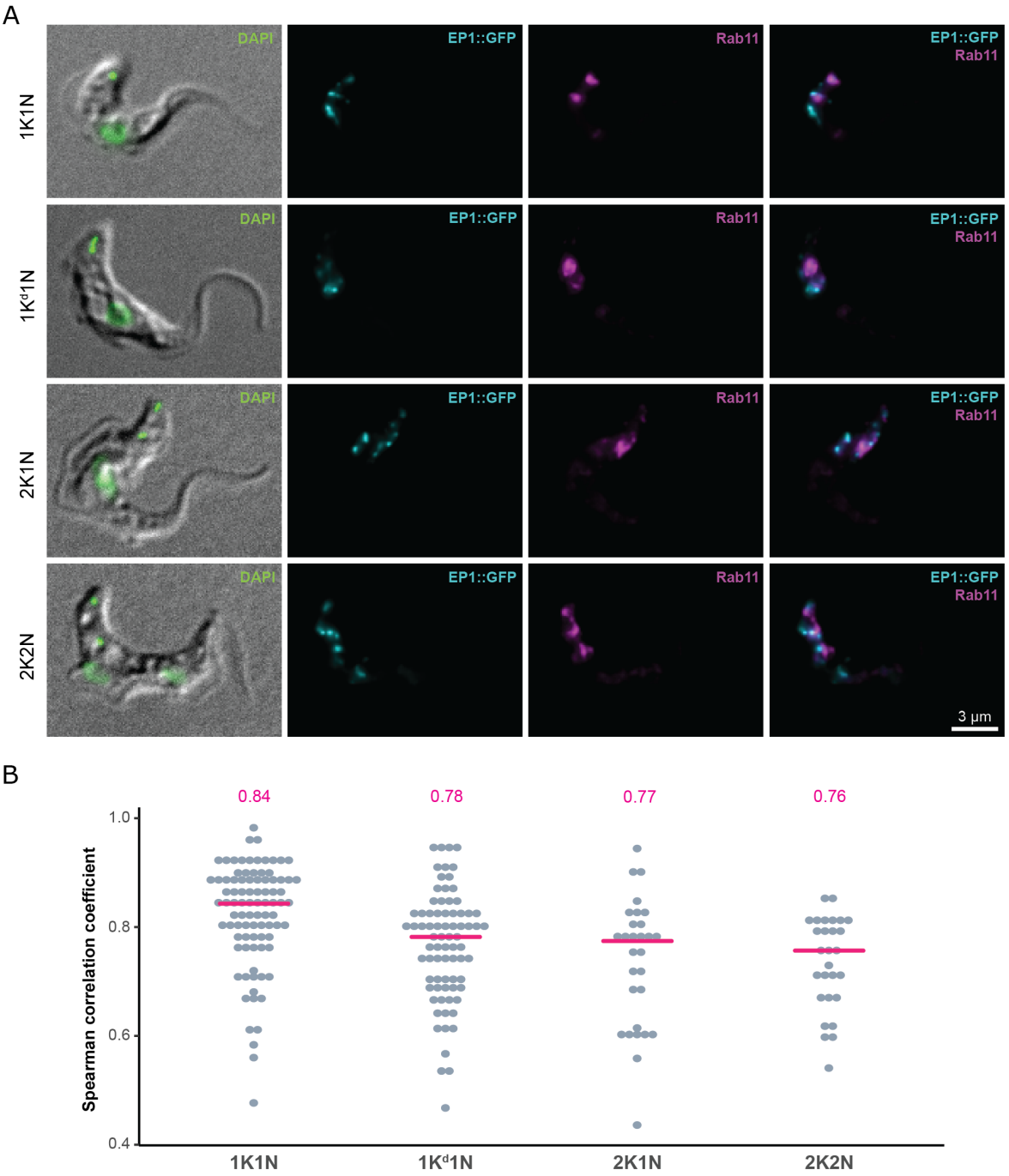

Figure 9. TbRab11 is localized in *Trypanosoma brucei* endosomes. (A) The GTPase TbRab11 (magenta) overlaps with the endosomal marker EP1::GFP (cyan) in fixed cells. The subcellular localization of both markers is shown in different cell cycle stages. Not all endosomal signal (EP1::GFP) coincides with TbRab11, which serves as a marker for the recycling compartment of the endosome. (B) TbRab11 and EP1::GFP strongly colocalize during division. The dot plot depicts the colocalization of EP1::GFP and TbRab11 grouped according to cell cycle stage of the analyzed cells. Each dot represents data from one cell, and pink bars and numbers represent median values. The Spearman's rank correlation was obtained from 221 cells (1K1N = 88; 1K^{d}1N = 76; 2K1N = 29; 2K2N = 28) analyzed in 3 independent experiments.

3.6 The markers of the endosomal subpopulations TbRab5A, TbRab7, and TbRab11 show spatial overlap

The colocalization between ferritin and the endosomal markers TbRab5A, TbRab7, and TbRab11 indicated that the endosomal subpopulations work as distinct functional compartments. This agrees with previous studies showing their subcellular localization and their different roles in endocytosis (Engstler et al., 2004; Hall et al., 2005, 2004a; Morgan et al., 2002, 2001; Silverman et al., 2011). However, it is important to note that the superimposition of fluorescence images also suggested the spatial colocalization of TbRab markers (see Figure 8 B). In addition, a certain co-distribution between ferritin and the recycling compartment was indicated. Thus, to explore this overlap and verify whether it means a possible recycling of ferritin, or the spatial overlap of different endosomal compartments, colocalization analyses between TbRab markers were performed.

Bloodstream forms of *T. brucei* growing in culture were harvested, fixed, and used in immunofluorescence assays. Only 1K1N cells were considered for the quantification to ensure that organelle duplication was not biasing the analysis. A total of 100 cells were analyzed.

All three Rab proteins were found in the posterior region of the cell (Figure 10 A) and seemed to overlap (Figure 10 B). The correlation analysis indicated colocalization between these markers. The strongest correlation was observed between TbRab5A and TbRab7 ($r = 0.77$), followed by TbRab5A and TbRab11 ($r = 0.65$), and TbRab7 and TbRab11 ($r = 0.60$) (Figure 10 C).

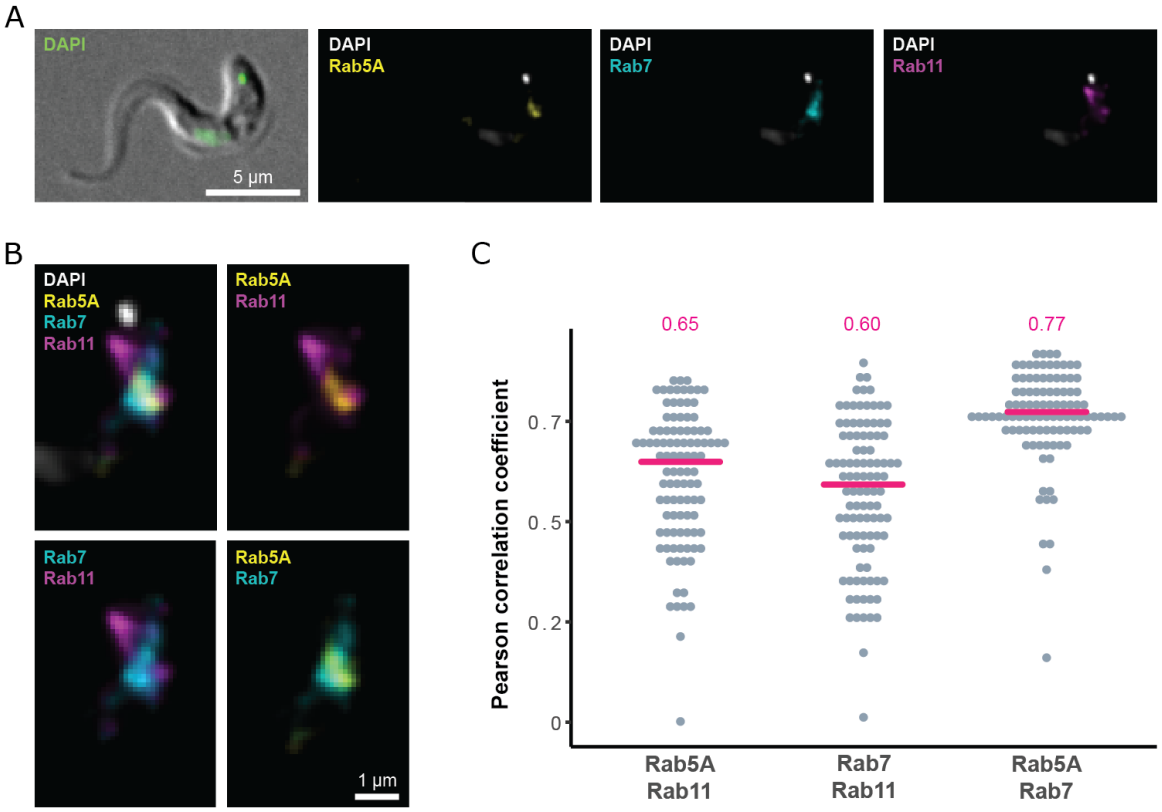

Figure 10. The endosomal subpopulations marked by TbRab5A, TbRab7, and TbRab11 colocalize in the posterior region of the *Trypanosoma brucei* cell. (A) Subcellular localization of TbRab markers in fixed bloodstream forms of *T. brucei*. 1K1N cells were observed with differential interference contrast (DIC) with nucleus and kinetoplast stained with DAPI (green). The endosomal markers TbRab5A (yellow), TbRab7 (cyan), and TbRab11 (magenta) localized between the nucleus and the kinetoplast (white). (B) The superposition of fluorescence images indicates spatial overlap of TbRab markers. The images represent the posterior region of the exemplary cell. (C) Colocalization analysis indicates a strong overlap between TbRab markers. The dot plot shows the correlation coefficient of TbRab markers obtained from single cells. Each dot represents data from one cell, and pink bars and numbers represent the median value. The Pearson correlation coefficient was obtained from a total of 100 cells analyzed in 3 independent experiments.

The high correlation coefficients obtained for all TbRab markers indicate their spatial overlap and proportional co-distribution. However, to measure the extent of this overlap, Manders' colocalization coefficients were measured in images obtained via structural illumination microscopy. All three Rabs were present in the posterior part of the cell (Figure 11 A) and presented overlapping regions with one another (Figure 11 B-C). The TbRab5A signal showed a virtually equal overlap with TbRab11 (27 %) and TbRab7 (26.2 %). On the other hand, approximately half of the TbRab7 signal overlapped with TbRab5A (47.6 %), while a smaller portion colocalized with TbRab11 (30.7 %). Similarly, TbRab11 showed higher colocalization with TbRab5A (19.5 %) when compared to its overlap ratio with

TbRab7 (9.1 %) (Figure 11 D). Overall, the lowest overlap was observed between TbRab11 and TbRab7 and the highest between TbRab7 and TbRab5A (Figure 11 D). Altogether, the colocalization results from super-resolved images suggest the simultaneous presence of the three Rab markers in the same structures. The overlap ratios are variable in the population (Supplementary Figure S1.2). In order to visualize these structures, attempts to employ immunogold labeling in ultrathin sections and correlative light and electron microscopy were performed. However, the results were not satisfactory due to inefficient antibody binding in immunogold labeling and the presence of potential artifacts in immunofluorescence experiments (Supplementary Figure S1.3).

Altogether, both high- and super-resolution microscopy suggest that *T. brucei* endosome subpopulations may have a physical connection instead of being composed of isolated and distinct vesicular/tubular compartments.

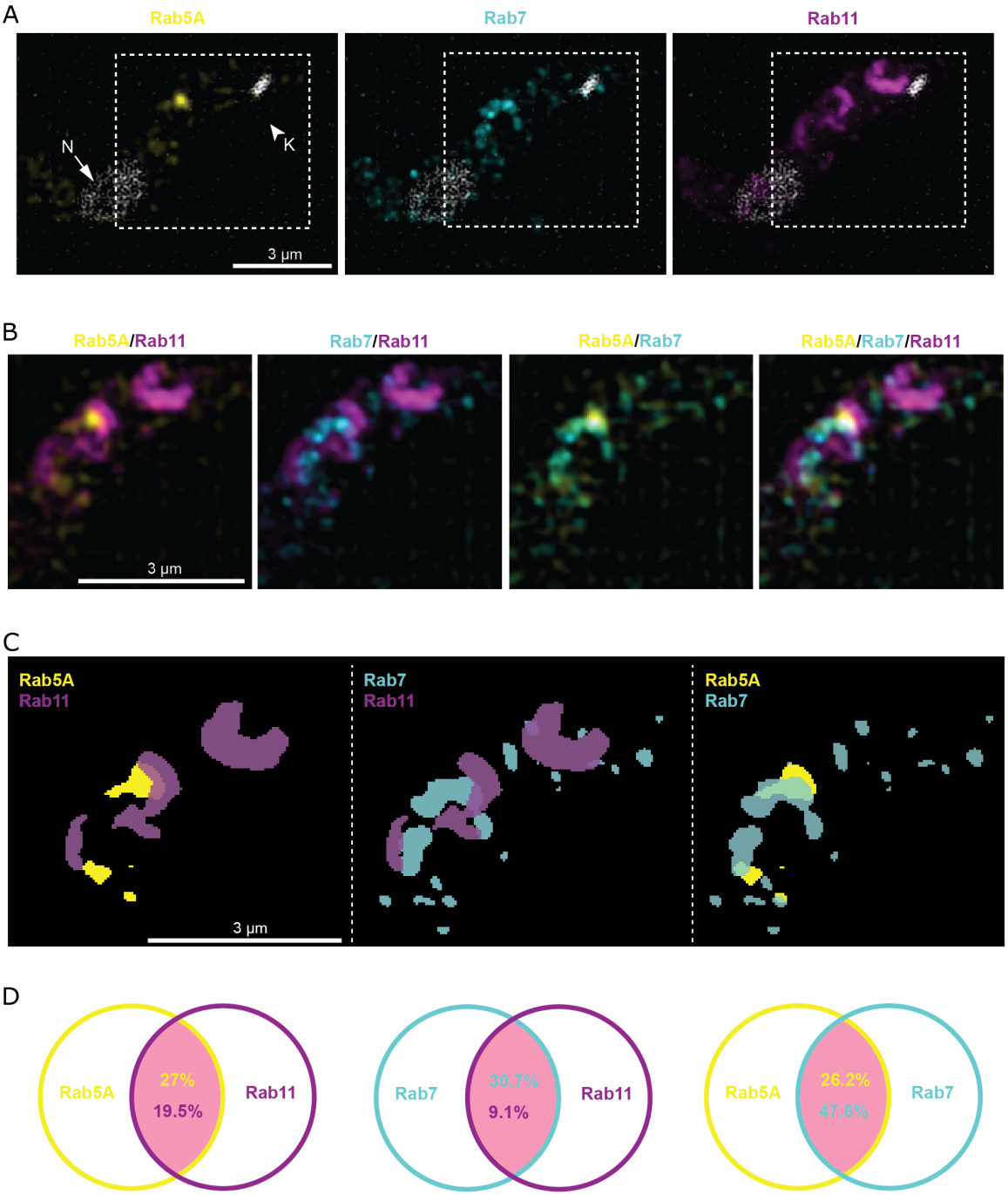

Figure 11. Structured illumination microscopy supports the presence of TbRab markers in the same structure (A) Subcellular localization of TbRab5A (yellow), TbRab7 (cyan), and TbRab11 (magenta) in the posterior region of a fixed cell. The dotted square indicates the region of interest (ROI) used in the colocalization analysis. (B) Enlarged image of the ROI showing the superposition of fluorescence channels. (C) Binary masks were generated for the colocalization analysis. Exemplary images show superimposed binary masks to emphasize the regions of overlap. (D) Venn diagram illustrating the overlap between the different TbRab markers. The fraction of co-occurrence was estimated using Manders' colocalization coefficients. The percentages are the median values of the colocalization coefficients (N = 31, 2 replicates).

3.7 The distribution of the endosomal TbRab markers changes during the *T. brucei* cell cycle

Having demonstrated that the endosomal subpopulations of *T. brucei* (defined by Rab proteins) seem to have a physical connection in 1K1N cells, it was unclear how this fit with the duplication and re-organization of the new endosomal system. Thus, to investigate whether changes in the endosomes during the cell cycle affect the distribution of the three TbRab markers, the colocalization analysis was applied to other *T. brucei* cell cycle stages.

Immunofluorescence assays were conducted, and a total of 242 cells were analyzed. All markers showed a sharp signal, and labeled structures with diverse morphologies, including punctate, round, or horseshoe-like shapes in 1K1N cells (N = 100). In $1K^d1N$ cells (N = 50), all markers exhibited a scattered pattern with signals around both kinetoplast disks. As the cell cycle progressed, differences in the signals of the different TbRabs were noticed. In 2K1N stages (N = 50), it was possible to distinguish two "groups" of signal: a smaller one close to the kinetoplast disk of the new-flagellum daughter and a bigger one between the kinetoplast disk of the old-flagellum daughter and the nucleus. In 2K2N cells (N = 42), some distribution patterns could be distinguished. TbRab5A was present in two main regions: between both kinetoplasts and both nuclei, corresponding to the cytoplasmic regions of the new and old-flagellum daughter, respectively. The signal of TbRab7 had a punctate morphology and scattered distribution located close to both nuclei and kinetoplast disks. The bulk of the TbRab11 signal was present between both kinetoplast disks (Figure 12 A). Because TbRab5A and TbRab7 have a similar distribution pattern in all cell cycle stages, their correlation remained high during cell division (1N1N = 0.77; $1K^d1N$ = 0.79; 2K1N = 0.71; 2K2N = 0.71). However, TbRab11 tended to remain close to the kinetoplast disks and not to the nucleus/nuclei, which explains the progressively decrease in the correlation of this marker with both TbRab5A (1K1N = 0.65; $1K^d1N$ = 0.51; 2K1N = 0.45; 2K2N = 0.45) and TbRab7 (1K1N = 0.60; $1K^d1N$ = 0.47; 2K1N = 0.35; 2K2N = 0.37) throughout the cell cycle (Figure 12 B).

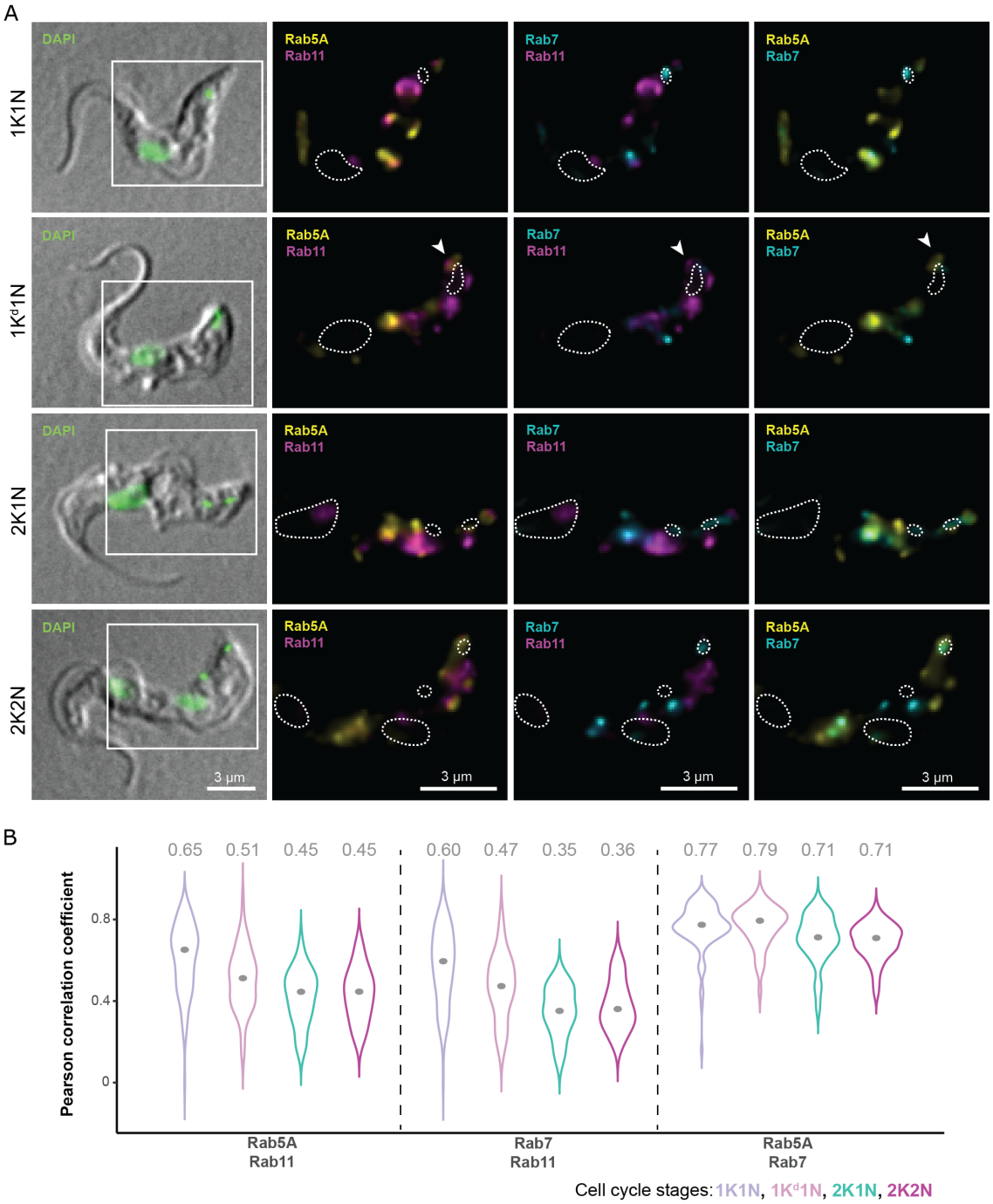

Figure 12. The distribution of the endosomal TbRab markers changes throughout the *Trypanosoma brucei* cell cycle (A) The localization of TbRab5A (yellow), TbRab7 (cyan), and TbRab11 (magenta) changes throughout the cell cycle. In 1K1N cells, all markers had sharp signals with punctate, round, or horseshoe-like morphology. In 1K^{d}1N, all markers had a scattered signal spread between the nucleus and kinetoplast. They were also found in proximity to the kinetoplast disk close to the posterior end of the cell (arrowhead). In the 2K1N stage, all markers kept the scattered distribution with an increase in the signal area in the vicinity of the kinetoplast disk of the new-flagellum daughter. In the 2K2N stages, the signal of TbRab5A was divided into two main regions: between both kinetoplast disks and both nuclei. The signal of TbRab7 had a punctate morphology and a scattered distribution located close to the nuclei and kinetoplast disks. The bulk of the TbRab11 signal extended between both kinetoplast disks, with some signal appearing in the cytoplasmic region of the old-flagellum daughter. Nucleus and kinetoplast were stained with DAPI (shown in green in the DIC images). The nucleus and kinetoplast are depicted in the fluorescent images with dashed white lines. (B) Violin plot showing the changes in colocalization of TbRab markers throughout the cell cycle. While the correlation between TbRab5A and TbRab7 remained high in all stages, the correlation of both with TbRab11 progressively decreased. The Pearson correlation was obtained from 242 cells (1K1N = 100; 1K^{d}1N = 50; 2K1N = 50; 2K2N = 42) in 3 independent experiments.

3.8 The lysosome of *T. brucei* shows morphological plasticity with indications of late duplication during the cell cycle

The lysosome is the final station for the endocytic pathway. Inside this organelle, endocytosed cargo can be broken down and used by the cell. However, the lysosome is not part of the VSG recycling pathway (Engstler et al., 2004). Thus, its duplication during the cell cycle may not be critical for the maintenance of the plasma membrane while the cell surface expands. To explore the duplication of the lysosome during the cell cycle, the morphological changes of this organelle were investigated.

Immunofluorescence assays using monoclonal and polyclonal antibodies against the lysosomal membrane protein p67 were conducted, and a total of 336 cells from three independent experiments were analyzed. The morphology of the lysosome was highly variable in 1K1N, 1K^{d}1N, or 2K1N cells. Among the different morphological patterns observed, it was possible to subdivide the lysosomes into three main groups: i) spherical, ii) extended (spherical or elongated signal presenting one or more protrusions), and iii) scattered (two or more punctate signals sometimes containing protrusions spreading in the posterior region of the cell) (Figure 13 A). In 2K2N cells, the p67 signal had migrated toward both nuclei (Figure 13 B). The rarely observed late cytokinesis cells showed a spherical p67 signal close to the nucleus (Figure 13 B). Such a morphological variety was also observed in images obtained after labeling the lysosome lumen with anti-cathepsin L, a lysosomal cysteine protease (Supplementary Figure S1.4). The area of the lysosome-associated signal (p67) was similar in 1K1N (1.20 ± 0.50 μm^2; N = 164) and 1K^{d}1N cells (1.29 ± 0.49 μm^2; N = 101). However, the organelle started growing in 2K1N cells (1.61 ± 0.58 μm^2; N = 41), achieving the maximum area in 2K2N cells (2.26 ± 0.78 μm^2; N = 30) (Figure 13 C). No significant changes in the lysosome area were noticed until the 2K1N stage (Figure 13 D). This indicates that the lysosome starts its duplication after kinetoplast division (2K1N) when the new endosomal system is already expanded. The most dramatic increase in the lysosomal area occurred during the 2K2N stage, in which the

organelle nearly doubled in size. Altogether, these results indicate that lysosome duplication starts after the duplication of the endosomes and finishes after nuclear duplication – in the last stage of the cell cycle.

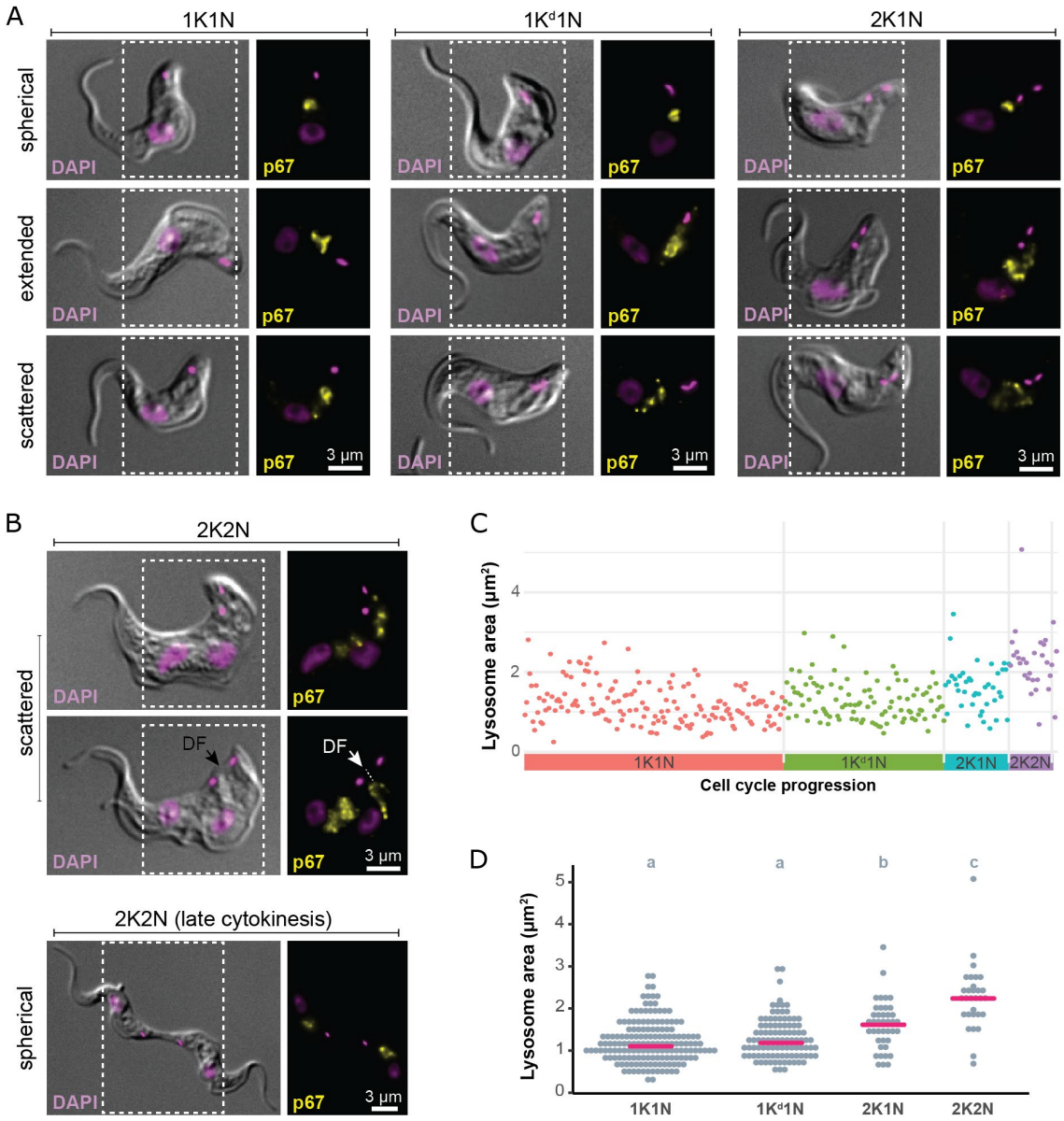

Figure 13. *Trypanosoma brucei* lysosome shows morphological plasticity with indications of late duplication during the cell cycle. (A) *T. brucei* lysosomes (p67) show three morphological patterns before nucleus duplication (1K1N, 1K^{d}1N, and 2K1N cells): spherical, extended (spherical or elongated signal presenting one or more protrusions), and scattered (two or more punctate signals with or without protrusions spreading in the posterior region of the cell). (B) Lysosomes show scattered morphology after nucleus duplication. The lysosome in 2K2N cells spreads into two cytoplasmic regions: one of the new-flagellum daughter and the other of the old-flagellum daughter. Observations of cells with a clear division fold (DF, arrow), the pathway for the cleavage furrow ingression, reveal a non-equivalent distribution of the signal. Cells in late cytokinesis presented a spherical lysosome. The white boxes in the DIC images represent the region of interest shown in the fluorescence images. (C) Lysosome duplication starts after kinetoplast division. The scatter plot depicts the area (µm^2) of the lysosome-associated signal (p67) obtained from single cells and classified according to their cell cycle stage (1K1N = pink; 1K^{d}1N = green; 2K1N = blue; 2K2N = lilac). Each dot represents measurements from one cell. Data is randomly distributed inside each progressive cell cycle stage. (D) The lysosome significantly increases after kinetoplast duplication. The dot plot shows the area (µm^2) of the lysosome-associated signal (p67) classified according to each cell cycle stage. Each dot represents measurements from one cell, and pink bars represent the median (1K1N = 1.1 µm^2; 1K^{d}1N = 1.2 µm^2; 2K1N = 1. 6 µm^2; 2K2N = 2.2 µm^2). Differences in the area of the lysosome-associated signal (p67) among the cell cycle stages were evaluated using a one-way ANOVA with Tukey's range test as the *post hoc* analysis. Groups with different letters (a/b/c) are significantly different from each other. The total area measurements were obtained from 336 cells (1K1N = 164; 1K^{d}1N = 101; 2K1N = 41; 2K2N = 30) in 3 independent experiments.

The morphological plasticity of the lysosome is a feature that has been observed in other eukaryotes (Bohnert and Johnson, 2022; Knapp and Swanson, 1990). In trypanosomes, however, the lysosome is usually referred to as a round structure (Engstler et al., 2004; Hall et al., 2004b; Peck et al., 2008). Thus, to check the morphological diversity of the lysosomes without the interference of chemical fixation, high-pressure frozen cells were used for correlative light and electron microscopy, using anti-cathepsin L as a lysosome marker. The cathepsin L-rich regions appeared as electron-lucent cytoplasmic areas with shapes varying from round to elongated (Figure 14 A-C).

To explore the structural flexibility of the lysosome in more detail, transmission electron microscopy of high-pressure frozen cells was performed. To this end, ultrathin sections were used in immunogold assays with antibodies against p67 and cathepsin L. The lysosome-associated membrane protein p67 was found in vesicular, circular, and irregular-shaped structures (Figure 15 A-D). Interestingly, cathepsin L evidenced the electron-dense lumen of irregular structures. These structures showed elongated regions with sheet-like morphology decorated with round/vesicular-like structures (Figure 15 E).

Overall, the duplication of the lysosome starts during the 2K1N stage and ends after the nucleus is divided. Such a late duplication is not surprising since the lysosome is assumed to have no participation in VSG recycling and, consequently, it is not essential for cell surface expansion. Another interesting finding of this study is the morphological plasticity of the lysosome, which does not seem to be related to the cell cycle. This is the first time that the structural flexibility of the lysosome has been described in *T. brucei*.

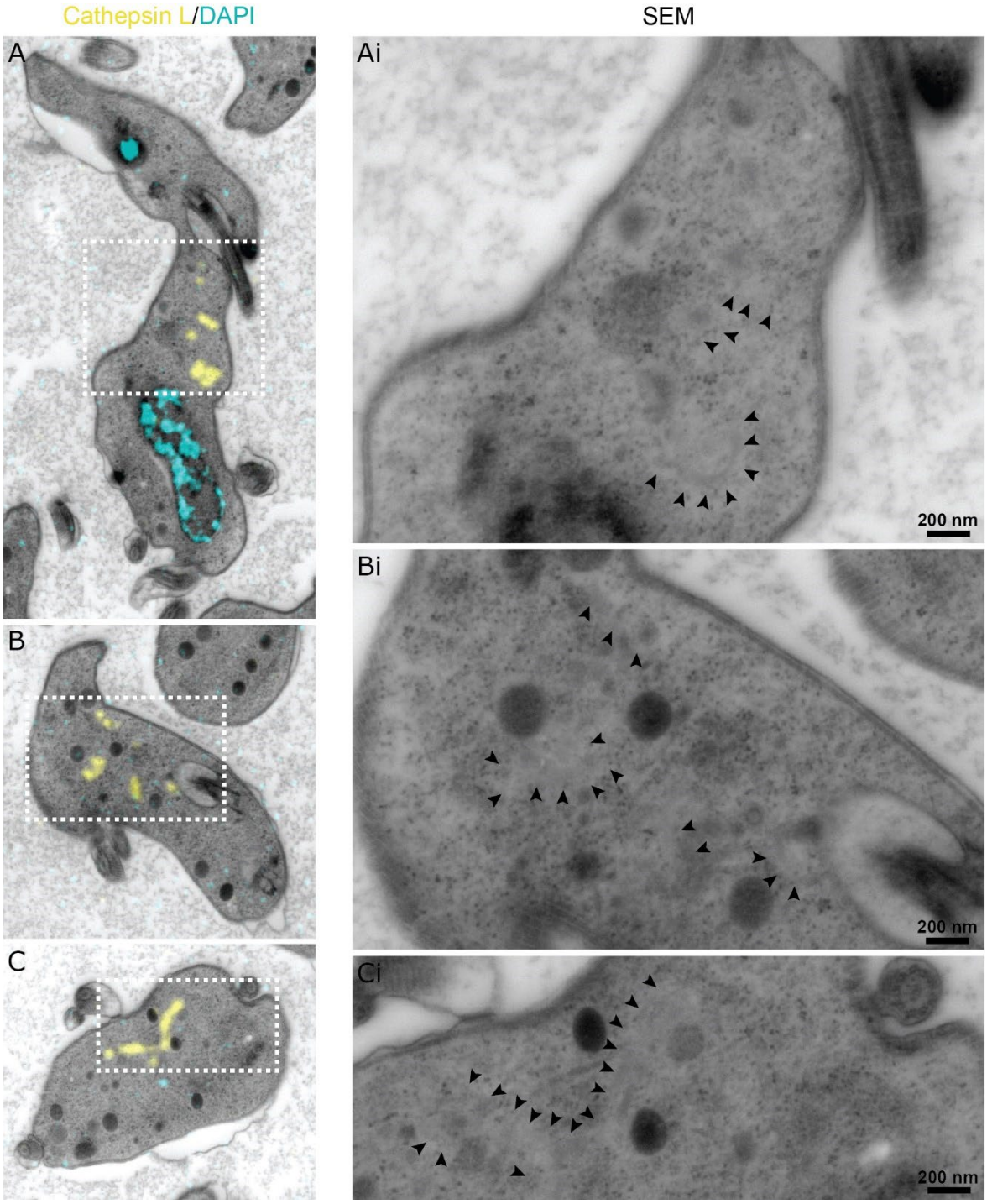

Figure 14. Correlative light and electron microscopy reveals diverse morphological shapes of the *Trypanosoma brucei* lysosome. High-pressure frozen *T. brucei* cells were embedded in LR-White and sectioned (100 nm). Sections were used for immunofluorescence assays and imaged via structured illumination microscopy. After imaging, sections were contrasted for electron microscopy and imaged in a scanning electron microscope. The fluorescence images and electron microscopy mosaics were manually correlated, using DAPI (nucleic acids) as a fiducial. The white box in the correlated images (A, B, C) represent the region of interest magnified for visualization of structures (Ai, Bi, Ci). (A/Ai) Cell with three regions rich in cathepsin L (arrowheads). The largest of these regions is observed close to the nucleus. (B/Bi) Cell with four regions rich in cathepsin L (arrowheads). One of these is placed close to the flagellar pocket. (C/Ci) Cell with long tubular-like structure rich in cathepsin L (arrowheads) close to vesicle-like shapes.

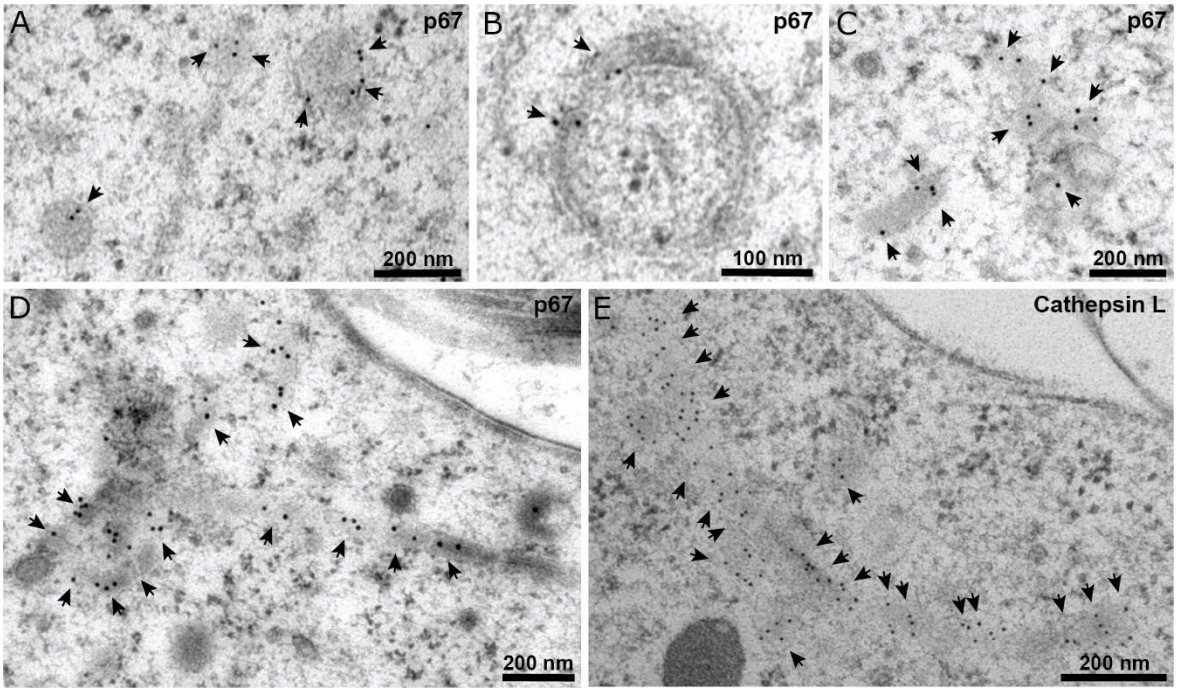

Figure 15. Transmission electron microscopy highlights the structural plasticity of the lysosomes. (A-D) p67 (arrows) is found in the membrane of structures with different shapes: vesicular-like (A), circular (B), irregular (C), and tubular (D). (E) Cathepsin L in the lumen of an irregular structure. The electron-dense region labeled with cathepsin L evidences an elongated sheet-like structure with vesicle-like shapes around it. A, B, E: 6 nm gold; C, D: 12 nm gold.

3.9 Summary of main findings

The results presented here suggest that in replicating *T. brucei* cells, the cell surface area underwent continuous growth. In contrast, endosomes initiated their duplication during kinetoplast division (1K^{d}1N) and showed a significant increase in the 2K1N stage. Additionally, clathrin recruitment experienced only a marginal increase in proliferating *T. brucei* cells. The duplication of the lysosome, however, occurred after the expansion of the endosomes (2K1N cells) and was completed during the 2K2N stage (Figure 16). These findings point to a potential relationship between plasma membrane growth and endocytosis, as well as coordination in the duplication of the endo-lysosomal system.

Regarding the endosomal subpopulations marked by TbRab5A (early endosomes), TbRab7 (late endosomes), and TbRab11 (recycling endosomes), they were shown to function as distinct compartments during fluid-phase cargo uptake. Interestingly, colocalization analyses suggested the presence of TbRabs in the same region/structure.

The different migration patterns observed between these markers during parasite division affected the colocalization between TbRab11 and both TbRab5A and TbRab7, while the overlap between TbRab5A and TbRab7 remained stable.

Furthermore, the lysosome exhibited high morphological plasticity, independent of the cell cycle, as explored through light and electron microscopy, making it the first examination of its structural flexibility in *T. brucei*. These results provide valuable insights into the dynamic processes within replicating *T. brucei* cells and the interplay between plasma membrane growth, endosomal behavior, and lysosome duplication.

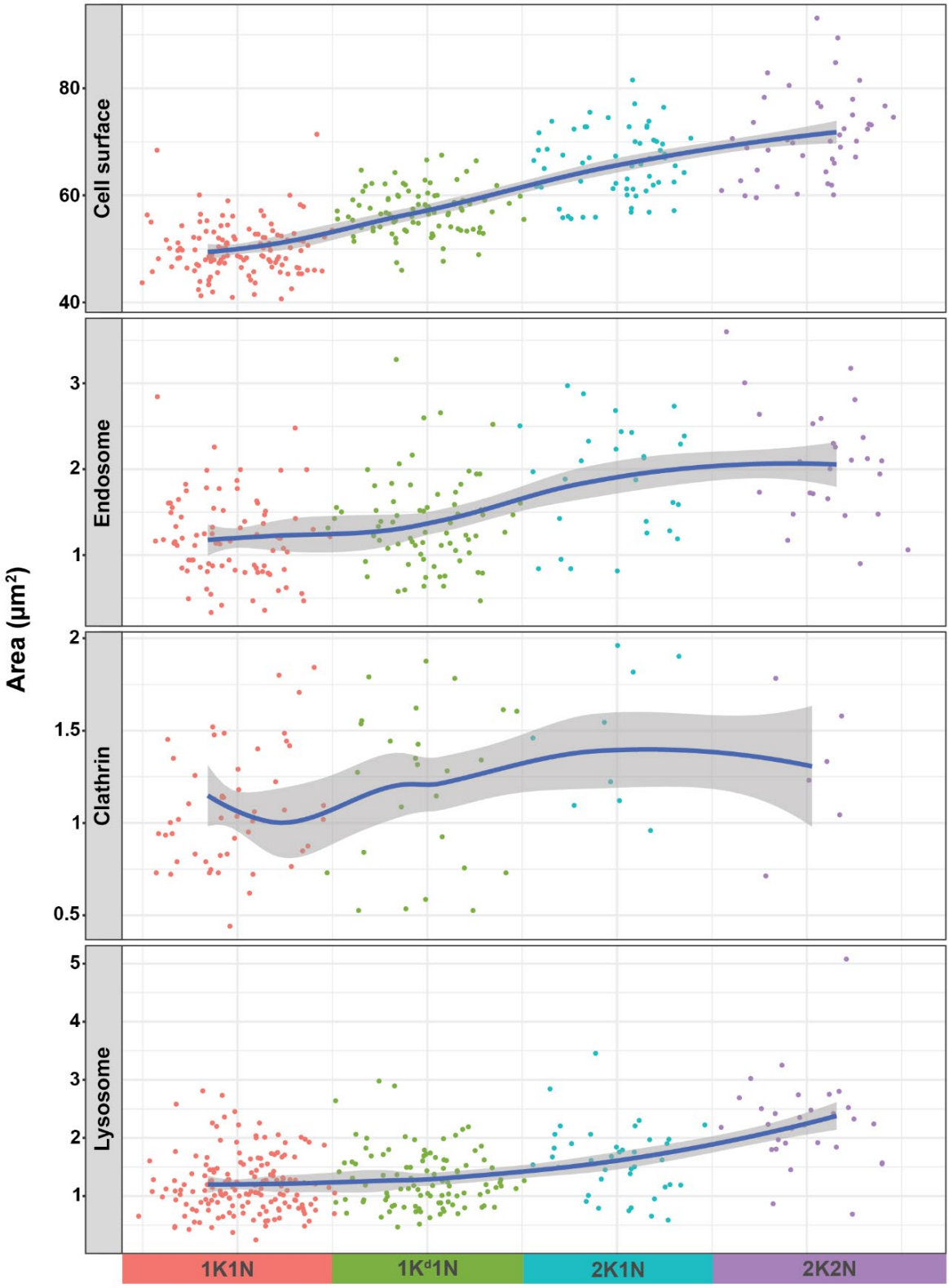

Figure 16. Area growth of *Trypanosoma brucei* cell surface, endosome, clathrin, and lysosome. The figure presents area measurements of the cell surface, endosome, clathrin-related signal, and the lysosome collected from fixed *T. brucei* cells. The findings indicate that cell surface area undergoes continuous growth in replicating *T. brucei* cells, while the endosomes demonstrate a pronounced increase in the 2K1N stage. Clathrin experiences a slight, yet stable, increase in proliferating *T. brucei* cells. As for the duplication of the lysosome, it occurs after the division of the kinetoplast (2K1N and 2K2N cells), subsequent to the expansion of the endosomes. Each dot represents one cell, and the data distribution within each cell cycle stage (1K1N, 1K^{d}1N, 2K1N, 2K2N) is randomized. The trend curve illustrates the overall pattern in the collected data.

4. Discussion

This study aimed to contribute to the understanding of plasma membrane growth dynamics and its potential relationship with the endo-lysosomal system during *T. brucei* proliferation. Despite the presence of artificial changes in the proportion of cell cycle stages caused by centrifugation, the analyses of fixed cells suggested a coordination between plasma membrane growth and the duplication of *T. brucei* endosomes. Additionally, this study provided evidence of morphological plasticity in the *T. brucei* lysosome, indicating its coordinated duplication with the *T. brucei* endosomes.

The discussion will be subdivided into four parts, focusing on the impacts of centrifugation in cell cycle analysis, plasma membrane growth dynamics, the potential physical connection of the endosomes, and the duplication of the lysosome and its morphological plasticity.

4.1 The impacts of centrifugation in the cell cycle analysis of *T. brucei*

As the central question of this study was related to the cell cycle, the first step was choosing a method that would allow the investigation of the different cell cycle stages. *Trypanosoma brucei* grows in asynchronous cultures and attempts at synchronization have proven inefficient or difficult (reviewed in Morriswood and Engstler, 2018). On the other hand, the events of both nuclear and kinetoplast division are well-documented in literature (Gluenz et al., 2011; Sherwin and Gull, 1989), and several studies used the morphology of these organelles to classify the cells when analyzing events related to the cell cycle (Hughes et al., 2017, 2013; Kurasawa et al., 2022; Matthews and Gull, 1994; Robinson, 1995; Wheeler et al., 2013). As this has proven to be a widely used and efficient method, it was decided that the same approach would be used in this study. Surprisingly, during the

investigation, it was noticed that the centrifugation of the parasites would interfere with an accurate cell cycle analysis by diminishing the number of cells in late cytokinesis. This fact becomes particularly relevant when applying an ergodic analysis to estimate the time of progression of the cell cycle. The ergodic principles are centered on the assumption that “the proportion of cells in any cycle stage observed in the population at a single time point is the same as the proportion of time spent in cycle stage as a single cell progresses through the cycle” (Wheeler, 2015, p. 3899). However, when the proportion of cells at a specific cell cycle stage is artificially changed, as demonstrated here, this proposition becomes weak.

Furthermore, the fact that *T. brucei* cells may re-enter the cell cycle before abscission adds an extra layer of complexity to this matter. Because the population of cells in late cytokinesis is composed of two connected cells with both 1K1N or 2K2N morphologies (Wheeler et al., 2013), the effects of the artificial breakage of the cytoplasmic bridges is not limited to the 1K1N stage. Consequently, applying a mathematical correction to the proportions of 1K1N/2K2N cells based on the results of the centrifugation experiments (which showed 13.8 % of cells in late cytokinesis) is not the ideal solution. Thus, the real impacts caused by the artificial breakage of the cytoplasmic bridges in the *T. brucei* population are, at this point, difficult to estimate. A more precise way to determine the duration of each cell cycle stage would be through live-cell microscopy. However, a potential challenge in live-cell imaging of trypanosomes is their constant motile behavior, which is essential for the parasite's virulence and viability (Engstler et al., 2007; Glogger et al., 2017; Saenz-Garcia et al., 2022; Shimogawa et al., 2018). To overcome this challenge, it is possible to use transient immobilization approaches using either agarose or hydrogels. However, a potential issue arises when using agarose, as it becomes challenging to maintain bloodstream forms of the parasite at 20 °C (Hartel et al., 2015), which is below their optimal temperature. Although the use of hydrogel offers a viable alternative for imaging the parasite at higher temperatures, effectively preserving the parasites' viability

for at least 60 minutes (Glogger et al., 2017), this time is still short when considering the entire cell cycle of *T. brucei*. Recently, Muniz and collaborators (2022) introduced an imaging approach for procyclic trypanosomes confined to microwells. Their strategy enabled the parasites to retain free mobility while limiting their movement to the imaging focal plane. With this approach, they showed that *T. brucei* procyclic forms are viable for cell cycle imaging for up to 24 hours (Muniz et al., 2022). Although the application of this strategy to bloodstream forms would require adaptations, such as precise temperature and CO_2 control, it holds great promise for enabling continuous imaging of cells undergoing an approximately 6-hour cell cycle.

4.2 Plasma membrane growth during *T. brucei* proliferation

After choosing the method for grouping cells into the successive cell cycle stages, this study investigated the changes in the cell surface and the endosomes during *T. brucei* proliferation. A previous study of Hughes and collaborators (2017) showed that the cell volume grows during the replication of *T. brucei* cells. To be sustainable, and keep cellular homeostasis, the increase in cell volume would demand expansion in the cell surface area, which was demonstrated by the present study. Because the plasma membrane area does not grow by stretching (Gauthier et al., 2009; Morris and Homann, 2001), its expansion is enabled by the insertion of new membrane components. In mammalian cells, the deposition of new plasma membrane can happen either via exocytosis, as seen in neurons (Craig et al., 1995; Urbina and Gupton, 2020), or via unfolding of plasma membrane prolongations, such as the microvilli present in epithelial cells (Figard and Sokac, 2014; Follett and Goldman, 1970). *Trypanosoma brucei* has a tight sub-pellicular microtubule cytoskeleton that defines the cell shape (Robinson, 1995) and no extensions of the cell surface are observed under normal conditions (Hempelmann et al., 2021). Thus, it seems unlikely that

plasma membrane growth would occur via unfolding leaving exocytosis as a possibility to be explored. It is known that *T. brucei* endosomes have an intimate connection with plasma membrane homeostasis – as demonstrated by the impressive rates of VSG recycling (Engstler et al., 2004). Thus, the main hypothesis of this study was that plasma membrane growth in proliferative *T. brucei* cells is sustained by the endosomes.

The results showed that both cell surface and endosomes started growing during the division of the kinetoplast ($1K^d1N$) and continued their expansion until the last stage of the cell cycle (2K2N). However, their growth dynamics differed. While the cell surface progressively increased from one cell cycle stage to another, the endosomes showed a marked expansion after the division of the kinetoplast (2K1N). Broadening the scope of this investigation to clathrin, it was possible to suggest a moderate increase in clathrin recruitment. In addition, the visualization of CCPs and CCVs close to each duplicated flagellar pocket, and the presence of clathrin and TbRabs (TbRab5A, TbRab7, and TbRab11) in the region where the new endosome is formed (close to the kinetoplast disk in the cytoplasmic region of the new-flagellum daughter in $1K^d1N$ stages) suggests the activity of the newly formed endosomal system. In fact, the highest recruitment of clathrin coincided with the expansion of the new endosome (2K1N). This result agrees with higher levels of YFP::CLC and VSG mRNA detected in *T. brucei* cells after the kinetoplast division obtained by Jamin Jung in his PhD thesis (Jung, 2015). Placed together, these results suggest that the duplication of the endosomes at an early stage of the cell cycle enables plasma membrane growth and cell surface homeostasis.

Nevertheless, two intriguing observations of this study remain to be explored. Why did the cell surface area not double its initial size in 2K2N cells? Why was the highest recruitment of clathrin not twice as large as was measured in 1K1N cells? To these, a few explanations are possible.

The first explanation lies in the method chosen to identify the cell cycle stages. Cells with 1K1N morphology represent a mixed population with cells that have either not started to proliferate and early division stages (with duplicated basal bodies and flagellum) (Hughes et al., 2017; Sherwin and Gull, 1989). Thus, it is possible that the average value presented for 1K1N cells is artificially inflated by the presence of early dividing cells. If this is true, the cell surface area and clathrin recruitment would have ultimately doubled but might have gone unrecognized as such due to the overestimate of the 1K1N value. This explanation agrees with the measurements obtained by Hughes and collaborators (2017) that show cell volume increase in the early division stages of 1K1N morphology. Another aspect that could have influenced the measurements of cell surface area presented here would be the division fold. The division fold is an inward projection of the plasma membrane formed along the long axis of 2K2N cells (Wheeler et al., 2013). Because the area measurements were taken in the x-y plane, the “in-fold” of plasma membrane was neglected when measuring the cell surface area of 2K2N cells. Nevertheless, the limitations of the method may have impacted the measurements but probably would not fully explain the lack of the twofold increase in cell surface area and clathrin recruitment.

Regarding the cell surface area, observations in *Caenorhabditis elegans* and sea urchins showed that membrane deposition is a necessary step during cytokinesis (Shuster and Burgess, 2002; Skop et al., 2001). In this way, the second explanation for not having observed a twofold increase in cell surface area is that the lack of measurements in cells in late cytokinesis did not allow this study to capture the plasma membrane growth in the very late stages of the cell cycle. Finally, a third explanation could be related to the surface-to-volume ratio of the cells. When contrasted with the volume measurements of Hughes and collaborators (2017), it appears that the volume of the cell doubles in 2K2N while the cell surface area does not. By increasing volume and area in different proportions, the surface-to-volume ratio would be diminished increasing membrane tension and reducing cell

resistance to deformation (Lipowsky, 2022; Mao et al., 2021). The longitudinal membrane invagination of 2K2N cells, named division fold, marks the path for the cleavage furrow, which begins at the anterior end of the fold (close to the flagellum), and progresses toward the posterior (Robinson, 1995; Sherwin and Gull, 1989; Wheeler et al., 2013). Although the dynamics of the cleavage furrow are well-documented, the understanding of the mechanisms that command it are still evolving. An Aurora B kinase ortholog (TbAUK1), polo-like kinase, and two other proteins, TbCPC1 and TbCPC2, were reported to localize in the division fold of *T. brucei* and be involved with the cleavage furrow ingression (Kurasawa et al., 2022; Li et al., 2008). The recruitment of TbAUK1 is influenced by the cytokinesis initiation factor 1 (CIF1; also known as TOEFAZ1), which also recruits several other molecules (Hilton et al., 2018; Kurasawa et al., 2022; Sinclair-Davis et al., 2017; Zhou et al., 2018a). It was previously suggested that the destabilization of CIF1 would enable an alternative furrow ingression from the posterior pole of the division fold (Zhou et al., 2016). However, cells entering this “alternative cytokinesis pathway” seem not to complete cell division (Muniz et al., 2022). It was proposed that the flagellar motility is an important element contributing to cytokinesis (Ralston et al., 2006), which could be related to the deformation forces caused by the incessant beating (Alizadehrad et al., 2015). In addition, it is known that increased membrane tension enables the fission of membranous organelles in mammalian cells (Mahecic et al., 2021) and that areas of membrane strangulation, such as the division fold, can facilitate fission in the presence of a force (Lipowsky, 2022). Considering that the involvement of a contractile actomyosin ring or similar mechanism in *T. brucei* fission has not been reported, it is possible to suggest that an increased membrane tension is a necessary stressor that facilitates the ingression of the cleavage furrow in *T. brucei*.

Studies in opisthokonts showed that clathrin triskelions form a cage-like structure surrounding vesicles that pinch off from the plasma membrane (Crowther and Pearse,

1981; Kirchhausen and Harrison, 1981; Sochacki and Taraska, 2019; Ungewickell and Branton, 1981). To fuse with the endosomes, CCVs must be uncoated, freeing the clathrin triskelions that become available for new recruitment (Prasad et al., 1993; Rothnie et al., 2011; Ungewickell et al., 1995). Since clathrin triskelions can be re-used multiple times by the cell, an increase in endocytosis might not directly or dramatically affect clathrin levels. Kinetics on endocytosis showed that after 15 seconds, clathrin levels achieved a steady-state (Engstler et al., 2004). Thus, it is plausible that clathrin levels would respond to the endocytic capacity of the cell. If this is true, and considering that the new endosomal system appears to be active during the cell cycle, then the discrete increase in clathrin recruitment could indicate that the new endosomal system is not functioning at its full capacity. Nevertheless, it is important to consider that complementary in-depth analyses on clathrin recruitment are necessary to sustain this hypothesis, such as fluorescence *in situ* hybridization (FISH) to analyze the level of clathrin transcripts or live-cell imaging.

4.3 The physical connection between endosomal subpopulations

The endosome markers TbRab5A, TbRab7, and TbRab11 play a key role in membrane recycling (Engstler et al., 2004; Grünfelder et al., 2003; Link et al., 2021; Overath and Engstler, 2004). Their involvement in the transport of membrane-bound cargo, such as LDL, transferrin, and VSG (Engstler et al., 2004; Field et al., 1998; Jeffries et al., 2001; Pal et al., 2002), as well as fluid-phase cargo, such as dextran and lucifer yellow (Engstler et al., 2004; Field et al., 1998; Hall et al., 2005), was previously demonstrated via fluorescence microscopy. Interestingly, although membrane-bound (VSG_{biotin}) and fluid-phase cargo (dextran) were shown to overlap at the beginning of endocytosis, a separation of both markers was observed after 20 seconds following uptake into the cell. A comparison between this cargo segregation and the kinetics of VSG_{biotin} endocytosis suggests that this

separation happened after VSGs had entered TbRab11-positive structures. In addition, both markers achieved maximum separation after ~1 minute, when dextran was localized to the lysosome (Engstler et al., 2004). Placed together, these studies indicate that TbRab11-positive structures would not be involved in fluid-phase cargo transport (Field et al., 1998; Hall et al., 2005). Electron microscopy studies using ferritin supported this idea, since ferritin was never observed inside narrow endosomal cisternae or exocytic carriers (Engstler et al., 2004; Langreth and Balber, 1975), which are TbRab11-positive structures (Grünfelder et al., 2003). However, horseradish peroxidase was observed inside narrow cisternal structures and exocytic carriers (Engstler et al., 2004), disagreeing with the exclusion of fluid-phase cargo from TbRab11-positive compartments. Trying to accommodate all of these observations, Engstler and collaborators (2004) proposed that fluid-phase cargo was transported in TbRab5A, TbRab7, and TbRab11 compartments and sorted into class II CCVs to be transported to the lysosome. However, the same authors also suggested that a possible interface between the early and the recycling compartments should be further investigated.

To contribute to the understanding of the possible interface of endosomal subpopulations, and the endocytic pathways for fluid-phase cargo, this study presented the first quantitative colocalization analysis of *T. brucei* endosomes and ferritin. Ferritin strongly overlapped with TbRab5A while showing a moderate colocalization with TbRab7 and a weak overlap with TbRab11. These results confirm the involvement of both TbRab5A and TbRab7 in the ferritin endocytic pathway. This is not surprising, since the early endosome (TbRab5A) was shown to be the first station of endocytosed cargo in *T. brucei* cells (Engstler et al., 2004), and that the depletion of TbRab7 impaired the delivery of endocytosed cargo to the lysosome (Silverman et al., 2011). As ferritin was never observed in recycling compartments (Engstler et al., 2004) and the structures marked by TbRab11 and TbRab5A were considered juxtaposed (Jeffries et al., 2001; Pal et al., 2002), the weak

colocalization between TbRab11 and ferritin observed here could be considered an artifact. However, the quantitative colocalization analysis of *T. brucei* endosomal markers indicated the simultaneous presence of the three TbRab markers in the same structures. Although this could be interpreted as a transitory double binding, similar to what would happen during a maturation process (Rink et al., 2005; Scott et al., 2014; Trivedi et al., 2020), data from our group suggest a non-stochastic distribution of TbRabs in specific regions of a complex endosomal network (Link et al., 2023, preprint).

Finally, the colocalization of TbRabs was explored during the duplication of *T. brucei*. During kinetoplast division ($1K^d1N$) all TbRab markers appeared around the kinetoplast disk in the cytoplasmic region of the new-flagellum daughter. Such a distribution suggests that all three markers are recruited early in the formation of the new endosomal system. After the kinetoplast division, the signal of all markers progressively enlarges, spreading within the posterior region, which is consistent with the observations of the endosomes reported here. These observations suggest a *de novo* formation of the endosomal system in *T. brucei*. Evidences for the *de novo* formation of endosomes were shown in mammalian cells, in which the maturation of early endosomes into late endosomes stimulates the *de novo* formation of early endosomes (Skjeldal et al., 2021). To confirm a *de novo* biogenesis of *T. brucei* endosomes further experiments would be necessary, such as live-cell imaging.

The distribution of the TbRab markers changed during the course of the cell cycle, with the bulk of TbRab11 signal concentrating close to the kinetoplasts while TbRab5A and TbRab7 appeared close to the kinetoplasts and also in proximity with the nucleus/nuclei as the cell cycle progressed. These differences in the migration patterns explain the changes in the colocalization of the markers during the cell cycle. The observed migration of TbRab signals seemed to accompany the expansion of the new endosomal system, as evidenced by the strong colocalization of TbRab11 and EP1::GFP in all cell cycle stages. In

mammalian cells, clusters of Rab5 and Rab11 were recorded around mitotic spindle poles (Carlton et al., 2020; Hehnly and Doxsey, 2014; Serio et al., 2011) while in *Drosophila* only Rab5 was observed in this region (Capalbo et al., 2011). Knockout of Rab5 revealed its requirement for proper chromosome alignment and nuclear envelope breakdown in mammalian and *Drosophila* cells (Capalbo et al., 2011; Serio et al., 2011). Because trypanosomes undergo a closed mitosis (Zhou et al., 2018b, 2014) such an activity of TbRab5 would not be expected. However, evidence collected in the yeast *S. pombe* suggest that a local disassembly of the nuclear envelope is necessary for spindle pole formation even in cells undergoing closed mitosis (Dey et al., 2020). While carrying out the present study, a few trypanosome cells showed TbRab11 and TbRab5A in proximity with the nucleus. However, these signals did not prevail in the population and were weaker than the signal in the posterior region of the cell – coinciding with the endosomes. Because this study focused on the endosomes, the possible involvement of TbRabs and chromosome segregation was not explored. Nevertheless, it is important to highlight that, to this point, the study of small Rab GTPases in trypanosomes was solely focused on the intracellular transport (Engstler et al., 2004; Field et al., 1998; Hall et al., 2005; Jeffries et al., 2001; Pal et al., 2002; Silverman et al., 2011; Umaer et al., 2018). Consequently, no other role for TbRabs is known for this organism, representing an open field to be explored.

4.4 Lysosome duplication and morphological plasticity

As the main organelle responsible for intracellular digestion, the lysosome is essential for cellular homeostasis acting in nutrient sensing, intracellular signaling, and metabolism (Ballabio and Bonifacino, 2020; Barral et al., 2022). It has a close relationship with endosomes, which secure delivery of endogenous or exogenous cargo to the lysosome (Barral et al., 2022). In *T. brucei*, the lysosome is usually studied in a context of

therapeutics, exploring its potential as a target for drug development (Caffrey et al., 2001; Koeller et al., 2021; Koeller and Bangs, 2019; Peck et al., 2008). Therefore, very little attention has been dedicated to the lysosome regarding its morphology, duplication, and inheritance.

This study shows that the lysosome started increasing in size after the endosomes had completed their duplication, during the 2K1N stage. In 2K2N cells it achieved double its area, indicating the completion of the duplication. This late replication has been reported previously for other small degradative organelles named acidocalcisomes, which also increase in number in 2K1N cells. It was suggested that the late duplication of acidocalcisomes indicates that they are not essential for cell volume growth (Hughes et al., 2017), which also could be the case for the lysosome. In addition, endocytosed VSG was never spotted in the lysosome (Engstler et al., 2004; Grünfelder et al., 2003; Overath and Engstler, 2004). Thus, it is possible to assume that the lysosome is not essential for plasma membrane homeostasis during *T. brucei* replication.

The morphology of the lysosome was highly heterogeneous even within the individual cell cycle stages, showing either a spherical shape or protrusions that varied in number and form. When studying the mechanisms of trypanosome resistance to the trypanolytic factor, Hager and Hajduk (1997) spotted distinct morphologies of the lysosome marked with dextran. In his PhD thesis, Jamin Jung reported that the lysosome protrusions “appeared and disappeared at different sites” (Jung, 2015, p. 53). However, the lysosome is still commonly referred to as a round structure (Engstler et al., 2004; Hall et al., 2004b; Koeller and Bangs, 2019; Peck et al., 2008), a shape that is usually used to emphasize differences to the tubular lysosome of *Leishmania* (Halliday et al., 2019; Wang et al., 2020). Here, electron microscopy was used to investigate the structure of the lysosome in more detail, revealing the membrane protein p67 to be associated with vesicular, circular, and irregular structures. With cathepsin L the lumen of the lysosome was visualized and the

irregular structures appeared to be formed by an elongated structure surrounded with vesicle-like regions.

The morphological heterogeneity of the lysosome has been previously documented in phagocytic cells, in which extended tubular projections were observed in lysosomal membranes. In these cells, the perinuclear lysosome showed a vesicular morphology until phagocytosis was stimulated and tubule-like protrusions started radiating from the vesicular endosome. These protrusions progressively diminished in concert with the digestion of the particles taken up and the lysosome returned to the vesicle-like morphology (Barois et al., 2002; Bohnert and Johnson, 2022; Knapp and Swanson, 1990; Swanson et al., 1987). Thus, it was proposed that the protrusions may accelerate particle digestion by increasing the internal holding capacity of lysosomes (Bohnert and Johnson, 2022). The function of the lysosomal plasticity in *T. brucei* remains to be elucidated but it is tempting to speculate that there is a similar physiological role.

5. Conclusions

This study showed that the cell surface area of proliferating *T. brucei* cells progressively grows during the cell cycle. In contrast, the endosomes exhibit pronounced growth after kinetoplast duplication (2K1N), which is followed by the duplication of the lysosome (2K2N). This points to a coordinated duplication of these organelles with complementary roles in trypanosome metabolism. In addition, the early duplication of the endosomes suggests a potential relationship with plasma membrane growth, which is different from what was observed for the lysosome. The duplication of the endosome happens in the cytoplasmic region of the new-flagellum daughter with recruitment of clathrin and TbRab GTPases to the same location suggesting the activity of the newly formed endosomal system. The recruitment of clathrin to both flagellar pockets reinforces this idea. The marginal increase in clathrin recruitment, allowed the proposition that endosomes sustain plasma membrane growth via imbalance in endo- and exocytosis. To confirm this, future studies could explore the endocytosis ratios during the different stages of the cell cycle using, for example, flow cytometry to measure the internalization of biotinylated VSG.

The in-depth colocalization analyses of TbRab markers indicated their presence in the same region/structure, demonstrating, for the first time, the potential physical connection of *T. brucei* endosome subpopulations. This finding was further investigated via electron tomography and immunoelectron microscopy and the results are available in the preprint of Link and collaborators (2023).

Chapter 2

18S rRNA gene sequence-structure phylogeny of the Trypanosomatida (Kinetoplastea, Euglenozoa) with special reference to *Trypanosoma*

This chapter is a reproduction of:

Borges, A.R., Engstler, M., Wolf, M., 2021. 18S rRNA gene sequence-structure phylogeny of the Trypanosomatida (Kinetoplastea, Euglenozoa) with special reference to *Trypanosoma*. European Journal of Protistology 81, 125824.

https://doi.org/10.1016/j.ejop.2021.125824.

Modifications in formatting were performed to fit in this thesis layout.

1. Introduction

Kinetoplastids (Kinetoplastea HONIGBERG, 1963) are a remarkable group of unicellular organisms. They include free-living and parasite protists of invertebrates, vertebrates, and plants (Adl et al., 2019; Cavalier-Smith, 2016; Lukeš et al., 2018). Among them, we find the obligatory parasites of the order Trypanosomatida KENT, 1880 (Adl et al., 2019; Moreira et al., 2004), including the human pathogens *T. brucei*, which causes African sleeping sickness, *T. cruzi*, the causative agent of Chagas disease in South America, and *Leishmania* ROSS, 1903 species which infect and harm hundreds of thousands of people each year (Akhoundi et al., 2016; Lukeš et al., 2018, 2014; WHO, 2012). African trypanosomes are likely the most well-known trypanosomatids. Due to their dixenic life cycle and the extracellular lifestyle in the vertebrate blood, they have evolved interesting, and sometimes unusual, mechanisms to deal with such different environments and challenges imposed by the immune system. Thus, it does not come as a surprise that major discoveries in cell biology have been made in trypanosomes, such as antigenic variation (Vickerman, 1978), glycolysis compartmented in unique organelles (Hart et al., 1987), GPI-anchoring of membrane proteins (Menon et al., 1988), and unprecedented nucleotide modifications (Gommers-Ampt et al., 1993).

For harboring such a diverse group of organisms, it is unsurprising that the evolution of parasitism inside Kinetoplastea has been intriguing scientists for decades. Given that each parasitic group has closely affiliated free-living relatives and reversion to a free-living state did not occur, it is probable that at least four independent adoptions of obligate parasitism or commensalism have occurred (Lukeš et al., 2018, 2014; Yazaki et al., 2017). Currently, the earliest diverging lineage inside Trypanosomatida is the genus *Paratrypanosoma* VOTÝPKA AND LUKEŠ, 2013, represented by one species found in mosquitoes, *Paratrypanosoma confusum* VOTÝPKA AND LUKEŠ, 2013 (Flegontov et al.,

2013; Skalický et al., 2017). The vast majority of trypanosomatids are monoxenic parasites of insects with few dixenic genera due to the capacity of infect vertebrates, such as *Leishmania* and *Trypanosoma* GRUBY, 1843 (Lukeš et al., 2018). Thus, the most likely origin of *Leishmania* and *Trypanosoma* is from within monoxenic trypanosomatids, implicating that their origins were no earlier than 370 million years ago, when the invasion of land by vertebrates occurred (Hamilton and Stevens, 2017; Lukeš et al., 2014; Stevens et al., 1999). The transmission of an insect-living trypanosomatid into a warm-blooded host has most likely occurred many times with rare successful cases (Flegontov et al., 2013; Hamilton and Stevens, 2017; Lukeš et al., 2014). So far, only *Trypanosoma*, *Leishmania*, *Endotrypanum*, and *Porcisia* have left surviving descendants in vertebrates.

Having passed the vertebrate colonization bottleneck, *Trypanosoma* radiation and adaptation to diverse vertebrate species became an unprecedented evolutionary success story. Today, these parasites prosper in essentially all vertebrate Classes, from fish to mammals (Fermino et al., 2019; Hamilton and Stevens, 2017; Lemos et al., 2015). The 18S rDNA marker has been extensively used to analyze the phylogenetic relationship inside this group (Hamilton et al., 2004, 2005, 2007; Lukeš et al., 2014; Maslov et al., 2001; Stevens et al., 1999). The incorporation of glycosomal glyceraldehyde phosphate dehydrogenase (gGAPDH) into the analysis allowed the generation of more resolved trees, consolidating, for example, the long-lasting question about the monophyly inside *Trypanosoma* (Fermino et al., 2019; Hamilton et al., 2009, 2007, 2005, 2004; Hamilton and Stevens, 2017; Lima et al., 2015).

The advent of modern sequencing technologies has greatly advanced our understanding of trypanosomatid phylogeny, with more new genera described in the last decade than within the past century (Adl et al., 2019; Lukeš et al., 2018, 2014). These days, trypanosomatid phylogeny has sufficiently advanced to provide a solid framework for comparative studies, with genomic data available for more than just the medically relevant

kinetoplastids. Interestingly, the basic layout of trypanosomatid genomes appears to be strikingly similar, with high overall synteny, within and between monoxenic and dixenic species (Lukeš et al., 2018). The constantly growing genome data might become a powerful tool for evolutionary inference. In the future, trypanosomatids will be studied not only as infective agents of devastating neglected tropical diseases, or powerful genetic and cellular model systems, but also to unravel basic principles of the evolution of unicellular eukaryotes. What we know today is just the tip of an iceberg. The origin of *Trypanosoma*, for example, remains enigmatic. Further, the presence of prokaryotic endosymbionts and viruses in trypanosomatids, or the full biodiversity and ecological role of insect trypanosomatids remain superficially explored (Lukeš et al., 2018; Teixeira et al., 2011).

Here, we present the first large scale case study in which trypanosomatid RNA secondary structure is used as an additional source of phylogenetic information. We use 18S rRNA sequence-structure data simultaneously in inferring alignments and trees. This approach was recently reviewed and shown to increase robustness and accuracy of reconstructed phylogenies (Keller et al., 2010; Wolf et al., 2014). So far, all conclusions have been made with multigene trees. In our study, there are only a few places in our robustly supported trees where branching does not match with multigene phylogenomic trees. In our discussion, we explore both the synergetic and the discrepant aspects of our trees and the literature, as they are potentially critical branches that are ambiguous and require more attention.

2. Material and Methods

2.1 Taxon sampling, secondary structure prediction, sequence–structure alignment, and phylogenetic tree reconstruction

For this study, 240 SSU 18S ribosomal RNA gene sequences from Trypanosomatida with a sequence length > 1500 nucleotides and a full taxonomic lineage, down to a complete species name, were retrieved from NCBI (GenBank) using a search string (Supplementary List S1). Of these sequences, 195 are from the *Trypanosoma* genus. For a closer look into the *Trypanosoma* phylogeny, a subset of 43 sequences of the automated search were used for analysis, which was further complemented with manually retrieved sequences from NCBI (Supplementary List S2). Secondary structures of the 18S rRNA gene sequences were obtained via homology modeling (Wolf et al., 2005) using *T. cruzi* (AF245382) and *T. brucei* (M12676) as templates (Supplementary Figure S1) in the ITS2 database (Ankenbrand et al., 2015). The two template-secondary structures (without pseudoknots) were obtained from the Comparative RNA Web (CRW) (Cannone et al., 2002). For sequence-structure alignments, the four RNA nucleotides, which were multiplied by three states (unpaired, paired left and paired right), are encoded by a 12-letter alphabet (Wolf et al., 2014). Using a specific 12 x 12 sequence-structure scoring matrix (Seibel et al., 2006), global multiple sequence-structure alignments were automatically generated in ClustalW2 1.83 (Larkin et al., 2007) as implemented in 4SALE 1.7.1 (Seibel et al., 2008, 2006). After alignment, the sequences were trimmed at start and end. The final alignments are available as supplementary data S1-S5. Based on Keller et al. (2010), using 12-letter encoded sequences, sequence-structure neighbor-joining (NJ) trees were determined using ProfDistS (Keller et al., 2010; Wolf et al., 2008). For further analysis of *Trypanosoma* using the 12-letter encoded sequences, sequence-structure maximum likelihood (ML) trees (Felsenstein, 1981) were calculated using phangorn (Schliep, 2011), as implemented in the

statistical framework R (R Core Team, 2014). The R script is available from the 4SALE homepage at http://4sale.bioapps.biozentrum.uniwuerzburg.de (Wolf et al., 2014). Bootstrap support for all sequence-structure trees was estimated (due to the complexity of the 12x12 approach) based on 100 pseudo-replicates. Trees were rooted with non-*Trypanosoma* sequences from Trypanosomatida.

3. Results and Discussion

3.1 Phylogeny of Trypanosomatida and trypanosomes based on the automated search

The analysis of 240 18S rRNA gene sequence-structure pairs (Figure 1) and selection of 43 different species (Figure 2) resulted in trees supported by high bootstraps values (>75) on sister groups displaying the following *Trypanosoma* clades: the *Trypanosoma pestanai* BETTENCOURT AND FRANÇA, 1905 clade, represented in our tree by this species found in the Eurasian badger (Hamilton and Stevens, 2017); the *T. brucei* clade, consisting of trypanosome species naturally transmitted by tsetse flies, such as *Trypanosoma vivax* ZIEMANN, 1905, *Trypanosoma congolense* BRODEN, 1904, and *T. brucei* (Hamilton et al., 2007, 2004; Hamilton and Stevens, 2017; Lima et al., 2015); the *T. cruzi* clade, comprising mammalian trypanosomes with worldwide distribution, such as *T. cruzi*, *Trypanosoma rangeli* TEJERA, 1920, and *Trypanosoma wauwau* TEIXEIRA AND CAMARGO, 2016, endemic of Latin America, *Trypanosoma conorhini* (DONOVAN, 1909) found in Europe, South America and Africa, and *Trypanosoma dionisii* BETTENCOURT AND FRANÇA, 1905 distributed in Latin America, Africa, Asia and Europe (Clément et al., 2020; Hamilton et al., 2009, 2007; Lima et al., 2015); the *Trypanosoma lewisi* (KENT, 1880) clade, including parasites of the subgenus *Herpetosoma* found majorly in rodents (Ortiz et al., 2018); the Crocodilian clade, harboring trypanosomes of terrestrial lineage found in crocodilians in Africa and alligators in South America (Fermino et al., 2019, 2013); the Avian clade, with *Trypanosoma corvi* STEPHENS AND CHRISTOPHERS, 1908, *Trypanosoma avium* DANILEWSKY, 1885 and *Trypanosoma thomasbancrofti* SLAPETA, 2016 (Šlapeta et al., 2016); the *Trypanosoma theileri* LAVERAN, 1902 clade, with *T. theileri*, a worldwide distributted cattle parasite, and the subclade representant *Trypanosoma cyclops* WEINMAN, 1972 (Hamilton and Stevens, 2017; Lima et al., 2015); and the Aquatic clade, harboring trypanosomes from fish, anurans and platypus (Attias et al., 2016; Lemos et al., 2015; Spodareva et al., 2018). Interestingly, the lizard/snake clade is also represented in our tree

with *Trypanosoma varani* WENYON, 1908, a snake trypanosome, branching together with the mammal parasite *Trypanosoma freitasi* REGO ET AL., 1957. The branching of marsupial and rodent trypanosomes inside this clade has been previously observed (Dobigny et al., 2011; Ortiz et al., 2018). Thus, our analysis corroborates the existence of the lizard-snake/marsupial-rodent clade composed by trypanosomes transmitted by sandflies (Ortiz et al., 2018).

The phylogenetic analyses using sequence-structure data of 18S rRNA genes (Figure 2) supports the monophyly of *Trypanosoma* as previously observed in trees constructed with partial/complete sequences of 18S rDNA and/or gGAPDH sequences (Fermino et al., 2019; Hamilton et al., 2007, 2005, 2004). Intriguingly, in the tree obtained using a greater number of sequences (Figure 1) *Strigomonas culicis* (WALLACE AND JOHNSON, 1961) (U05679.1 and HQ659564.1) appear as a basal group of African trypanosomes. To date, studies on Trypanosomatida showed a basal position of *Trypanosoma* in relation to *Strigomonas* LWOFF AND LWOFF, 1931 (Du et al., 1994; Lukeš et al., 2018; Teixeira et al., 2011). To confirm/refute this positioning it would be necessary to increase the analysis with other representants of Strigomonadinae subfamily. It is important to note that the inclusion of representants of *T. brucei* clade in extensive phylogenetic analysis of Kinetoplastea potentially generate artifacts, such as the suggestion of paraphyly inside *Trypanosoma* due to the clustering with other trypanosomatid genera (Hughes and Piontkivska, 2003). This could be related not only to the positioning observed for *Strigomonas*, but would also explain the clustering of one sequence of the bat parasite *T. dionisii* within the *T. brucei* clade (Figure 1). This species is distributed worldwide, with its origin in Africa, and presents a high phyletic diversity (Clément et al., 2020). However, its branching inside *T. cruzi* clade is strongly supported (Hamilton et al., 2007, 2005, 2004; Hamilton and Stevens, 2017; Lima et al., 2015).

The first branching of *Trypanosoma* (Figure 2) forms two major groups: one lineage composed by *T. brucei* and *T. pestanai* clades, and another with trypanosomes from Terrestrial (*T. cruzi*, *T. lewisi*, *T. theileri*, snake-lizard/marsupial-rodent, avian and

crocodilian clades) and Aquatic lineages. Thus, this tree corroborates the hypothesis of the independent evolutionary history of both human pathogens, *T. brucei* and *T. cruzi* (Hamilton and Stevens, 2017). The topology of our tree shows the Aquatic clade as a solid lineage, in accordance with previous observations (Fermino et al., 2019; Hamilton et al., 2007, 2005; Lima et al., 2015). However, the origin of this clade is still under debate. Many studies using different DNA markers, such as long (>1.4 kb) 18S rDNA sequences, v7v8 hypervariable region of 18S rDNA and/or partial sequences of gGAPDH, showed either an early division between Aquatic and Terrestrial lineages as a single event (Fermino et al., 2019; Hamilton et al., 2007, 2005; Lima et al., 2015) or in subsequent events with amphibian trypanosomes and *Trypanosoma therezieni* BRYGOO, 1963 at the basis of *Trypanosoma* (Botero et al., 2016, 2013; Hamilton et al., 2004). Interestingly, our tree suggests a later evolution of the Aquatic clade from Terrestrial trypanosomes (Figure 2), which agrees with the insect first hypothesis (Hamilton and Stevens, 2017; Ortiz et al., 2018). This hypothesis assumes that trypanosomes were originated from a monogenetic insect parasite that adapted to live inside terrestrial vertebrates and later spread to leeches and other aquatic animals, most likely through amphibians (Hamilton and Stevens, 2017).

Trypanosomes of the *T. brucei* clade are virtually restricted to Africa, with one exception being *T. vivax* (Rodrigues et al., 2008; Silva Pereira et al., 2020). The early divergence of *T. vivax* inside the *T. brucei* clade (Figures 1, 2) is in accordance to previous results showing a higher evolutionary rate of this species among the salivarian trypanosomes (Hamilton et al., 2007; Lima et al., 2015; Stevens and Rambaut, 2001). It is interesting to consider that a previous analysis of 18S rDNA sequences revealed that members of the *T. brucei* clade show an evolutionary rate higher than other trypanosomes (Stevens and Rambaut, 2001). However, this high divergence has proven not to alter the topology of sequence-based trees (Hamilton et al., 2004). Inside this clade, *T. brucei*, *Trypanosoma evansi* STEEL, 1885 and *Trypanosoma equiperdum* DOFLEIN, 1901 branched together (Figure 2). In fact, the relationship between these species has been a topic of discussion for many years. Although a high genetic variation among *T. evansi* strains has

been recorded, phylogenetic studies support their similarities with *T. equiperdum* and *T. brucei* (Carnes et al., 2015; Kamidi et al., 2017; Lai et al., 2008). Thus, the reclassification of *T. equiperdum* and *T. evansi* as a subspecies of *T. brucei* was suggested, but would be against the Principle of Priority of the International Code of Zoological Nomenclature due to the seniority of the name *T. evansi* (Molinari and Moreno, 2018).

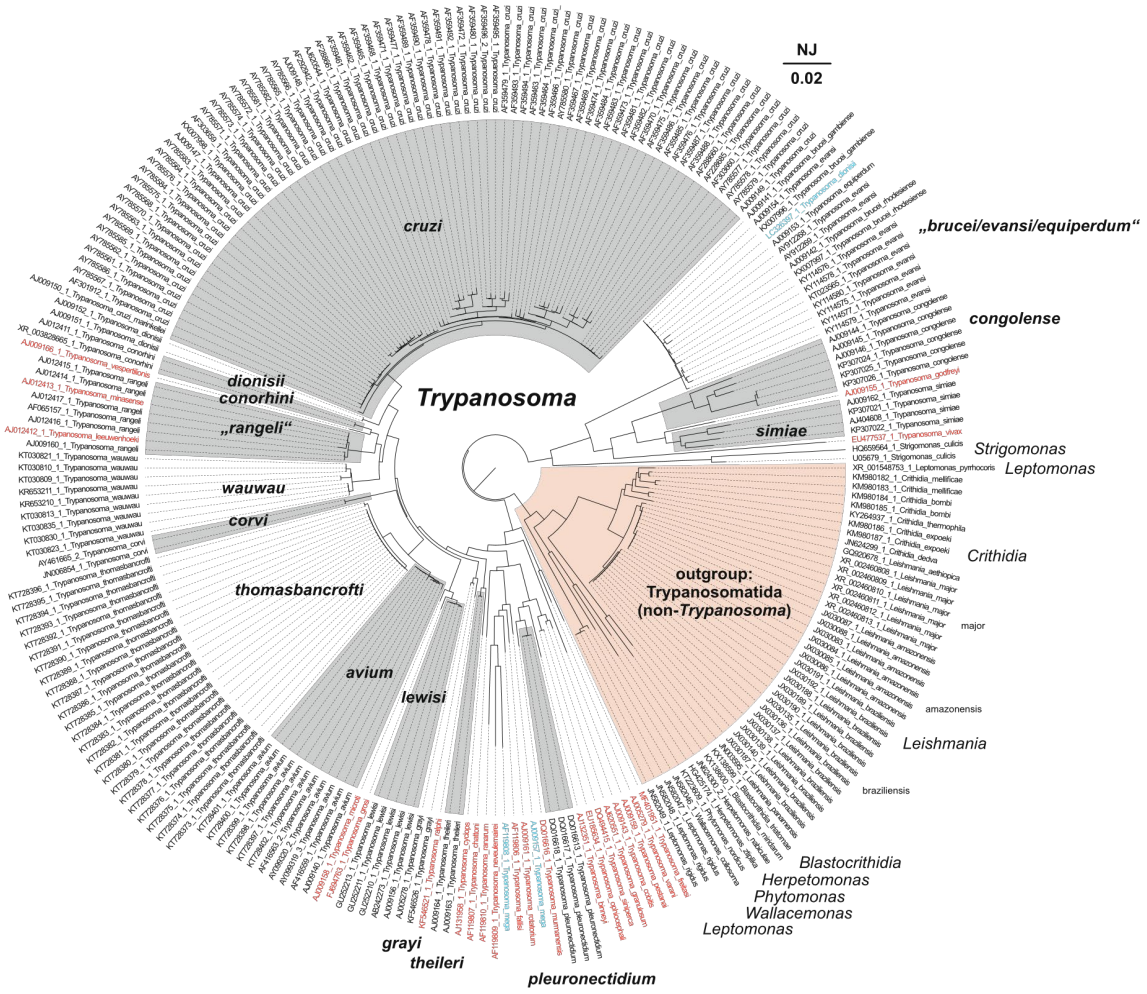

Figure 1. 18S rDNA sequence-structure neighbor-joining (NJ) tree obtained by ProfDistS (Wolf et al., 2008). All 240 18S rDNA sequences from Trypanosomatida (Kinetoplastea, Euglenozoa) available at NCBI (GenBank) with a sequence length > 1500 nucleotides and with a full taxonomic lineage down to a complete species name have been used for the analysis. For tree reconstruction the global multiple sequence-structure alignment (.xfasta format) as derived by 4SALE (Seibel et al., 2008, 2006) was automatically encoded by a 12-letter alphabet (Wolf et al., 2014). GenBank accession numbers accompany each taxon name. Key taxa are off and on marked in gray and additionally named alongside the tree. Non-monophyletic taxa are indicated by quotation marks. Singletons are highlighted red and polyphyletic taxa are highlighted blue. The scale bar indicates evolutionary distances. The tree is rooted at non-*Trypanosoma* sequences.

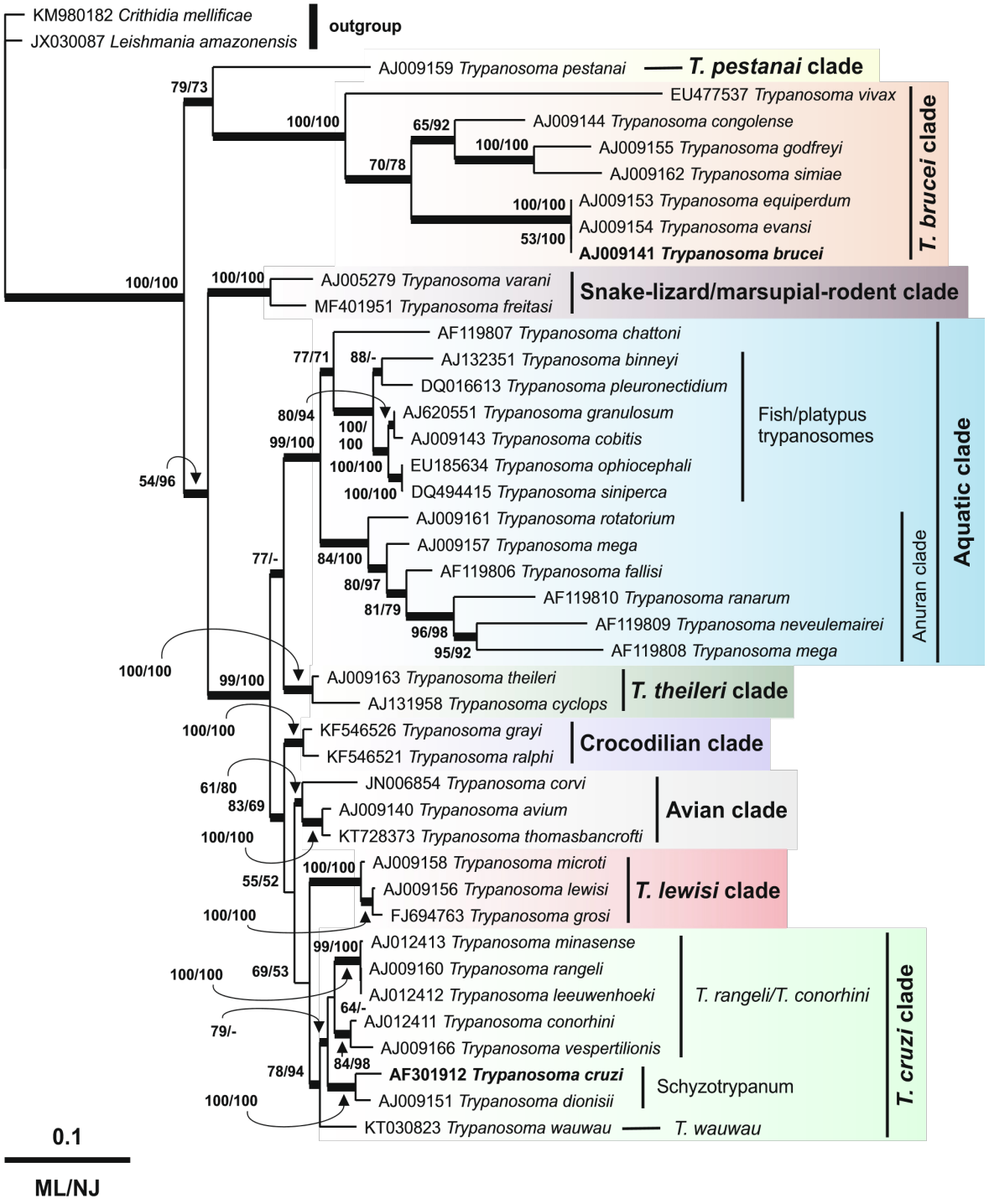

Figure 2. 18S rDNA sequence-structure maximum likelihood (ML) tree, representative subset of 43 sequences from Figure 1, obtained by phangorn as implemented in R (Schliep, 2011). Bootstrap values from 100 pseudo-replicates, mapped at the appropriate internodes, are from maximum likelihood- (ML) and neighbor-joining- (NJ, obtained by ProfDistS (Wolf et al., 2008)) analyses. For NJ tree reconstruction the global multiple sequence-structure alignment (.xfasta format) as derived by 4SALE (Seibel et al., 2008, 2006) was automatically encoded by a 12-letter alphabet (Wolf et al., 2014). For ML tree reconstruction the "one letter encoded" fasta format (12letter alphabet) as derived by 4SALE (Seibel et al., 2008, 2006) was used. GenBank identifiers accompany each taxon name. The scale bar indicates evolutionary distances. Highly supported branches are indicated by thicker lines. The tree is rooted at *Crithridia mellificae* (KM980182) and *Leishmania amazonensis* (JX030087). Clades discussed in the text are highlighted.

Regarding the other major group of our analysis (Terrestrial/Aquatic lineages), the first branching inside this group suggests the differentiation of the snake-lizard/marsupial-rodent clade as a basal group of other trypanosomes (Figure 2). However, other studies have suggested avian trypanosomes as a basal group among terrestrial lineages (Hamilton et al., 2004). This can be associated with the low bootstrap values of our tree in either three events: the snake-lizard/marsupial-rodent clade (ML = 54) differentiation, the divergence of crocodilian trypanosomes (ML = 55), and the internal branch of avian trypanosomes (ML = 61), which will be further explored in our discussion.

The *T. cruzi* and *T. lewisi* clades appear as sister groups in our analysis (Figure 2), as has been previously demonstrated (Hamilton et al., 2007, 2005, 2004; Lima et al., 2015). The *T. cruzi* clade can be subdivided into three subclades: Schizotrypanum, *T. wauwau* (and other Neotropical bat trypanosomes), and *T. rangeli/T. conorhini* (Clément et al., 2020; Lima et al., 2015). The specific sequences of *Trypanosoma minasense* CHAGAS, 1908 and *Trypanosoma leeuwenhoeki* SHAW, 1969 (AJ012413.1 and AJ012412.1, respectively) grouped with *T. rangeli* in our tree were previously considered synonyms of this species by 18S rDNA sequence analysis, explaining their positioning (Hamilton and Stevens, 2017; Sato et al., 2008). Regarding the *T. lewisi* clade, our results suggest the existence of two subclades inside the group (ML = 100), one harboring *Trypanosoma microti* LAVERAN AND PETIT, 1910, and the other with *T. lewisi* and *Trypanosoma grosi* LAVERAN AND PETIT, 1909. This finding is in accordance with a recent analysis of long fragments of 18S rDNA which demonstrated this subdivision despite the similarities in the v7v8 hypervariable region (Egan et al., 2020).

Concerning avian trypanosomes, our tree reflects previous findings in both the divergence between *T. avium* and *T. corvi* and the maximum supported (ML = 100) proximity between *T. avium* and *T. thomasbancrofti* (Sato et al., 2008; Šlapeta et al., 2016). A low bootstrap value (ML = 61) is observed in the divergence of *T. corvi* and *T. avium/T. thomasbancrofti*. It is interesting to note that we currently have two topologies known in literature, with the possibility of paraphyly demonstrated by analysis of long sequences of

18S rDNA (Hamilton et al., 2007; Šlapeta et al., 2016; Votýpka et al., 2004). This, however, was not observed in trees constructed with v7v8 hypervariable region of 18S rDNA, gGAPDH sequences, or concatenated trees using both (Fermino et al., 2019, 2015, 2013). Thus, our tree corroborates the data of phylogenies using only the long sequences of 18S rDNA. This controversy indicates the need for a better resolution on avian trypanosome positioning.

In our analysis we see the crocodilian/alligator trypanosomes (*T. grayi* and *T. ralphi*) branching together with the maximum support value (ML = 100) (Figure 2). Although *T. grayi* is found in Africa and *T. ralphi* in South America (Fermino et al., 2019, 2015, 2013), in a tree with distant external groups like ours, this topology is expected due to their proximity inside the Crocodilian clade (Fermino et al., 2019, 2013). Our tree reflects the proximity of the crocodilian trypanosomes with *T. cruzi* clade, as previously observed through full genome analysis (Kelly et al., 2014). Interestingly, crocodilian trypanosomes, such as *T. grayi* and *Trypanosoma kaiowa* TEIXEIRA AND CAMARGO, 2019 are tsetse-transmitted species that are not restricted to the sub-Saharan belt (Fermino et al., 2019, 2013; Kelly et al., 2014), suggesting higher adaptive plasticity of crocodilian trypanosomes.

The trypanosomes of the Aquatic lineage branched together (Figure 2). The subgroups observed are anuran trypanosomes (*Trypanosoma rotatorium* (MAYER, 1843), *Trypanosoma mega* DUTTON AND TODD, 1903, *Trypanosoma fallisi* MARTIN AND DESSER, 1990, *Trypanosoma ranarum* (LANKESTER, 1871), and *Trypanosoma neveulemairei* BRUMPT, 1928) and fish trypanosomes (*Trypanosoma siniperca* CHANG, 1964, *Trypanosoma ophiocephali* CHEN, 1964, *Trypanosoma cobitis* MITROPHANOW, 1884, *Trypanosoma granulosum* LAVERAN AND MESNIL, 1902, *Trypanosoma pleuronectidium* ROBERTSON, 1906) along with the platypus parasite *Trypanosoma binneyi* MACKERRAS, 1959, which is in accordance to the literature (Attias et al., 2016; Fermino et al., 2019; Lemos et al., 2015; Spodareva et al., 2018). Interestingly, the anuran parasite, *Trypanosoma chattoni* MATHIS AND LEGER, 1911, appears in our analysis more related to fish and platypus trypanosomes than to the anuran clade. This positioning of *T. chattoni*

was shown in a previous study using complete 18S rDNA sequences and non-trypanosomes as the outgroup (Martin et al., 2002). Recent trees using complete 18S rDNA sequences and concatenated analysis of v7v8 hypervariable region and gGAPDH rooted by other trypanosomes sustained either a monophyletic anuran clade (Attias et al., 2016) or the paraphyly of the group (Spodareva et al., 2018).

3.2 Expanding the analysis of *Trypanosoma*

To expand our discussion and gain insights into the questions opened by our first analysis of *Trypanosoma*, we manually included sequences of 24 species to generate a new tree. This new assembly contained representatives from all *Trypanosoma* clades and was rendered in a slightly different topology. We comparatively present the new subgenera classification, proposed to unify phylogeny and the traditional morphological descriptions (Kostygov et al., 2021), along with the former, and extensively used, clades classification (Hamilton and Stevens, 2017) (Figure 3).

In this new tree, the *T. brucei* clade (subdivided in *Duttonella*, *Nannomonas*, and *Trypanozoon*) occupies a basal position within *Trypanosoma*. Despite this change, the internal branches were not altered, confirming the solid cluster of salivarian trypanosomes (Hamilton and Stevens, 2017), which have an evolutionary origin confined to Africa, with differentiation likely occurring after continental separation in the mid-Cretaceous (Stevens et al., 1999).

The positioning of the *T. pestanai* clade changed, now resulting from a differentiation event posterior to the Salivaria. The low bootstrap value (ML = 60) highlights its unresolved positioning. While some analysis place *T. pestanai* as a sister group of the *T. brucei* clade (Hamilton et al., 2007, 2005; Yazaki et al., 2017), others present the relationship closer to trypanosomes of the Terrestrial lineage, such as snake and lizard trypanosomes (Hamilton et al., 2007) and the *T. theileri* clade (*Herpetosoma*) (McInnes et al., 2011; Stevens et al., 1999). The elucidation of the positioning of this clade would require

a detailed analysis with the inclusion of other representants, such as *Trypanosoma copemani* AUSTEN ET AL., 2009 and *Trypanosoma giletti* MCINNES ET AL., 2010. However, the inclusion of these sequences was not possible using our method. Of notice, the subgenera of *T. pestanai* in the new classification remains undetermined while *T. copemani* and *T. giletti* were placed in the subgenera *Australotrypanum* (Kostygov et al., 2021).

One of the contradictory points resulting from our first analysis was the derived position of the Avian clade. The expansion of the tree confirmed the ancestrality of Crocodilian and *T. theileri* clades (*Crocotrypanum* and *Herpetosoma*, respectively) to the *T. irwini* clade, consisting of the avian trypanosome *Trypanosoma bennetti* VALKIUNAS ET AL., 2011 and the koala parasite *Trypanosoma irwini* MCINNES ET AL., 2009. This clade is the closest ancestor of the Avian clade and the positioning of *T. bennetti* within *T. irwini* corroborates the paraphyly of avian trypanosomes (Hamilton et al., 2007; Šlapeta et al., 2016; Votýpka et al., 2004). Considering the use of only five species of avian and three species of crocodilian trypanosomes in our reconstruction, our approach represents an interesting method to be applied in further studies. In the most recent classification, the former paraphyletic Avian clade is divided into three monophyletic subgenera *Avitrypanum*, *Trypanomorpha*, and *Ornithotrypanum* while the parasite of koalas *T. irwini* has still an uncertain placement (Kostygov et al., 2021).

The inclusion of sequences from *Trypanosoma lainsoni* NAIFF AND BARRET, 2013, a mammalian parasite, and *Trypanosoma scelopori* AYALA, 1970 and *Trypanosoma cascavelli* PESSOA AND DE BIASI, 1972, reptilian parasites, increased the bootstrap support for the earlier differentiation of the snake-lizard/marsupial-rodent clade (*Squamatrypanum*), placing it as an ancestor of the Aquatic clade. The increased number of representatives in the Aquatic clade confirmed the paraphyly of anuran trypanosomes (placed in the subgenus *Trypanosoma*). This paraphyly was previously proposed based on positioning of *Trypanosoma loricatum* (MAYER, 1843) (Spodareva et al., 2018). In our analysis, *T. loricatum*, *T. chattoni*, and *Trypanosoma herthameyeri* DE SOUZA AND CAMARGO, 2015 branched as ancestors of fish, platypus, and tortoise trypanosomes (subgenus

Haematomonas). Despite the proposition of the origin of the Terrestrial lineage from amphibian trypanosomes (Spodareva et al., 2018), our data advocates the ancestrality of Terrestrial trypanosomes. Dipterans are vectors of trypanosomes from the snake-lizard/marsupial-rodent clade and were also suggested as vectors of frog trypanosomes, such as *T. rotatorium*, which are potentially transmitted by *Culex territans* WALKER, 1856 (Desser et al., 1973). Thus, it seems likely that the Aquatic clade differentiated from a successful infection of an anuran by a terrestrial trypanosome. The proximity of anurans and leeches in the aquatic environment could have engendered the perfect opportunity for the transition to this invertebrate and the further spread to other aquatic animals.

Expanding the number of representatives in the *T. lewisi* clade (*Herpetosoma*), as well as including *Trypanosoma sapaensis* MAFIE ET AL., 2019 and *Trypanosoma anourosoricis* MAFIE ET AL., 2019 in the analysis reveals two major subclades: one composed by *T. sapaensis* and *T. anourosoricis* and another formed by *T. microti*, *T. grosi*, *T. lewisi*, *Trypanosoma niviventerae* MAFIE ET AL., 2019, *Trypanosoma blanchardi* HOMMEL AND ROBERTSON, 1976, and *Trypanosoma musculi* (THIROUX, 1905). Based on morphological analysis, *T. sapaensis* and *T. anourosoricis* were proposed to belong to the *Megatrypanum* subgenus (Mafie et al., 2019). However, the same study placed both as a sister group of *T. lewisi* (Mafie et al., 2019). The taxonomical inconsistencies generated by morphological analysis of trypanosomes are well known. In fact, due to the polyphyly observed in the subgenera of stercorarian trypanosomes, it was proposed to use the subgenus *Herpetosoma* for species closely related to *T. lewisi* while *Megatrypanum* should be used for species related to *T. theileri* (Hamilton and Stevens, 2017). Thus, our tree places *T. sapaensis* and *T. anourosoricis* within the *T. lewisi* clade with a maximal support value (ML = 100), suggesting their classification as *Herpetosoma*.

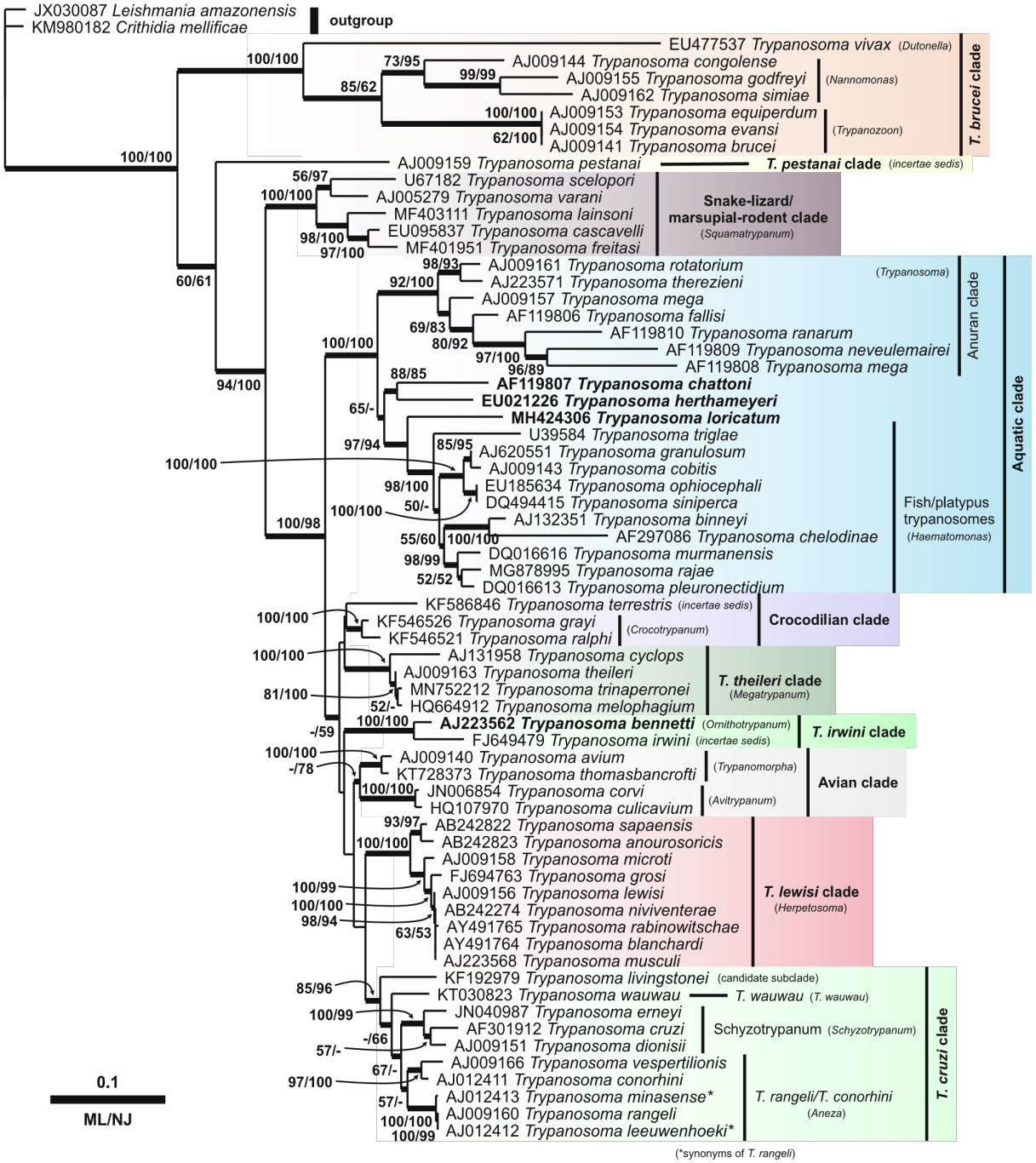

Figure 3. 18S rDNA sequence-structure maximum likelihood (ML) tree (cf. Fig. 2), with additional taxa included (cf. List S2). The previous, and extensively studied, clades (Hamilton and Stevens, 2017; Ortiz et al., 2018) and the new system based in monophyletic subgenera (Kostygov et al., 2021) are comparatively depicted.

4. Conclusions

18S rDNA is one of the most used markers in inferring phylogenies at higher taxonomic levels. However, this molecule has often been claimed to be inadequate for reconstructing phylogenetic relationships at lower taxonomic levels, in particular, because of its conservative rate of evolution. Thus, the use of the v7v8 hypervariable region has become popular inside the trypanosome community as a barcode suitable to describe new species along with gGAPDH (Hamilton and Stevens, 2017). However, some questions regarding the positioning of the groups still need to be answered. To this, evaluating bigger sequences and using different genetic markers can bring more information to the analysis improving resolution of the trees (Hamilton and Stevens, 2017). The inclusion of RNA secondary structures was shown to improve accuracy and robustness in reconstruction of phylogenetic trees through simulation studies for ITS2 rRNA gene sequence-structure data (Keller et al., 2010). Then, this approach was applied in a large number of biological case studies for ITS2 as well as exemplary for 18S rRNA gene sequence-structure data (Buchheim et al., 2017; Czech and Wolf, 2020; Heeg and Wolf, 2015; Lim et al., 2016).

In this work, we demonstrate that the simultaneous use of trypanosome 18S rRNA gene sequence and secondary structure data (i.e., the consideration of the individual secondary structures of the rRNA genes) results in reliable and robustly supported trees, which are generally in accordance with the current knowledge in the field. Our topology highlights the need for further exploration of some groups, such as the *T. pestanai*, avian and snake-lizard/marsupial-rodent clades, which are less explored in trypanosome phylogenies. Thus, the analysis of 18S rRNA gene sequence-structure data generates consistent trees, encouraging its use as an additional tool for upcoming phylogenetic reconstructions.

Summarizing discussion

A complex task of this thesis was to integrate information from the different research lines presented here – the classical cell biology and phylogenetics. While it is true that an overview of the macroevolution of the different *Trypanosoma* subgenera can provide insights into the conservation of cellular processes and/or structures, a detailed description of the endo-lysosomal system in other trypanosome species is currently lacking. Details such as the description of cargo uptake pathways, the GTPases involved in the transport, modifications in endocytosis and the endo-lysosomal system throughout the cell cycle, and plasma membrane homeostasis are still missing. Therefore, tracing a parallel between the main results of this thesis with the evolutionary history of *Trypanosoma* is remarkably difficult. Nevertheless, considering *T. brucei* as a less extensively studied organism in eukaryotic cell biology, which is deeply focused on opisthokonts (e.g., *Drosophila*, mammalian, and yeast cells), this brief discussion will be used to highlight areas of investigation for modern comparative cell biology. Whenever pertinent for the comparison, available information on other trypanosomatids will be presented.

In *T. brucei*, the cell surface constantly grows during the cell cycle (see Figure 2 – Chapter 1) but it does not double in size. This could lead to an increased cell surface tension in 2K2N cells, which may be necessary to trigger and facilitate the ingression of the cleavage furrow in the region of the division fold (see Discussion 4.2 – Chapter 1). It is tempting to speculate that the division fold acts as cytokinesis precursor, similarly to cytokinesis nodes of fission yeast (Laplante et al., 2016; Sayyad and Pollard, 2022), since molecules involved in cytokinesis (e.g., TbAUK1, TbCPC1 and TbCPC2), were recorded in this region (Kurasawa et al., 2022; Li et al., 2008). These molecules relocate from the mitotic spindle to the anterior pole of the fold in 2K2N cells (Li et al., 2008), showing a similar behavior to the chromosomal passenger complex (CPC). The CPC is found in opisthokonts and is composed of four subunits named Aurora B kinase, INCENP, Borealin, and Survivin/BORI. The last two are missing in *T. brucei* and orthologues have not been

reported (Komaki et al., 2022). In spite of the similar behavior found in the CPC-like machinery of *T. brucei*, TbCPC1 and TbCPC2 did not show sequence similarities with any CPC component of opisthokonts but conserved homologs were detected in *T. cruzi* and *Leishmania major* (Li et al., 2008), suggesting conservation among trypanosomatids and the presence of a CPC-like machinery in their common ancestor (see Figure 1 – Chapter 2).

The results presented here point to the coordinated duplication and segregation of endosomes and lysosome into the two non-equivalent daughter cells (see Figures 3 and 13 – Chapter 1). In opisthokonts, the endo-lysosomal system is believed to be inherited via stochastic segregation (Bergeland et al., 2001; Carlton et al., 2020). However, observations in *Drosophila* have suggested a coordinated inheritance of the endosomes during asymmetric cell division (Derivery et al., 2015). In *Leishmania*, the lysosome (multivesicular tubule) was shown to extend and disassemble prior to division, being reassembled in the daughter cells. This lysosomal disassembly was connected to decreased endocytosis rates (Wang et al., 2020). In *T. brucei*, endocytosis seemed not impaired during the cell cycle, as indicated by clathrin recruitment (see Figure 4 – Chapter 1). Clathrin is recruited to the flagellar pocket forming pits and vesicles (see Figures 5 and 6 – Chapter 1). Analyses in clathrin evolution showed that its heavy chain is conserved within *T. brucei* and opisthokonts while the light chain is more variable (Santos et al., 2022). AP-2, one of the primary agents involved in clathrin recruitment within opisthokonts has not been identified in *T. brucei* or any other African trypanosome. However, it is present in the genome of other trypanosomes, such as *T. cruzi*, *T. theileri*, *T. grayi*, and *T. carassii* (Kostygov et al., 2021; Link et al., 2021; Manna et al., 2013; Morgan et al., 2002). These trypanosome species are placed in subgenera with independent evolutionary history from African trypanosomes, as was shown by the phylogenetic reconstructions presented here (see Figures 2 and 3 – Chapter 2), which suggests the loss of AP-2 in the common ancestor of African trypanosomes. To move the endocytosed cargo to early endosomes, clathrin vesicles are uncoated (reviewed in Link et al., 2021). Interestingly, in *T. brucei* only one uncoating

accessory molecule was found so far, the ATPase TbHsc70, but several trypanosomatid-exclusive clathrin-associating proteins were reported (Adung'a et al., 2013). Considering that the clathrin uncoating motif "QLMLT" appears to be only present in opisthokonts (Santos et al., 2022), there is a possibility that clathrin uncoating follows a different mechanism in trypanosomes.

The colocalization analyses indicated that the endosomal subpopulations work as functionally distinct compartments (see Figure 8 – Chapter 1) but may have a physical connection (see Figures 10 and 11 – Chapter 1). Previous studies in *T. brucei* treated endosomal subpopulations as distinct compartments (reviewed in Link et al., 2021). However, the visualization of fluid-phase cargo inside Rab11 structures had already pointed to the need of further investigation of possible connections between the early and the recycling endosomes (Engstler et al., 2004). In mammals, connections between early endosomes with Rab11-positive structures have been shown (reviewed in Goldenring, 2015; Hsu and Prekeris, 2010; Scott et al., 2014). In addition, live-cell microscopy studies have suggested that Rab5-positive endosomal carrier vesicles mature into late endosomes showing a gradual substitution of Rab5 by Rab7 (Langemeyer et al., 2018; Rink et al., 2005; Scott et al., 2014). This was corroborated by colocalization analyses using CLEM showing both markers in the same structures with variable ratios within the population (van der Beek et al., 2021). In the same study, Rab7 was shown to colocalize with the lysosome (van der Beek et al., 2021), which is consistent with the proposed mechanism of fusion between late endosomes and lysosomes to form a hybrid organelle that matures into the classical lysosome (Rink et al., 2005; Scott et al., 2014). The potential physical connection of the endosomal compartments presented in this study was further investigated via electron microscopy and 3D reconstruction of electron tomograms and shows the presence of TbRab markers in regions of a long endosomal network (Link et al., 2023, preprint). The presence of cargo in continuous tubule-vesicular structures has also been recorded in *T. cruzi* (Alcantara et al., 2018). It would be tempting to suggest that the endosomal architecture is a conserved feature of the trypanosome cell. However, data on other

trypanosome species and non-opisthokont models are still insufficient, making such a proposition a mere speculation.

Finally, the morphological plasticity of the lysosome observed here (see Figures 13, 14, and 15 – Chapter 1) has been documented in mammalian cells where it was associated with a temporary boost in endocytosis (see Discussion 4.4 – Chapter 1). It is tempting to connect the structural flexibility of the *T. brucei* lysosome to the high endocytosis rates of the parasite (Engstler et al., 2007, 2004). However, the observations made here are just the tip of the iceberg in an open investigation field.

Although major progress has been made in the past years regarding the events and mechanisms underlying the cell cycle of *T. brucei*, many topics remain to be elucidated, such as how changes to organelle structure and function relate with the cell division machinery. Despite the evolutionary distance between trypanosomes (placed in the group Discoba) and Opisthokonta (Burki et al., 2020), similarities in some cellular processes can be observed between them, such as clathrin-mediated endocytosis and the presence of a CPC-like apparatus, which highlight the importance of these processes for the eukaryotic cell. At the same time, *T. brucei* and other African trypanosomes also show unique characteristics even within *Trypanosoma,* such as the absence of AP-2. Because eukaryote cell biology has been overwhelmingly focused on opisthokonts, our whole comprehension of cell biology is still limited. Thus, extending the focus to other models, as demonstrated in this thesis with *T. brucei*, would not only enhance our understanding of the evolution of eukaryotic cells but also unveil crucial biological processes of this parasite. Ultimately, such insights could significantly contribute to drug development and therapeutics.

References

Absalon, S., Kohl, L., Branche, C., Blisnick, T., Toutirais, G., Rusconi, F., Cosson, J., Bonhivers, M., Robinson, D., Bastin, P. 2007. Basal body positioning is controlled by flagellum formation in *Trypanosoma bruce*i. *PLoS One* 2, e437. https://doi.org/10.1371/journal.pone.0000437

Adikes, R.C., Kohrman, A.Q., Martinez, M.A.Q., Palmisano, N.J., Smith, J.J., Medwig-Kinney, T.N., Min, M., Sallee, M.D., Ahmed, O.B., Kim, N., Liu, S., Morabito, R.D., Weeks, N., Zhao, Q., Zhang, W., Feldman, J.L., Barkoulas, M., Pani, A.M., Spencer, S.L., Martin, B.L., Matus, D.Q. 2020. Visualizing the metazoan proliferation-quiescence decision *in vivo*. *eLife* 9, e63265. https://doi.org/10.7554/eLife.63265

Adl, S.M., Bass, D., Lane, C.E., Lukeš, J., Schoch, C.L., Smirnov, A., Agatha, S., Berney, C., Brown, M.W., Burki, F., Cárdenas, P., Čepička, I., Chistyakova, L., Campo, J. del, Dunthorn, M., Edvardsen, B., Eglit, Y., Guillou, L., Hampl, V., Heiss, A.A., Hoppenrath, M., James, T.Y., Karnkowska, A., Karpov, S., Kim, E., Kolisko, M., Kudryavtsev, A., Lahr, D.J.G., Lara, E., Gall, L.L., Lynn, D.H., Mann, D.G., Massana, R., Mitchell, E.A.D., Morrow, C., Park, J.S., Pawlowski, J.W., Powell, M.J., Richter, D.J., Rueckert, S., Shadwick, L., Shimano, S., Spiegel, F.W., Torruella, G., Youssef, N., Zlatogursky, V., Zhang, Q. 2019. Revisions to the classification, nomenclature, and diversity of eukaryotes. *Journal of Eukaryotic Microbiology* 66, 4-119. https://doi.org/10.1111/jeu.12691

Adung'a, V.O., Gadelha, C., Field, M.C. 2013. Proteomic analysis of clathrin interactions in trypanosomes reveals dynamic evolution of endocytosis. *Traffic* 14, 440-457. https://doi.org/10.1111/tra.12040

Agliarulo, I., Parashuraman, S. 2022. Golgi apparatus regulates plasma membrane composition and function. *Cells* 11, 368. https://doi.org/10.3390/cells11030368

Akhoundi, M., Kuhls, K., Cannet, A., Votýpka, J., Marty, P., Delaunay, P., Sereno, D. 2016. A historical overview of the classification, evolution, and dispersion of *Leishmania* parasites and sandflies. *PLoS Neglected Tropical Diseases* 10, e0004349. https://doi.org/10.1371/journal.pntd.0004349

Alberts, B., Johnson, A., Lewis, J., Raff, M., Roberts, K., Walter, P. 2002. An overview of the cell cycle, in Alberts, B., Johnson, A., Lewis, J., Raff, M., Roberts, K., Walter, P (eds.). Molecular Biology of the Cell. 4th Edition. New Yok: Garland Science. Available at: https://www.ncbi.nlm.nih.gov/books/NBK26869/ (Accessed: 24 July 2023).

Albertson, R., Cao, J., Hsieh, T., Sullivan, W. 2008. Vesicles and actin are targeted to the cleavage furrow via furrow microtubules and the central spindle. *Journal of Cell Biology* 181, 777-790. https://doi.org/10.1083/jcb.200803096

Alcantara, C.L., de Souza, W., Cunha E Silva, N.L. 2018. Tridimensional electron microscopy analysis of the early endosomes and endocytic traffic in *Trypanosoma cruzi* epimastigotes. *Protist* 169, 887–910. https://doi.org/10.1016/j.protis.2018.09.004

Alizadehrad, D., Krüger, T., Engstler, M., Stark, H. 2015. Simulating the complex cell design of *Trypanosoma brucei* and its motility. *PLoS Computational Biology* 11, e1003967. https://doi.org/10.1371/journal.pcbi.1003967

Allen, C.L., Goulding, D., Field, M.C. 2003. Clathrin-mediated endocytosis is essential in *Trypanosoma brucei*. *The EMBO Journal* 22, 4991-5002. https://doi.org/10.1093/emboj/cdg481

Almacellas, E., Pelletier, J., Day, C., Ambrosio, S., Tauler, A., Mauvezin, C. 2021. Lysosomal degradation ensures accurate chromosomal segregation to prevent chromosomal instability. *Autophagy* 17, 796-813. https://doi.org/10.1080/15548627.2020.1764727

Ankenbrand, M.J., Keller, A., Wolf, M., Schultz, J., Förster, F. 2015. ITS2 database V: Twice as much. *Molecular Biology and Evolution* 32, 3030-3032. https://doi.org/10.1093/molbev/msv174

Aslett, M., Aurrecoechea, C., Berriman, M., Brestelli, J., Brunk, B.P., Carrington, M., Depledge, D.P., Fischer, S., Gajria, B., Gao, X., Gardner, M.J., Gingle, A., Grant, G., Harb, O.S., Heiges, M., Hertz-Fowler, C., Houston, R., Innamorato, F., Iodice, J., Kissinger, J.C., Kraemer, E., Li, W., Logan, F.J., Miller, J.A., Mitra, S., Myler, P.J., Nayak, V., Pennington, C., Phan, I., Pinney, D.F.,

Ramasamy, G., Rogers, M.B., Roos, D.S., Ross, C., Sivam, D., Smith, D.F., Srinivasamoorthy, G., Stoeckert, C.J., Subramanian, S., Thibodeau, R., Tivey, A., Treatman, C., Velarde, G., Wang, H. 2010. TriTrypDB: a functional genomic resource for the Trypanosomatidae. *Nucleic Acids Research* 38, D457-462. https://doi.org/10.1093/nar/gkp851

Attias, M., Sato, L.H., Ferreira, R.C., Takata, C.S.A., Campaner, M., Camargo, E.P., Teixeira, M.M.G., de Souza, W. 2016. Developmental and ultrastructural characterization and phylogenetic analysis of *Trypanosoma herthameyeri* n. sp. of Brazilian Leptodactilydae frogs. *Journal of Eukaryotic Microbiology* 63, 610-622. https://doi.org/10.1111/jeu.12310

Bajorek, M., Schubert, H.L., McCullough, J., Langelier, C., Eckert, D.M., Stubblefield, W.-M.B., Uter, N.T., Myszka, D.G., Hill, C.P., Sundquist, W.I. 2009. Structural basis for ESCRT-III protein autoinhibition. *Nature Structural & Molecular Biology* 16, 754-762. https://doi.org/10.1038/nsmb.1621

Ballabio, A., Bonifacino, J.S. 2020. Lysosomes as dynamic regulators of cell and organismal homeostasis. *Nature Reviews Molecular Cell Biology* 21, 101-118. https://doi.org/10.1038/s41580-019-0185-4

Barois, N., de Saint-Vis, B., Lebecque, S., Geuze, H.J., Kleijmeer, M.J. 2002. MHC class II compartments in human dendritic cells undergo profound structural changes upon activation. *Traffic* 3, 894-905. https://doi.org/10.1034/j.1600-0854.2002.31205.x

Barral, D.C., Staiano, L., Guimas Almeida, C., Cutler, D.F., Eden, E.R., Futter, C.E., Galione, A., Marques, A.R.A., Medina, D.L., Napolitano, G., Settembre, C., Vieira, O.V., Aerts, J.M.F.G., Atakpa-Adaji, P., Bruno, G., Capuozzo, A., De Leonibus, E., Di Malta, C., Escrevente, C., Esposito, A., Grumati, P., Hall, M.J., Teodoro, R.O., Lopes, S.S., Luzio, J.P., Monfregola, J., Montefusco, S., Platt, F.M., Polishchuck, R., De Risi, M., Sambri, I., Soldati, C., Seabra, M.C. 2022. Current methods to analyze lysosome morphology, positioning, motility and function. *Traffic* 23, 238-269. https://doi.org/10.1111/tra.12839

Bartossek, T., Jones, N.G., Schäfer, C., Cvitković, M., Glogger, M., Mott, H.R., Kuper, J., Brennich, M., Carrington, M., Smith, A.-S., Fenz, S., Kisker, C., Engstler, M. 2017. Structural basis for the shielding function of the dynamic trypanosome variant surface glycoprotein coat. *Nature Microbiology* 2, 1523-1532. https://doi.org/10.1038/s41564-017-0013-6

Batram, C., Jones, N.G., Janzen, C.J., Markert, S.M., Engstler, M. 2014. Expression site attenuation mechanistically links antigenic variation and development in *Trypanosoma brucei*. *eLife* 3, e02324. https://doi.org/10.7554/eLife.02324

Bergeland, T., Widerberg, J., Bakke, O., Nordeng, T.W. 2001. Mitotic partitioning of endosomes and lysosomes. *Current Biology* 11, 644-651. https://doi.org/10.1016/S0960-9822(01)00177-4

Bi, E., Maddox, P., Lew, D.J., Salmon, E.D., McMillan, J.N., Yeh, E., Pringle, J.R. 1998. Involvement of an actomyosin contractile ring in *Saccharomyces cerevisiae* cytokinesis. *Journal of Cell Biology* 142, 1301-1312. https://doi.org/10.1083/jcb.142.5.1301

Bohl, B., Jabali, A., Ladewig, J., Koch, P. 2022. Asymmetric notch activity by differential inheritance of lysosomes in human neural stem cells. *Science Advances* 8, eabl5792. https://doi.org/10.1126/sciadv.abl5792

Bohnert, K.A., Johnson, A.E. 2022. Branching off: new insight into lysosomes as tubular organelles. *Frontiers in Cell and Developmental Biology* 10, 863922. https://doi.org/10.3389/fcell.2022.863922

Borges, A.R., Link, F., Engstler, M., Jones, N.G. 2021. The glycosylphosphatidylinositol anchor: a linchpin for cell surface versatility of trypanosomatids. *Frontiers in Cell and Developmental Biology* 9, 720536. https://doi.org/10.3389/fcell.2021.720536

Botero, A., Cooper, C., Thompson, C.K., Clode, P.L., Rose, K., Thompson, R.C.A. 2016. Morphological and phylogenetic description of *Trypanosoma noyesi* sp. nov.: an Australian wildlife trypanosome within the *T. cruzi* clade. *Protist* 167, 425-439. https://doi.org/10.1016/j.protis.2016.07.002

Botero, A., Thompson, C.K., Peacock, C.S., Clode, P.L., Nicholls, P.K., Wayne, A.F., Lymbery, A.J., Thompson, R.C.A. 2013. Trypanosomes genetic diversity, polyparasitism and the population decline of the critically endangered Australian marsupial, the brush tailed bettong or woylie

(*Bettongia penicillata*). *International Journal for Parasitology: Parasites and Wildlife* 2, 77-89. https://doi.org/10.1016/j.ijppaw.2013.03.001

Boucrot, E., Kirchhausen, T. 2008. Mammalian cells change volume during mitosis. *PLoS One* 3, e1477. https://doi.org/10.1371/journal.pone.0001477

Boucrot, E., Kirchhausen, T. 2007. Endosomal recycling controls plasma membrane area during mitosis. *Proceedings of the National Academy of Sciences of the United States of America* 104, 7939-7944. https://doi.org/10.1073/pnas.0702511104

Bright, N.A., Gratian, M.J., Luzio, J.P. 2005. Endocytic delivery to lysosomes mediated by concurrent fusion and kissing events in living cells. *Current Biology* 15, 360-365. https://doi.org/10.1016/j.cub.2005.01.049

Brocher, J. 2023. BioVoxxel_Toolbox. Available at: https://doi.org/10.5281/zenodo.5986130 (Accessed: 24 July 2023).

Bruce, D. 1895. Preliminary report on the tsetse fly disease or nagana, in Zululand. Durban: Bennett & Davis.

Bucci, C., Thomsen, P., Nicoziani, P., McCarthy, J., van Deurs, B. 2000. Rab7: a key to lysosome biogenesis. *Molecular Biology of the Cell* 11, 467-480. https://doi.org/10.1091/mbc.11.2.467

Buchheim, M.A., Müller, T., Wolf, M. 2017. 18S rDNA sequence-structure phylogeny of the Chlorophyceae with special emphasis on the Sphaeropleales. *Plant Gene* 10, 45-50. https://doi.org/10.1016/j.plgene.2017.05.005

Bülow, R., Overath, P., Davoust, J. 1988. Rapid lateral diffusion of the variant surface glycoprotein in the coat of *Trypanosoma brucei*. *Biochemistry* 27, 2384-2388. https://doi.org/10.1021/bi00407a020

Burki, F., Roger, A.J., Brown, M.W., Simpson, A.G.B. 2020. The new tree of eukaryotes. *Trends in Ecology & Evolution* 35, 43-55. https://doi.org/10.1016/j.tree.2019.08.008

Caffrey, C.R., Hansell, E., Lucas, K.D., Brinen, L.S., Alvarez Hernandez, A., Cheng, J., Gwaltney, S.L., Roush, W.R., Stierhof, Y.D., Bogyo, M., Steverding, D., McKerrow, J.H. 2001. Active site mapping, biochemical properties and subcellular localization of rhodesain, the major cysteine protease of *Trypanosoma brucei rhodesiense*. *Molecular and Biochemical Parasitology* 118, 61-73. https://doi.org/10.1016/s0166-6851(01)00368-1

Cannone, J.J., Subramanian, S., Schnare, M.N., Collett, J.R., D'Souza, L.M., Du, Y., Feng, B., Lin, N., Madabusi, L.V., Müller, K.M., Pande, N., Shang, Z., Yu, N., Gutell, R.R. 2002. The comparative RNA web (CRW) site: an online database of comparative sequence and structure information for ribosomal, intron, and other RNAs. *BMC Bioinformatics* 3, 2. https://doi.org/10.1186/1471-2105-3-2

Capalbo, L., D'Avino, P.P., Archambault, V., Glover, D.M. 2011. Rab5 GTPase controls chromosome alignment through Lamin disassembly and relocation of the NuMA-like protein Mud to the poles during mitosis. *Proceedings of the National Academy of Sciences of the United States of America* 108, 17343-17348. https://doi.org/10.1073/pnas.1103720108

Carbajo, C.G., Cornell, L.J., Madbouly, Y., Lai, Z., Yates, P.A., Tinti, M., Tiengwe, C. 2021. Novel aspects of iron homeostasis in pathogenic bloodstream form *Trypanosoma brucei*. *PLoS Pathogens* 17, e1009696. https://doi.org/10.1371/journal.ppat.1009696

Cardona, A., Saalfeld, S., Schindelin, J., Arganda-Carreras, I., Preibisch, S., Longair, M., Tomancak, P., Hartenstein, V., Douglas, R.J. 2012. TrakEM2 software for neural circuit reconstruction. *PLoS One* 7, e38011. https://doi.org/10.1371/journal.pone.0038011

Carlton, J.G., Jones, H., Eggert, U.S. 2020. Membrane and organelle dynamics during cell division. *Nature Reviews Molecular Cell Biology* 21, 151-166. https://doi.org/10.1038/s41580-019-0208-1

Carnes, J., Anupama, A., Balmer, O., Jackson, A., Lewis, M., Brown, R., Cestari, I., Desquesnes, M., Gendrin, C., Hertz-Fowler, C., Imamura, H., Ivens, A., Kořený, L., Lai, D.-H., MacLeod, A., McDermott, S.M., Merritt, C., Monnerat, S., Moon, W., Myler, P., Phan, I., Ramasamy, G., Sivam, D., Lun, Z.-R., Lukeš, J., Stuart, K., Schnaufer, A. 2015. Genome and phylogenetic analyses of *Trypanosoma evansi* reveal extensive similarity to *T. brucei* and multiple

independent origins for dyskinetoplasty. *PLoS Neglected Tropical Diseases* 9, e3404. https://doi.org/10.1371/journal.pntd.0003404

Cavalier-Smith, T. 2016. Higher classification and phylogeny of Euglenozoa. *European Journal of Protistology* 56, 250-276. https://doi.org/10.1016/j.ejop.2016.09.003

Cerón-Romero, M.A., Fonseca, M.M., de Oliveira Martins, L., Posada, D., Katz, L.A. 2022. Phylogenomic analyses of 2,786 genes in 158 lineages support a root of the eukaryotic tree of life between opisthokonts and all other lineages. *Genome Biology and Evolution* 14, evac119. https://doi.org/10.1093/gbe/evac119

Champion, L., Linder, M.I., Kutay, U. 2017. Cellular reorganization during mitotic entry. *Trends in Cell Biology* 27, 26-41. https://doi.org/10.1016/j.tcb.2016.07.004

Cheng, J., Grassart, A., Drubin, D.G. 2012. Myosin 1E coordinates actin assembly and cargo trafficking during clathrin-mediated endocytosis. *Molecular Biology of the Cell* 23, 2891-2904. https://doi.org/10.1091/mbc.E11-04-0383

Chung, J.Y.M., Steen, J.A., Schwarz, T.L. 2016. Phosphorylation-induced motor shedding is required at mitosis for proper distribution and passive inheritance of mitochondria. *Cell Reports* 16, 2142-2155. https://doi.org/10.1016/j.celrep.2016.07.055

Chung, W.L., Carrington, M., Field, M.C. 2004. Cytoplasmic targeting signals in transmembrane invariant surface glycoproteins of trypanosomes. *Journal of Biological Chemistry* 279, 54887-54895. https://doi.org/10.1074/jbc.M409311200

Clément, L., Dietrich, M., Markotter, W., Fasel, N.J., Monadjem, A., López-Baucells, A., Scaravelli, D., Théou, P., Pigeault, R., Ruedi, M., Christe, P. 2020. Out of Africa: the origins of the protozoan blood parasites of the *Trypanosoma cruzi* clade found in bats from Africa. *Molecular Phylogenetics and Evolution* 145, 106705. https://doi.org/10.1016/j.ympev.2019.106705

Cocucci, E., Aguet, F., Boulant, S., Kirchhausen, T. 2012. The first five seconds in the life of a clathrin-coated pit. *Cell* 150, 495-507. https://doi.org/10.1016/j.cell.2012.05.047

Craig, A.M., Wyborski, R.J., Banker, G. 1995. Preferential addition of newly synthesized membrane protein at axonal growth cones. *Nature* 375, 592-594. https://doi.org/10.1038/375592a0

Crilly, N.P., Mugnier, M.R. 2021. Thinking outside the blood: Perspectives on tissue-resident *Trypanosoma brucei*. *PLoS Pathogens* 17, e1009866. https://doi.org/10.1371/journal.ppat.1009866

Cross, G.A. 1975. Identification, purification and properties of clone-specific glycoprotein antigens constituting the surface coat of *Trypanosoma brucei*. *Parasitology* 71, 393-417. https://doi.org/10.1017/s003118200004717x

Cross, G.A., Kim, H.S., Wickstead, B. 2014. Capturing the variant surface glycoprotein repertoire (the VSGnome) of *Trypanosoma brucei* Lister 427. *Molecular and Biochemical Parasitology 195*, 59-73. https://doi.org/10.1016/j.molbiopara.2014.06.004

Crowther, R.A., Pearse, B.M. 1981. Assembly and packing of clathrin into coats. *Journal of Cell Biology* 91, 790-797. https://doi.org/10.1083/jcb.91.3.790

Cullen, P.J., Steinberg, F. 2018. To degrade or not to degrade: mechanisms and significance of endocytic recycling. *Nature Reviews Molecular Cell Biology* 19, 679-696. https://doi.org/10.1038/s41580-018-0053-7

Czech, V., Wolf, M. 2020. RNA consensus structures for inferring green algal phylogeny: a three-taxon analysis for *Golenkinia*/*Jenufa*, Sphaeropleales and Volvocales (Chlorophyta, Chlorophyceae). *Fottea* 20, 68-74. https://doi.org/10.5507/fot.2019.016

de França, L.R., Ghosh, S., Ye, S.J., Russell, L.D. 1993. Surface and surface-to-volume relationships of the Sertoli cell during the cycle of the seminiferous epithelium in the rat1. *Biology of Reproduction* 49, 1215-1228. https://doi.org/10.1095/biolreprod49.6.1215

Dean, S., Sunter, J.D., Wheeler, R.J. 2017. TrypTag.org: a trypanosome genome-wide protein localisation resource. *Trends in Parasitology* 33, 80-82. https://doi.org/10.1016/j.pt.2016.10.009

Derivery, E., Seum, C., Daeden, A., Loubéry, S., Holtzer, L., Jülicher, F., Gonzalez-Gaitan, M. 2015. Polarized endosome dynamics by spindle asymmetry during asymmetric cell division. *Nature* 528, 280-285. https://doi.org/10.1038/nature16443

Desser, S.S., McIver, S.B., Ryckman, A. 1973. *Culex territans* as a potential vector of *Trypanosoma rotatorium*. I. Development of the flagellate in the mosquito. *The Journal of Parasitology* 59, 353-358. https://doi.org/10.2307/3278833

Dey, G., Culley, S., Curran, S., Schmidt, U., Henriques, R., Kukulski, W., Baum, B. 2020. Closed mitosis requires local disassembly of the nuclear envelope. *Nature* 585, 119–123. https://doi.org/10.1038/s41586-020-2648-3

Dobigny, G., Poirier, P., Hima, K., Cabaret, O., Gauthier, P., Tatard, C., Costa, J.M., Bretagne, S. 2011. Molecular survey of rodent-borne *Trypanosoma* in Niger with special emphasis on *T. lewisi* imported by invasive black rats. *Acta Tropica* 117, 183-188. https://doi.org/10.1016/j.actatropica.2010.11.004

Du, Y., Maslov, D.A., Chang, K.P. 1994. Monophyletic origin of (division proteobacterial endosymbionts and their coevolution with insect trypanosomatid protozoa *Blastocrithidia culicis* and *Crithidia* spp. *Proceedings of the National Academy of Sciences of the United States of America* 91, 8437-8441. https://doi.org/10.1073/pnas.91.18.8437

Edgar, J.R. 2016. Q&A: What are exosomes, exactly? *BMC Biology* 14, 46. https://doi.org/10.1186/s12915-016-0268-z

Egan, S.L., Taylor, C.L., Austen, J.M., Banks, P.B., Ahlstrom, L.A., Ryan, U.M., Irwin, P.J., Oskam, C.L. 2020. Molecular identification of the *Trypanosoma* (*Herpetosoma*) *lewisi* clade in black rats (*Rattus rattus*) from Australia. *Parasitology Research* 119, 1691-1696. https://doi.org/10.1007/s00436-020-06653-z

Encarnação, M., Espada, L., Escrevente, C., Mateus, D., Ramalho, J., Michelet, X., Santarino, I., Hsu, V.W., Brenner, M.B., Barral, D.C., Vieira, O.V. 2016. A Rab3a-dependent complex essential for lysosome positioning and plasma membrane repair. *Journal of Cell Biology* 213, 631-640. https://doi.org/10.1083/jcb.201511093

Engstler, M., Boshart, M. 2004. Cold shock and regulation of surface protein trafficking convey sensitization to inducers of stage differentiation in *Trypanosoma brucei*. *Genes & Development* 18, 2798-2811. https://doi.org/10.1101/gad.323404

Engstler, M., Pfohl, T., Herminghaus, S., Boshart, M., Wiegertjes, G., Heddergott, N., Overath, P. 2007. Hydrodynamic flow-mediated protein sorting on the cell surface of trypanosomes. *Cell* 131, 505-515. https://doi.org/10.1016/j.cell.2007.08.046

Engstler, M., Thilo, L., Weise, F., Grünfelder, C.G., Schwarz, H., Boshart, M., Overath, P. 2004. Kinetics of endocytosis and recycling of the GPI-anchored variant surface glycoprotein in *Trypanosoma brucei*. *Journal of Cell Science* 117, 1105-1115. https://doi.org/10.1242/jcs.00938

Esau, K., Gill, R.H. 1965. Observations on cytokinesis. *Planta* 67, 168–181.

Faria, J.R.C. 2021. A nuclear enterprise: zooming in on nuclear organization and gene expression control in the African trypanosome. *Parasitology* 148, 1237-1253. https://doi.org/10.1017/S0031182020002437

Feliciano, D., Di Pietro, S.M. 2012. SLAC, a complex between Sla1 and Las17, regulates actin polymerization during clathrin-mediated endocytosis. *Molecular Biology of the Cell* 23, 4256-4272. https://doi.org/10.1091/mbc.E11-12-1022

Felsenstein, J. 1981. Evolutionary trees from gene frequencies and quantitative characters: finding maximum likelihood estimates. *Evolution* 35, 1229-1242. https://doi.org/10.1111/j.1558-5646.1981.tb04991.x

Ferguson, M.A. 1997. The surface glycoconjugates of trypanosomatid parasites. *Philosophical Transactions of the Royal Society B: Biological Sciences* 352, 1295-1302. https://doi.org/10.1098/rstb.1997.0113

Ferguson, M.A., Homans, S.W., Dwek, R.A., Rademacher, T.W. 1988. Glycosyl-phosphatidylinositol moiety that anchors *Trypanosoma brucei* variant surface glycoprotein to the membrane. *Science* 239, 753-759. https://doi.org/10.1126/science.3340856

Fermino, B.R., Paiva, F., Soares, P., Tavares, L.E.R., Viola, L.B., Ferreira, R.C., Botero-Arias, R., de-Paula, C.D., Campaner, M., Takata, C.S.A., Teixeira, M.M.G., Camargo, E.P. 2015. Field and experimental evidence of a new caiman trypanosome species closely phylogenetically related to fish trypanosomes and transmitted by leeches. *International Journal for Parasitology: Parasites and Wildlife* 4, 368-378. https://doi.org/10.1016/j.ijppaw.2015.10.005

Fermino, B.R., Paiva, F., Viola, L.B., Rodrigues, C.M.F., Garcia, H.A., Campaner, M., Takata, C.S.A., Sheferaw, D., Kisakye, J.J., Kato, A., Jared, C.A.G.S., Teixeira, M.M.G., Camargo, E.P. 2019. Shared species of crocodilian trypanosomes carried by tabanid flies in Africa and South America, including the description of a new species from caimans, *Trypanosoma kaiowa* n. sp. *Parasites & Vectors* 12, 225. https://doi.org/10.1186/s13071-019-3463-2

Fermino, B.R., Viola, L.B., Paiva, F., Garcia, H.A., de Paula, C.D., Botero-Arias, R., Takata, C.S.A., Campaner, M., Hamilton, P.B., Camargo, E.P., Teixeira, M.M.G. 2013. The phylogeography of trypanosomes from South American alligatorids and African crocodilids is consistent with the geological history of South American river basins and the transoceanic dispersal of *Crocodylus* at the Miocene. *Parasites & Vectors 6*, 313. https://doi.org/10.1186/1756-3305-6-313

Field, H., Farjah, M., Pal, A., Gull, K., Field, M.C. 1998. Complexity of trypanosomatid endocytosis pathways revealed by Rab4 and Rab5 isoforms in *Trypanosoma brucei*. *Journal of Biological Chemistry* 273, 32102-32110. https://doi.org/10.1074/jbc.273.48.32102

Fielding, A.B., Willox, A.K., Okeke, E., Royle, S.J. 2012. Clathrin-mediated endocytosis is inhibited during mitosis. *Proceedings of the National Academy of Sciences of the United States of America* 109, 6572-6577. https://doi.org/10.1073/pnas.1117401109

Figard, L., Sokac, A.M. 2014. A membrane reservoir at the cell surface. *Bioarchitecture* 4, 39–46. https://doi.org/10.4161/bioa.29069

Flegontov, P., Votýpka, J., Skalický, T., Logacheva, M.D., Penin, A.A., Tanifuji, G., Onodera, N.T., Kondrashov, A.S., Volf, P., Archibald, J.M., Lukeš, J. 2013. *Paratrypanosoma* is a novel early-branching trypanosomatid. *Current Biology* 23, 1787-1793. https://doi.org/10.1016/j.cub.2013.07.045

Follett, E.A.C., Goldman, R.D. 1970. The occurrence of microvilli during spreading and growth of BHK21/C13 fibroblasts. *Experimental Cell Research* 59, 124-136. https://doi.org/10.1016/0014-4827(70)90631-2

Frappaolo, A., Piergentili, R., Giansanti, M.G. 2022. Microtubule and actin cytoskeletal dynamics in male meiotic cells of *Drosophila melanogaster*. *Cells* 11, 695. https://doi.org/10.3390/cells11040695

Fraschini, R. 2020. Cytokinesis in eukaryotic cells: the furrow complexity at a glance. *Cells* 9, 271. https://doi.org/10.3390/cells9020271

Fujimoto, L.M., Roth, R., Heuser, J.E., Schmid, S.L. 2000. Actin assembly plays a variable, but not obligatory role in receptor-mediated endocytosis in mammalian cells. *Traffic* 1, 161-171. https://doi.org/10.1034/j.1600-0854.2000.010208.x

Futter, C.E., Pearse, A., Hewlett, L.J., Hopkins, C.R. 1996. Multivesicular endosomes containing internalized EGF-EGF receptor complexes mature and then fuse directly with lysosomes. *Journal of Cell Biology* 132, 1011-1023. https://doi.org/10.1083/jcb.132.6.1011

Gabernet-Castello, C., Dacks, J.B., Field, M.C. 2009. The single ENTH-domain protein of trypanosomes; endocytic functions and evolutionary relationship with epsin. *Traffic* 10, 894-911. https://doi.org/10.1111/j.1600-0854.2009.00910.x

Gadelha, C., Rothery, S., Morphew, M., McIntosh, J.R., Severs, N.J., Gull, K. 2009. Membrane domains and flagellar pocket boundaries are influenced by the cytoskeleton in African trypanosomes. *Proceedings of the National Academy of Sciences of the United States of America* 106, 17425-17430. https://doi.org/10.1073/pnas.0909289106

Galletta, B.J., Chuang, D.Y., Cooper, J.A. 2008. Distinct roles for Arp2/3 regulators in actin assembly and endocytosis. *PLoS Biology* 6, e1. https://doi.org/10.1371/journal.pbio.0060001

Gao, C.H., Yu, G., Cai, P. 2021. ggVennDiagram: An intuitive, easy-to-use, and highly customizable R package to generate Venn diagram. *Frontiers in Genetics* 12, 706907. https://doi.org/10.3389/fgene.2021.706907

García-Salcedo, J.A., Pérez-Morga, D., Gijón, P., Dilbeck, V., Pays, E., Nolan, D.P. 2004. A differential role for actin during the life cycle of *Trypanosoma brucei*. *The EMBO Journal* 23, 780-789. https://doi.org/10.1038/sj.emboj.7600094

Gauthier, N.C., Rossier, O.M., Mathur, A., Hone, J.C., Sheetz, M.P. 2009. Plasma membrane area increases with spread area by exocytosis of a GPI-anchored protein compartment. *Molecular Biology of the Cell* 20, 3261-3272. https://doi.org/10.1091/mbc.e09-01-0071

Geuze, H.J., Slot, J.W., Strous, G.J., Hasilik, A., von Figura, K. 1985. Possible pathways for lysosomal enzyme delivery. *Journal of Cell Biology* 101, 2253-2262. https://doi.org/10.1083/jcb.101.6.2253

Geuze, H.J., Slot, J.W., Strous, G.J., Lodish, H.F., Schwartz, A.L. 1983. Intracellular site of asialoglycoprotein receptor-ligand uncoupling: double-label immunoelectron microscopy during receptor-mediated endocytosis. *Cell* 32, 277-287. https://doi.org/10.1016/0092-8674(83)90518-4

Geuze, H.J., Stoorvogel, W., Strous, G.J., Slot, J.W., Bleekemolen, J.E., Mellman, I. 1988. Sorting of mannose 6-phosphate receptors and lysosomal membrane proteins in endocytic vesicles. *Journal of Cell Biology* 107, 2491-2501. https://doi.org/10.1083/jcb.107.6.2491

Gilden, J.K., Umaer, K., Kruzel, E.K., Hecht, O., Correa, R.O., Mansfield, J.M., Bangs, J.D. 2017. The role of the PI(3,5)P2 kinase TbFab1 in endo/lysosomal trafficking in *Trypanosoma brucei*. *Molecular and Biochemical Parasitology* 214, 52-61. https://doi.org/10.1016/j.molbiopara.2017.03.005

Glogger, M., Stichler, S., Subota, I., Bertlein, S., Spindler, M.C., Teßmar, J., Groll, J., Engstler, M., Fenz, S.F. 2017. Live-cell super-resolution imaging of intrinsically fast moving flagellates. *Journal of Physics D: Applied Physics* 50, 074004. https://doi.org/10.1088/1361-6463/aa54eb

Gluenz, E., Povelones, M.L., Englund, P.T., Gull, K. 2011. The kinetoplast duplication cycle in *Trypanosoma brucei* is orchestrated by cytoskeleton-mediated cell morphogenesis. *Molecular and Cellular Biology* 31, 1012-1021. https://doi.org/10.1128/MCB.01176-10

Goldenring, J.R. 2015. Recycling endosomes. *Current Opinion in Cell Biology* 35, 117-122. https://doi.org/10.1016/j.ceb.2015.04.018

Gommers-Ampt, J.H., Van Leeuwen, F., de Beer, A.L., Vliegenthart, J.F., Dizdaroglu, M., Kowalak, J.A., Crain, P.F., Borst, P. 1993. Beta-D-glucosyl-hydroxymethyluracil: a novel modified base present in the DNA of the parasitic protozoan *T. brucei*. *Cell* 75, 1129-1136. https://doi.org/10.1016/0092-8674(93)90322-h

Gottlieb, T.A., Ivanov, I.E., Adesnik, M., Sabatini, D.D. 1993. Actin microfilaments play a critical role in endocytosis at the apical but not the basolateral surface of polarized epithelial cells. *Journal of Cell Biology* 120, 695-710. https://doi.org/10.1083/jcb.120.3.695

Granot, D., Snyder, M. 1991. Glucose induces cAMP-independent growth-related changes in stationary-phase cells of *Saccharomyces cerevisiae*. *Proceedings of the National Academy of Sciences of the United States of America* 88, 5724-5728. https://doi.org/10.1073/pnas.88.13.572

Gruenberg, J., Griffiths, G., Howell, K.E. 1989. Characterization of the early endosome and putative endocytic carrier vesicles *in vivo* and with an assay of vesicle fusion *in vitro*. *Journal of Cell Biology* 108, 1301-1316. https://doi.org/10.1083/jcb.108.4.1301

Grünfelder, C.G., Engstler, M., Weise, F., Schwarz, H., Stierhof, Y.D., Boshart, M., Overath, P. 2002. Accumulation of a GPI-anchored protein at the cell surface requires sorting at multiple intracellular levels. *Traffic* 3, 547-559. https://doi.org/10.1034/j.1600-0854.2002.30805.x

Grünfelder, C.G., Engstler, M., Weise, F., Schwarz, H., Stierhof, Y.D., Morgan, G.W., Field, M.C., Overath, P. 2003. Endocytosis of a glycosylphosphatidylinositol-anchored protein via clathrin-coated vesicles, sorting by default in endosomes, and exocytosis via RAB11-positive carriers. *Molecular Biology of the Cell* 14, 2029-2040. https://doi.org/10.1091/mbc.e02-10-0640

Gull, K. 2003. Host–parasite interactions and trypanosome morphogenesis: a flagellar pocketful of goodies. *Current Opinion in Microbiology* 6, 365-370. https://doi.org/10.1016/S1369-5274(03)00092-4

Gulluni, F., Prever, L., Li, H., Krafcikova, P., Corrado, I., Lo, W.-T., Margaria, J.P., Chen, A., De Santis, M.C., Cnudde, S.J., Fogerty, J., Yuan, A., Massarotti, A., Sarijalo, N.T., Vadas, O., Williams, R.L., Thelen, M., Powell, D.R., Schueler, M., Wiesener, M.S., Balla, T., Baris, H.N., Tiosano, D., McDermott, B.M., Perkins, B.D., Ghigo, A., Martini, M., Haucke, V., Boura, E., Merlo, G.R., Buchner, D.A., Hirsch, E. 2021. PI(3,4)P2-mediated cytokinetic abscission prevents early senescence and cataract formation. *Science* 374, eabk0410. https://doi.org/10.1126/science.abk0410

Günzel, M. 2010. Charakterisierung des Transportweges von GPI-verankerten Proteinen in *T. brucei*. PhD Thesis. Universität Darmstadt, Darmstadt.

Hager, K.M., Hajduk, S.L. 1997. Mechanism of resistance of African trypanosomes to cytotoxic human HDL. *Nature* 385, 823-826. https://doi.org/10.1038/385823a0

Halcrow, E.F.J., Mazza, R., Diversi, A., Enright, A., D'Avino, P.P. 2022. Midbody proteins display distinct dynamics during cytokinesis. *Cells* 11, 3337. https://doi.org/10.3390/cells11213337

Hall, B., Allen, C.L., Goulding, D., Field, M.C. 2004a. Both of the Rab5 subfamily small GTPases of *Trypanosoma brucei* are essential and required for endocytosis. *Molecular and Biochemical Parasitology* 138, 67-77. https://doi.org/10.1016/j.molbiopara.2004.07.007

Hall, B., Pal, A., Goulding, D., Field, M.C. 2004b. Rab4 is an essential regulator of lysosomal trafficking in trypanosomes. *Journal of Biological Chemistry* 279, 45047-45056. https://doi.org/10.1074/jbc.M407271200

Hall, B., Smith, E., Langer, W., Jacobs, L.A., Goulding, D., Field, M.C. 2005. Developmental variation in Rab11-dependent trafficking in *Trypanosoma brucei*. *Eukaryotic Cell* 4, 971-980. https://doi.org/10.1128/EC.4.5.971-980.2005

Halliday, C., Billington, K., Wang, Z., Madden, R., Dean, S., Sunter, J.D., Wheeler, R.J. 2019. Cellular landmarks of *Trypanosoma brucei* and *Leishmania mexicana*. *Molecular and Biochemical Parasitology* 230, 24-36. https://doi.org/10.1016/j.molbiopara.2018.12.003

Hamilton, P.B., Adams, E.R., Njiokou, F., Gibson, W.C., Cuny, G., Herder, S. 2009. Phylogenetic analysis reveals the presence of the *Trypanosoma cruzi* clade in African terrestrial mammals. *Infection, Genetics and Evolution* 9, 81-86. https://doi.org/10.1016/j.meegid.2008.10.011

Hamilton, P.B., Gibson, W.C., Stevens, J.R. 2007. Patterns of co-evolution between trypanosomes and their hosts deduced from ribosomal RNA and protein-coding gene phylogenies. *Molecular Phylogenetics and Evolution* 44, 15-25. https://doi.org/10.1016/j.ympev.2007.03.023

Hamilton, P.B., Stevens, J.R. 2017. Classification and phylogeny of *Trypanosoma cruzi*, in: Telleria, J., Tibayrenc, M. (eds.). American trypanosomiasis Chagas disease. London: Elsevier, pp. 321–344.

Hamilton, P.B., Stevens, J.R., Gaunt, M.W., Gidley, J., Gibson, W.C. 2004. Trypanosomes are monophyletic: evidence from genes for glyceraldehyde phosphate dehydrogenase and small subunit ribosomal RNA. *International Journal for Parasitology* 34, 1393-1404. https://doi.org/10.1016/j.ijpara.2004.08.011

Hamilton, P.B., Stevens, J.R., Gidley, J., Holz, P., Gibson, W.C. 2005. A new lineage of trypanosomes from Australian vertebrates and terrestrial bloodsucking leeches (Haemadipsidae). *International The Journal of Parasitology* 35, 431-443. https://doi.org/10.1016/j.ijpara.2004.12.005

Harding, C., Heuser, J., Stahl, P. 1983. Receptor-mediated endocytosis of transferrin and recycling of the transferrin receptor in rat reticulocytes. *Journal of Cell Biology* 97, 329-339. https://doi.org/10.1083/jcb.97.2.329

Hart, D.T., Baudhuin, P., Opperdoes, F.R., de Duve, C. 1987. Biogenesis of the glycosome in *Trypanosoma brucei*: the synthesis, translocation and turnover of glycosomal polypeptides. *The EMBO Journal* 6, 1403–1411. https://doi.org/10.1002/j.1460-2075.1987.tb02381.x

Hartel, A.J.W., Glogger, M., Guigas, G., Jones, N.G., Fenz, S.F., Weiss, M., Engstler, M. 2015. The molecular size of the extra-membrane domain influences the diffusion of the GPI-anchored VSG on the trypanosome plasma membrane. *Scientific Reports* 5, 10394. https://doi.org/10.1038/srep10394

Hartel, A.J.W., Glogger, M., Jones, N.G., Abuillan, W., Batram, C., Hermann, A., Fenz, S.F., Tanaka, M., Engstler, M. 2016. N-glycosylation enables high lateral mobility of GPI-anchored proteins at a molecular crowding threshold. *Nature Communications* 7, 12870. https://doi.org/10.1038/ncomms12870

Haucke, V., Kozlov, M.M. 2018. Membrane remodeling in clathrin-mediated endocytosis. *Journal of Cell Science* 131, jcs216812. https://doi.org/10.1242/jcs.216812

Heddergott, N. 2006. Clathrin-mediated endocytosis in *Trypanosoma brucei*. Master thesis. LMU München, München.

Heeg, J.S., Wolf, M. 2015. ITS2 and 18S rDNA sequence-structure phylogeny of *Chlorella* and allies (Chlorophyta, Trebouxiophyceae, Chlorellaceae). *Plant Gene* 4, 20-28. https://doi.org/10.1016/j.plgene.2015.08.001

Hehnly, H., Doxsey, S. 2014. Rab11 endosomes contribute to mitotic spindle organization and orientation. *Developmental Cell* 28, 497-507. https://doi.org/10.1016/j.devcel.2014.01.014

Hempelmann, A., Hartleb, L., van Straaten, M., Hashemi, H., Zeelen, J.P., Bongers, K., Papavasiliou, F.N., Engstler, M., Stebbins, C.E., Jones, N.G. 2021. Nanobody-mediated macromolecular crowding induces membrane fission and remodeling in the African trypanosome. *Cell Reports* 37, 109923. https://doi.org/10.1016/j.celrep.2021.109923

Hilton, N.A., Sladewski, T.E., Perry, J.A., Pataki, Z., Sinclair-Davis, A.N., Muniz, R.S., Tran, H.L., Wurster, J.I., Seo, J., de Graffenried, C.L. 2018. Identification of TOEFAZ1-interacting proteins reveals key regulators of *Trypanosoma brucei* cytokinesis. *Molecular Microbiology* 109, 306-326. https://doi.org/10.1111/mmi.13986

Hoffmann, A., Käser, S., Jakob, M., Amodeo, S., Peitsch, C., Týč, J., Vaughan, S., Zuber, B., Schneider, A., Ochsenreiter, T. 2018. Molecular model of the mitochondrial genome segregation machinery in *Trypanosoma brucei*. *Proceedings of the National Academy of Sciences of the United States of America* 115, 1809-1818. https://doi.org/10.1073/pnas.1716582115

Hsu, V.W., Prekeris, R. 2010. Transport at the recycling endosome. *Current Opinion in Cell Biology, Membranes and organelles* 22, 528-534. https://doi.org/10.1016/j.ceb.2010.05.008

Hu, H., An, T., Kurasawa, Y., Zhou, Q., Li, Z. 2019. The trypanosome-specific proteins FPRC and CIF4 regulate cytokinesis initiation by recruiting CIF1 to the cytokinesis initiation site. *Journal of Biological Chemistry* 294, 16672-16683. https://doi.org/10.1074/jbc.RA119.010538

Hughes, A.L., Piontkivska, H. 2003. Phylogeny of Trypanosomatidae and Bodonidae (Kinetoplastida) based on 18S rRNA: evidence for paraphyly of *Trypanosoma* and six other genera. *Molecular Biology and Evolution* 20, 644-652. https://doi.org/10.1093/molbev/msg062

Hughes, L., Towers, K., Starborg, T., Gull, K., Vaughan, S. 2013. A cell-body groove housing the new flagellum tip suggests an adaptation of cellular morphogenesis for parasitism in the bloodstream form of *Trypanosoma brucei*. *Journal of Cell Science* 126, 5748-5757. https://doi.org/10.1242/jcs.139139

Hughes, L., Borrett, S., Towers, K., Starborg, T., Vaughan, S. 2017. Patterns of organelle ontogeny through a cell cycle revealed by whole-cell reconstructions using 3D electron microscopy. *Journal of Cell Science* 130, 637-647. https://doi.org/10.1242/jcs.198887

Jackson, D.G., Owen, M.J., Voorheis, H.P. 1985. A new method for the rapid purification of both the membrane-bound and released forms of the variant surface glycoprotein from *Trypanosoma brucei*. *Biochemical Journal* 230, 195-202. https://doi.org/10.1042/bj2300195

Jeffries, T.R., Morgan, G.W., Field, M.C. 2001. A developmentally regulated Rab11 homologue in *Trypanosoma brucei* is involved in recycling processes. *Journal of Cell Science* 114, 2617-2626. https://doi.org/10.1242/jcs.114.14.2617

Ji, H.H., Yao, L.L., Liu, C., Li, X. 2019. Regulation of Myosin-5b by Rab11a and the Rab11 family interacting protein 2. *Bioscience Reports* 39, BSR20181252. https://doi.org/10.1042/BSR20181252

Jin, H., Tang, Y., Yang, L., Peng, X., Li, B., Fan, Q., Wei, S., Yang, S., Li, X., Wu, B., Huang, M., Tang, S., Liu, J., Li, H. 2021. Rab GTPases: central coordinators of membrane trafficking in cancer. *Frontiers in Cell and Developmental Biology* 9, 648384. https://doi.org/10.3389/fcell.2021.648384

Johnstone, R.M., Adam, M., Hammond, J.R., Orr, L., Turbide, C. 1987. Vesicle formation during reticulocyte maturation. Association of plasma membrane activities with released vesicles (exosomes). *Journal of Biological Chemistry* 262, 9412-9420. https://doi.org/10.1016/S0021-9258(18)48095-7

Jongsma, M.L.M., Berlin, I., Neefjes, J. 2015. On the move: organelle dynamics during mitosis. *Trends in Cell Biology* 25, 112-124. https://doi.org/10.1016/j.tcb.2014.10.005

Jung, J. 2015. Precise timing of the trypanosome cell division cycle. PhD Thesis. Julius-Maximilians-Universität Würzburg, Würzburg.

Kaksonen, M., Roux, A. 2018. Mechanisms of clathrin-mediated endocytosis. *Nature Reviews Molecular Cell Biology* 19, 313-326. https://doi.org/10.1038/nrm.2017.132

Kamentseva, R., Kosheverova, V., Kharchenko, M., Zlobina, M., Salova, A., Belyaeva, T., Nikolsky, N., Kornilova, E. 2020. Functional cycle of EEA1-positive early endosome: Direct evidence for pre-existing compartment of degradative pathway. *PLoS One* 15, e0232532. https://doi.org/10.1371/journal.pone.0232532

Kamidi, C.M., Saarman, N.P., Dion, K., Mireji, P.O., Ouma, C., Murilla, G., Aksoy, S., Schnaufer, A., Caccone, A. 2017. Multiple evolutionary origins of *Trypanosoma evansi* in Kenya. *PLoS Neglected Tropical Diseases* 11, e0005895. https://doi.org/10.1371/journal.pntd.0005895

Karim, M.A., Samyn, D.R., Mattie, S., Brett, C.L. 2018. Distinct features of multivesicular body-lysosome fusion revealed by a new cell-free content-mixing assay. *Traffic* 19, 138-149. https://doi.org/10.1111/tra.12543

Kassambara, A. 2023a. ggpubr: “ggplot2” based publication ready plots. Available at: https://rpkgs.datanovia.com/ggpubr/ (Accessed: 24 July 2023).

Kassambara, A. 2023b. rstatix: Pipe-friendly framework for basic statistical tests. Available at: https://cran.r-project.org/web/packages/rstatix/index.html (Accessed: 24 July 2023).

Katzmann, D.J., Babst, M., Emr, S.D. 2001. Ubiquitin-dependent sorting into the multivesicular body pathway requires the function of a conserved endosomal protein sorting complex, ESCRT-I. *Cell* 106, 145-155. https://doi.org/10.1016/S0092-8674(01)00434-2

Keller, A., Förster, F., Müller, T., Dandekar, T., Schultz, J., Wolf, M. 2010. Including RNA secondary structures improves accuracy and robustness in reconstruction of phylogenetic trees. *Biology Direct* 5, 4. https://doi.org/10.1186/1745-6150-5-4

Kelly, S., Ivens, A., Manna, P.T., Gibson, W., Field, M.C. 2014. A draft genome for the African crocodilian trypanosome *Trypanosoma grayi*. *Scientific Data* 1, 140024. https://doi.org/10.1038/sdata.2014.24

Kirchhausen, T., Harrison, S.C. 1981. Protein organization in clathrin trimers. *Cell* 23, 755–761. https://doi.org/10.1016/0092-8674(81)90439-6

Klumperman, J., Raposo, G. 2014. The complex ultrastructure of the endolysosomal system. *Cold Spring Harbor Perspectives in Biology* 6, a016857. https://doi.org/10.1101/cshperspect.a016857

Knapp, P.E., Swanson, J.A. 1990. Plasticity of the tubular lysosomal compartment in macrophages. *Journal of Cell Science* 95, 433-439. https://doi.org/10.1242/jcs.95.3.433

Koeller, C.M., Bangs, J.D. 2019. Processing and targeting of cathepsin L (TbCatL) to the lysosome in *Trypanosoma brucei*. *Cellular Microbiology* 21, e12980. https://doi.org/10.1111/cmi.12980

Koeller, C.M., Smith, T.K., Gulick, A.M., Bangs, J.D. 2021. p67: a cryptic lysosomal hydrolase in *Trypanosoma brucei*? *Parasitology* 148, 1271-1276. https://doi.org/10.1017/S003118202000195X

Kok, J.W., Hoekstra, K., Eskelinen, S., Hoekstra, D. 1992. Recycling pathways of glucosylceramide in BHK cells: Distinct involvement of early and late endosomes. *Journal of Cell Science* 103, 1139-1152. https://doi.org/10.1242/jcs.103.4.1139

Komaki, S., Tromer, E.C., De Jaeger, G., De Winne, N., Heese, M., Schnittger, A. 2022. Molecular convergence by differential domain acquisition is a hallmark of chromosomal passenger complex evolution. *Proceedings of the National Academy of Sciences of the United States of America* 119, e2200108119. https://doi.org/10.1073/pnas.2200108119

Korolchuk, V.I., Saiki, S., Lichtenberg, M., Siddiqi, F.H., Roberts, E.A., Imarisio, S., Jahreiss, L., Sarkar, S., Futter, M., Menzies, F.M., O'Kane, C.J., Deretic, V., Rubinsztein, D.C. 2011. Lysosomal positioning coordinates cellular nutrient responses. *Nature Cell Biology* 13, 453-460. https://doi.org/10.1038/ncb2204

Kostygov, A.Y., Karnkowska, A., Votýpka, J., Tashyreva, D., Maciszewski, K., Yurchenko, V., Lukeš, J. 2021. Euglenozoa: taxonomy, diversity and ecology, symbioses and viruses. *Open Biology* 11, 200407. https://doi.org/10.1098/rsob.200407

Kurasawa, Y., Lee, K.J., Hu, H., Pham, K.T.M., Li, Z. 2022. Polo-like kinase and Aurora B kinase phosphorylate and cooperate with the CIF1-CIF2 complex to promote cytokinesis initiation in *Trypanosoma brucei*. *Open Biology* 12, 220197. https://doi.org/10.1098/rsob.220197

Lacomble, S., Vaughan, S., Gadelha, C., Morphew, M.K., Shaw, M.K., McIntosh, J.R., Gull, K. 2010. Basal body movements orchestrate membrane organelle division and cell morphogenesis in *Trypanosoma brucei*. *Journal of Cell Science* 123, 2884-2891. https://doi.org/10.1242/jcs.074161

Lai, D.H., Hashimi, H., Lun, Z.R., Ayala, F.J., Lukes, J. 2008. Adaptations of *Trypanosoma brucei* to gradual loss of kinetoplast DNA: *Trypanosoma equiperdum* and *Trypanosoma evansi* are petite mutants of *T. brucei*. *Proceedings of the National Academy of Sciences of the United States of America* 105, 1999-2004. https://doi.org/10.1073/pnas.0711799105

Lamaze, C., Fujimoto, L.M., Yin, H.L., Schmid, S.L. 1997. The actin cytoskeleton is required for receptor-mediated endocytosis in mammalian cells. *Journal of Biological Chemistry* 272, 20332-20335. https://doi.org/10.1074/jbc.272.33.20332

Langemeyer, L., Fröhlich, F., Ungermann, C. 2018. Rab GTPase function in endosome and lysosome biogenesis. *Trends in Cell Biology* 28, 957-970. https://doi.org/10.1016/j.tcb.2018.06.007

Langreth, S.G., Balber, A.E. 1975. Protein uptake and digestion in bloodstream and culture forms of *Trypanosoma brucei*. *Journal of Protozoology* 22, 40-53. https://doi.org/10.1111/j.1550-7408.1975.tb00943.x

Laplante, C., Huang, F., Tebbs, I.R., Bewersdorf, J., Pollard, T.D. 2016. Molecular organization of cytokinesis nodes and contractile rings by super-resolution fluorescence microscopy of live fission yeast. *Proceedings of the National Academy of Sciences of the United States of America* 113, 5876-5885. https://doi.org/10.1073/pnas.1608252113

Larkin, M.A., Blackshields, G., Brown, N.P., Chenna, R., McGettigan, P.A., McWilliam, H., Valentin, F., Wallace, I.M., Wilm, A., Lopez, R., Thompson, J.D., Gibson, T.J., Higgins, D.G. 2007. Clustal W and Clustal X version 2.0. *Bioinformatic*s 23, 2947-2948. https://doi.org/10.1093/bioinformatics/btm404

Lehane, M.J., Allingham, P.G., Weglicki, P. 1996. Composition of the peritrophic matrix of the tsetse fly, *Glossina morsitans morsitans*. *Cell Tissue Research* 283, 375-384. https://doi.org/10.1007/s004410050548

Lemos, M., Fermino, B.R., Simas-Rodrigues, C., Hoffmann, L., Silva, R., Camargo, E.P., Teixeira, M.M.G., Souto-Padrón, T. 2015. Phylogenetic and morphological characterization of trypanosomes from Brazilian armoured catfishes and leeches reveal high species diversity, mixed infections and a new fish trypanosome species. *Parasites & Vectors* 8, 573. https://doi.org/10.1186/s13071-015-1193-7

Leung, K.F., Dacks, J.B., Field, M.C. 2008. Evolution of the multivesicular body ESCRT machinery; retention across the eukaryotic lineage. *Traffic* 9, 1698-1716. https://doi.org/10.1111/j.1600-0854.2008.00797.x

Li, C.H., Lee, C.K. 1993. Minimum cross entropy thresholding. *Pattern Recognition* 26, 617-625. https://doi.org/10.1016/0031-3203(93)90115-D

Li, D., Shao, L., Chen, B.C., Zhang, X., Zhang, M., Moses, B., Milkie, D.E., Beach, J.R., Hammer, J.A., Pasham, M., Kirchhausen, T., Baird, M.A., Davidson, M.W., Xu, P., Betzig, E. 2015. Extended-resolution structured illumination imaging of endocytic and cytoskeletal dynamics. *Science* 349, aab3500. https://doi.org/10.1126/science.aab3500

Li, Z., Lee, J.H., Chu, F., Burlingame, A.L., Günzl, A., Wang, C.C. 2008. Identification of a novel chromosomal passenger complex and its unique localization during cytokinesis in *Trypanosoma brucei*. *PLoS One* 3, e2354. https://doi.org/10.1371/journal.pone.0002354

Lim, H.C., Teng, S.T., Lim, P.T., Wolf, M., Leaw, C.P. 2016. 18S rDNA phylogeny of *Pseudo-nitzschia* (Bacillariophyceae) inferred from sequence-structure information. *Phycologia* 55, 134-146. https://doi.org/10.2216/15-78.1

Lima, L., Espinosa-Álvarez, O., Ortiz, P.A., Trejo-Varón, J.A., Carranza, J.C., Pinto, C.M., Serrano, M.G., Buck, G.A., Camargo, E.P., Teixeira, M.M.G. 2015. Genetic diversity of *Trypanosoma cruzi* in bats, and multilocus phylogenetic and phylogeographical analyses supporting Tcbat as an independent DTU (discrete typing unit). *Acta Tropica* 151, 166-177. https://doi.org/10.1016/j.actatropica.2015.07.015

Link, F., Borges, A., Karo, O., Jungblut, M., Mueller, T., Meyer-Natus, E., Krueger, T., Sachs, S., Jones, N.G., Morphew, M., Sauer, M., Stigloher, C., McIntosh, J.R., Engstler, M. 2023. Continuous endosomes form functional subdomains and orchestrate rapid membrane trafficking in trypanosomes [Preprint]. Available at: https://www.biorxiv.org/content/10.1101/2023.07.20.549860v1 (Accessed: 24 July 2023).

Link, F., Borges, A.R., Jones, N.G., Engstler, M. 2021. To the surface and back: exo- and endocytic pathways in *Trypanosoma brucei*. *Frontiers in Cell and Developmental Biology* 9, 720521. https://doi.org/10.3389/fcell.2021.720521

Lipowsky, R. 2022. Remodeling of membrane shape and topology by curvature elasticity and membrane tension. *Advanced Biology* 6, 2101020. https://doi.org/10.1002/adbi.202101020

Lippincott, J., Li, R. 1998. Sequential assembly of myosin II, an IQGAP-like protein, and filamentous actin to a ring structure involved in budding yeast cytokinesis. *Journal of Cell Biology* 140, 355-366. https://doi.org/10.1083/jcb.140.2.355

Lizarrondo, J., Klebl, D.P., Niebling, S., Abella, M., Schroer, M.A., Mertens, H.D.T., Veith, K., Thuenauer, R., Svergun, D.I., Skruzny, M., Sobott, F., Muench, S.P., Garcia-Alai, M.M. 2021. Structure of the endocytic adaptor complex reveals the basis for efficient membrane anchoring during clathrin-mediated endocytosis. *Nature Communications* 12, 2889. https://doi.org/10.1038/s41467-021-23151-7

Loeffler, D., Schneiter, F., Wang, W., Wehling, A., Kull, T., Lengerke, C., Manz, M.G., Schroeder, T. 2022. Asymmetric organelle inheritance predicts human blood stem cell fate. *Blood* 139, 2011-2023. https://doi.org/10.1182/blood.2020009778

Loeffler, D., Wehling, A., Schneiter, F., Zhang, Y., Müller-Bötticher, N., Hoppe, P.S., Hilsenbeck, O., Kokkaliaris, K.D., Endele, M., Schroeder, T. 2019. Asymmetric lysosome inheritance predicts activation of haematopoietic stem cells. *Nature* 573, 426-429. https://doi.org/10.1038/s41586-019-1531-6

Lukeš, J., Butenko, A., Hashimi, H., Maslov, D.A., Votýpka, J., Yurchenko, V. 2018. Trypanosomatids are much more than just trypanosomes: clues from the expanded family tree. *Trends in Parasitology* 34, 466-480. https://doi.org/10.1016/j.pt.2018.03.002

Lukeš, J., Skalický, T., Týč, J., Votýpka, J., Yurchenko, V. 2014. Evolution of parasitism in kinetoplastid flagellates. *Molecular and Biochemical Parasitology* 195, 115-122. https://doi.org/10.1016/j.molbiopara.2014.05.007

Ma, L., Umasankar, P.K., Wrobel, A.G., Lymar, A., McCoy, A.J., Holkar, S.S., Jha, A., Pradhan-Sundd, T., Watkins, S.C., Owen, D.J., Traub, L.M. 2016. Transient Fcho1/2·Eps15/R·AP-2 nanoclusters prime the AP-2 Clathrin adaptor for cargo binding. *Developmental Cell* 37, 428-443. https://doi.org/10.1016/j.devcel.2016.05.003

Machado, H., Bizarra-Rebelo, T., Costa-Sequeira, M., Trindade, S., Carvalho, T., Rijo-Ferreira, F., Rentroia-Pacheco, B., Serre, K., Figueiredo, L.M. 2021. *Trypanosoma brucei* triggers a broad immune response in the adipose tissue. *PLoS Pathogens* 17, e1009933. https://doi.org/10.1371/journal.ppat.1009933

Mafie, E., Saito-Ito, A., Kasai, M., Hatta, M., Rivera, P.T., Ma, X.-H., Chen, E.-R., Sato, H., Takada, N. 2019. Integrative taxonomic approach of trypanosomes in the blood of rodents and soricids in Asian countries, with the description of three new species. *Parasitology Research* 118, 97-109. https://doi.org/10.1007/s00436-018-6120-3

Magez, S., Pinto Torres, J.E., Obishakin, E., Radwanska, M. 2020. Infections with extracellular trypanosomes require control by efficient innate immune mechanisms and can result in the destruction of the mammalian humoral immune system. *Frontiers in Immunology* 11, 382. https://doi.org/10.3389/fimmu.2020.00382

Mahecic, D., Carlini, L., Kleele, T., Colom, A., Goujon, A., Matile, S., Roux, A., Manley, S. 2021. Mitochondrial membrane tension governs fission. *Cell Reports* 35, 108947. https://doi.org/10.1016/j.celrep.2021.108947

Maia da Silva, F., Noyes, H., Campaner, M., Junqueira, A.C.V., Coura, J.R., Añez, N., Shaw, J.J., Stevens, J.R., Teixeira, M.M.G. 2004. Phylogeny, taxonomy and grouping of *Trypanosoma rangeli* isolates from man, triatomines and sylvatic mammals from widespread geographical origin based on SSU and ITS ribosomal sequences. *Parasitology* 129, 549-561. https://doi.org/10.1017/S0031182004005931

Majumdar, S., Liu, S.T., 2020. Cell division symmetry control and cancer stem cells. *AIMS Molecular Science* 7, 82-98. https://doi.org/10.3934/molsci.2020006

Manna, P.T., Gadelha, C., Puttick, A.E., Field, M.C. 2015. ENTH and ANTH domain proteins participate in AP2-independent clathrin-mediated endocytosis. *Journal of Cell Science* 128, 2130-2142. https://doi.org/10.1242/jcs.167726

Manna, P.T., Kelly, S., Field, M.C. 2013. Adaptin evolution in kinetoplastids and emergence of the variant surface glycoprotein coat in African trypanosomatids. *Molecular Phylogenetics and Evolution* 67, 123-128. https://doi.org/10.1016/j.ympev.2013.01.002

Mao, F., Yang, Y., Jiang, H. 2021. Endocytosis and exocytosis protect cells against severe membrane tension variations. *Biophysical Journal* 120, 5521-5529. https://doi.org/10.1016/j.bpj.2021.11.019

Martin, D.S., Wright, A.-D.G., Barta, J.R., Desser, S.S. 2002. Phylogenetic position of the giant anuran trypanosomes *Trypanosoma chattoni*, *Trypanosoma fallisi*, *Trypanosoma mega*, *Trypanosoma neveulemairei*, and *Trypanosoma ranarum* inferred from 18S rRNA gene sequences. *The Journal of Parasitology* 88, 566-571. https://doi.org/10.1645/0022-3395(2002)088[0566:PPOTGA]2.0.CO;2

Mascanzoni, F., Ayala, I., Colanzi, A. 2019. Organelle inheritance control of mitotic entry and progression: implications for tissue homeostasis and disease. *Frontiers in Cell and Developmental Biology* 7, 133. https://doi.org/10.3389/fcell.2019.00133

Maslov, D.A., Podlipaev, S.A., Lukes, J. 2001. Phylogeny of the kinetoplastida: taxonomic problems and insights into the evolution of parasitism. *Memórias do Instituto Oswaldo Cruz* 96, 397-402. https://doi.org/10.1590/s0074-02762001000300021

Matsui, W., Kirchhausen, T. 1990. Stabilization of clathrin coats by the core of the clathrin-associated protein complex AP-2. *Biochemistry* 29, 10791-10798. https://doi.org/10.1021/bi00500a011

Matthews, K.R., Gull, K. 1994. Evidence for an interplay between cell cycle progression and the initiation of differentiation between life cycle forms of African trypanosomes. *Journal of Cell Biology* 125, 1147-1156. https://doi.org/10.1083/jcb.125.5.1147

McCusker, D., Kellogg, D.R. 2012. Plasma membrane growth during the cell cycle: unsolved mysteries and recent progress. *Current Opinion in Cell Biology* 24, 845-851. https://doi.org/10.1016/j.ceb.2012.10.008

McInnes, L.M., Hanger, J., Simmons, G., Reid, S.A., Ryan, U.M. 2011. Novel trypanosome *Trypanosoma gilletti* sp. (Euglenozoa: Trypanosomatidae) and the extension of the host range of *Trypanosoma copemani* to include the koala (*Phascolarctos cinereus*). *Parasitology* 138, 59-70. https://doi.org/10.1017/S0031182010000971

Menon, A.K., Mayor, S., Ferguson, M.A., Duszenko, M., Cross, G.A. 1988. Candidate glycophospholipid precursor for the glycosylphosphatidylinositol membrane anchor of *Trypanosoma brucei* variant surface glycoproteins. *Journal of Biological Chemistry* 263, 1970-1977.

Mettlen, M., Pucadyil, T., Ramachandran, R., Schmid, S.L. 2009. Dissecting dynamin's role in clathrin-mediated endocytosis. *Biochemical Society Transactions* 37, 1022-1026. https://doi.org/10.1042/BST0371022

Molinari, J., Moreno, S.A. 2018. *Trypanosoma brucei* Plimmer & Bradford, 1899 is a synonym of *T. evansi* (Steel, 1885) according to current knowledge and by application of nomenclature rules. *Systematic Parasitology* 95, 249-256. https://doi.org/10.1007/s11230-018-9779-z

Moore, A.S., Coscia, S.M., Simpson, C.L., Ortega, F.E., Wait, E.C., Heddleston, J.M., Nirschl, J.J., Obara, C.J., Guedes-Dias, P., Boecker, C.A., Chew, T.L., Theriot, J.A., Lippincott-Schwartz, J., Holzbaur, E.L.F. 2021. Actin cables and comet tails organize mitochondrial networks in mitosis. *Nature* 591, 659-664. https://doi.org/10.1038/s41586-021-03309-5

Moreira, D., López-García, P., Vickerman, K. 2004. An updated view of kinetoplastid phylogeny using environmental sequences and a closer outgroup: proposal for a new classification of the class Kinetoplastea. *International Journal of Systematic and Evolutionary Microbiology* 54, 1861-1875. https://doi.org/10.1099/ijs.0.63081-0

Morgan, G.W., Allen, C.L., Jeffries, T.R., Hollinshead, M., Field, M.C. 2001. Developmental and morphological regulation of clathrin-mediated endocytosis in *Trypanosoma brucei*. *Journal of Cell Science* 114, 2605-2615. https://doi.org/10.1242/jcs.114.14.2605

Morgan, G.W., Hall, B.S., Denny, P.W., Carrington, M., Field, M.C. 2002. The kinetoplastida endocytic apparatus. Part I: a dynamic system for nutrition and evasion of host defences. *Trends in Parasitology* 18, 491-496. https://doi.org/10.1016/s1471-4922(02)02391-7

Morris, C.E., Homann, U. 2001. Cell surface area regulation and membrane tension. *Journal of Membrane Biology* 179, 79-102. https://doi.org/10.1007/s002320010040

Morriswood, B., Engstler, M. 2018. Let's get fISSical: fast *in silico* synchronization as a new tool for cell division cycle analysis. Parasitology 145, 196-209. https://doi.org/10.1017/S0031182017000038

Moser, J., Miller, I., Carter, D., Spencer, S.L. 2018. Control of the restriction point by Rb and p21. *Proceedings of the National Academy of Sciences of the United States of America* 115, 8219–8227. https://doi.org/10.1073/pnas.1722446115

Mugnier, M.R., Cross, G.A., Papavasiliou, F.N. 2015. The *in vivo* dynamics of antigenic variation in *Trypanosoma brucei*. *Science* 347, 1470-1473. https://doi.org/10.1126/science.aaa4502

Mugnier, M.R., Stebbins, C.E., Papavasiliou, F.N. 2016. Masters of disguise: antigenic variation and the VSG coat in *Trypanosoma brucei*. *PLoS Pathogens* 12, e1005784. https://doi.org/10.1371/journal.ppat.1005784

Muniz, R.S., Campbell, P.C., Sladewski, T.E., Renner, L.D., de Graffenried, C.L. 2022. Revealing spatio-temporal dynamics with long-term trypanosomatid live-cell imaging. *PLoS Pathogens* 18, e1010218. https://doi.org/10.1371/journal.ppat.1010218

Neuwirth, E. 2022. RColorBrewer: ColorBrewer palettes. Available at: https://cran.r-project.org/web/packages/RColorBrewer/RColorBrewer.pdf (Accessed: 24 July 2023).

Nolan, D.P., Rolin, S., Rodriguez, J.R., Van Den Abbeele, J., Pays, E. 2000. Slender and stumpy bloodstream forms of *Trypanosoma brucei* display a differential response to extracellular acidic

and proteolytic stress. *European Journal of Biochemistry* 267, 18-27. https://doi.org/10.1046/j.1432-1327.2000.00935.x

Odle, R.I., Walker, S.A., Oxley, D., Kidger, A.M., Balmanno, K., Gilley, R., Okkenhaug, H., Florey, O., Ktistakis, N.T., Cook, S.J. 2020. An mTORC1-to-CDK1 switch maintains autophagy suppression during mitosis. *Molecular Cell* 77, 228-240. https://doi.org/10.1016/j.molcel.2019.10.016

Onyilagha, C., Uzonna, J.E. 2019. Host immune responses and immune evasion strategies in African trypanosomiasis. *Frontiers in Immunology* 10, 2738. https://doi.org/10.3389/fimmu.2019.02738

Ortiz, P.A., Garcia, H.A., Lima, L., da Silva, F.M., Campaner, M., Pereira, C.L., Jittapalapong, S., Neves, L., Desquesnes, M., Camargo, E.P., Teixeira, M.M.G. 2018. Diagnosis and genetic analysis of the worldwide distributed *Rattus*-borne *Trypanosoma* (*Herpetosoma*) *lewisi* and its allied species in blood and fleas of rodents. *Infection, Genetics and Evolution* 63, 380-390. https://doi.org/10.1016/j.meegid.2017.09.001

Otsu, N. 1979. A threshold selection method from gray-level histograms. *IEEE Transactions on Systems, Man, and Cybernetics* 9, 62-66. https://doi.org/10.1109/TSMC.1979.4310076

Ouellet, J., Barral, Y. 2012. Organelle segregation during mitosis: lessons from asymmetrically dividing cells. *Journal of Cell Biology* 196, 305-313. https://doi.org/10.1083/jcb.201102078

Overath, P., Engstler, M. 2004. Endocytosis, membrane recycling and sorting of GPI-anchored proteins: *Trypanosoma brucei* as a model system. *Molecular Microbiology* 53, 735-744. https://doi.org/10.1111/j.1365-2958.2004.04224.x

Overath, P., Stierhof, Y.D., Wiese, M. 1997. Endocytosis and secretion in trypanosomatid parasites — Tumultuous traffic in a pocket. *Trends in Cell Biology* 7, 27-33. https://doi.org/10.1016/S0962-8924(97)10046-0

Pal, A., Hall, B.S., Nesbeth, D.N., Field, H.I., Field, M.C. 2002. Differential endocytic functions of *Trypanosoma brucei* Rab5 isoforms reveal a glycosylphosphatidylinositol-specific endosomal pathway. *Journal of Biological Chemistry* 277, 9529-9539. https://doi.org/10.1074/jbc.M110055200

Palade, G.E. 1955. A small particulate component of the cytoplasm. *Journal of Biophysical and Biochemical Cytology* 1, 59-68. https://doi.org/10.1083/jcb.1.1.59

Pan, B.T., Teng, K., Wu, C., Adam, M., Johnstone, R.M. 1985. Electron microscopic evidence for externalization of the transferrin receptor in vesicular form in sheep reticulocytes. *Journal of Cell Biology* 101, 942-948. https://doi.org/10.1083/jcb.101.3.942

Pantazopoulou, M., Lamprokostopoulou, A., Karampela, D.S., Alexaki, A., Delis, A., Coens, A., Samiotaki, M., Kriebardis, A.G., Melki, R., Pagakis, S.N., Stefanis, L., Vekrellis, K. 2023. Differential intracellular trafficking of extracellular vesicles in microglia and astrocytes. *Cellular and Molecular Life Sciences* 80, 193. https://doi.org/10.1007/s00018-023-04841-5

Paweletz, N. 2001. Walther Flemming: pioneer of mitosis research. *Nature Reviews Molecular Cell Biology* 2, 72-75. https://doi.org/10.1038/35048077

Peck, R.F., Shiflett, A.M., Schwartz, K.J., McCann, A., Hajduk, S.L., Bangs, J.D. 2008. The LAMP-like protein p67 plays an essential role in the lysosome of African trypanosomes. *Molecular Microbiology* 68, 933-946. https://doi.org/10.1111/j.1365-2958.2008.06195.x

Podinovskaia, M., Prescianotto-Baschong, C., Buser, D.P., Spang, A. 2021. A novel live-cell imaging assay reveals regulation of endosome maturation. *eLife* 10, e70982. https://doi.org/10.7554/eLife.70982

Poteryaev, D., Datta, S., Ackema, K., Zerial, M., Spang, A. 2010. Identification of the switch in early-to-late endosome transition. *Cell* 141, 497-508. https://doi.org/10.1016/j.cell.2010.03.011

Prasad, K., Barouch, W., Greene, L., Eisenberg, E. 1993. A protein cofactor is required for uncoating of clathrin baskets by uncoating ATPase. *Journal of Biological Chemistry* 268, 23758-23761.

Presle, A., Frémont, S., Salles, A., Commere, P.H., Sassoon, N., Berlioz-Torrent, C., Gupta-Rossi, N., Echard, A. 2021. The viral restriction factor tetherin/BST2 tethers cytokinetic midbody

remnants to the cell surface. *Current Biology* 31, 2203-2213. https://doi.org/10.1016/j.cub.2021.02.039

Prichard, K.L., O'Brien, N.S., Murcia, S.R., Baker, J.R., McCluskey, A. 2022. Role of clathrin and dynamin in clathrin mediated endocytosis/synaptic vesicle recycling and implications in neurological diseases. *Frontiers in Cellular Neuroscience* 15, 754110. https://doi.org/10.3389/fncel.2021.754110

Puertollano, R., Aguilar, R.C., Gorshkova, I., Crouch, R.J., Bonifacino, J.S. 2001. Sorting of mannose 6-phosphate receptors mediated by the GGAs. *Science* 292, 1712-1716. https://doi.org/10.1126/science.1060750

R Core Team. 2021. R: A language and environment for statistical computing. Available at: https://www.r-project.org/index.html (Accessed: 24 July 2023).

R Core Team. 2014. R: a language and environment for statistical computing. Available at: https://www.r-project.org/index.html (Accessed: 24 July 2023).

Rackevei, A.S., Borges, A., Engstler, M., Dandekar, T., Wolf, M. 2022. About the analysis of 18S rDNA sequence data from trypanosomes in barcoding and phylogenetics: tracing a continuation error occurring in the literature. *Biology (Basel)* 11, 1612. https://doi.org/10.3390/biology11111612

Raiborg, C., Bache, K.G., Gillooly, D.J., Madshus, I.H., Stang, E., Stenmark, H. 2002. Hrs sorts ubiquitinated proteins into clathrin-coated microdomains of early endosomes. *Nature Cell Biology* 4, 394-398. https://doi.org/10.1038/ncb791

Ralston, K.S., Lerner, A.G., Diener, D.R., Hill, K.L. 2006. Flagellar motility contributes to cytokinesis in *Trypanosoma brucei* and is modulated by an evolutionarily conserved dynein regulatory system. *Eukaryotic Cell* 5, 696-711. https://doi.org/10.1128/EC.5.4.696-711.2006

Rappaport, R. 1986. Establishment of the mechanism of cytokinesis in animal cells. *International Review of Cytology* 105, 245-281. https://doi.org/10.1016/s0074-7696(08)61065-7

Rennick, J.J., Johnston, A.P.R., Parton, R.G. 2021. Key principles and methods for studying the endocytosis of biological and nanoparticle therapeutics. *Nature Nanotechnology* 16, 266-276. https://doi.org/10.1038/s41565-021-00858-8

Revelle, W. 2022. psych: Procedures for psychological, psychometric, and personality research. Available at: https://cran.r-project.org/web/packages/psych/index.html (Accessed: 24 July 2023).

Rico, E., Rojas, F., Mony, B.M., Szoor, B., MacGregor, P., Matthews, K.R. 2013. Bloodstream form pre-adaptation to the tsetse fly in *Trypanosoma brucei*. *Frontiers in Cellular and Infection Microbiology* 3, 78. https://doi.org/10.3389/fcimb.2013.00078

Rink, J., Ghigo, E., Kalaidzidis, Y., Zerial, M. 2005. Rab conversion as a mechanism of progression from early to late endosomes. *Cell* 122, 735-749. https://doi.org/10.1016/j.cell.2005.06.043

Robertson, M. 1912. Notes on the polymorphism of *Trypanosoma gambiense* in the blood and its relation to the exogenous cycle in *Glossina palpalis*. *Proceedings of the Royal Society of London Series B* 85, 527-539. https://doi.org/10.1098/rspb.1912.0080

Robertson, M., Bradford, J.R. 1912. Notes on certain aspects of the development of *Trypanosoma gambiense* in *Glossina palpalis*. *Proceedings of the Royal Society of London Series B* 85, 241-248. https://doi.org/10.1098/rspb.1912.0048

Robinson, D.R. 1995. Microtubule polarity and dynamics in the control of organelle positioning, segregation, and cytokinesis in the trypanosome cell cycle. *Journal of Cell Biology* 128, 1163-1172. https://doi.org/10.1083/jcb.128.6.1163

Rodrigues, A.C., Neves, L., Garcia, H.A., Viola, L.B., Marcili, A., Da Silva, F.M., Sigauque, I., Batista, J.S., Paiva, F., Teixeira, M.M.G. 2008. Phylogenetic analysis of *Trypanosoma vivax* supports the separation of South American/West African from East African isolates and a new *T. vivax*-like genotype infecting a nyala antelope from Mozambique. Parasitology 135, 1317-1328. https://doi.org/10.1017/S0031182008004848

Rogerson, E., Pelletier, J., Acosta-Serrano, A., Rose, C., Taylor, S., Guimond, S., Lima, M., Skidmore, M., Yates, E., 2018. Variations in the peritrophic matrix composition of heparan sulphate from the tsetse fly, *Glossina morsitans morsitans*. *Pathogens* 7, 32. https://doi.org/10.3390/pathogens7010032

Rojas, F., Matthews, K.R. 2019. Quorum sensing in African trypanosomes. *Current Opinion in Microbiology* 52, 124-129. https://doi.org/10.1016/j.mib.2019.07.001

Rose, C., Belmonte, R., Armstrong, S.D., Molyneux, G., Haines, L.R., Lehane, M.J., Wastling, J., Acosta-Serrano, A. 2014. An Investigation into the protein composition of the teneral *Glossina morsitans morsitans* peritrophic matrix. *PLoS Neglected Tropical Diseases* 8, e2691. https://doi.org/10.1371/journal.pntd.0002691

Rose, C., Casas-Sánchez, A., Dyer, N.A., Solórzano, C., Beckett, A.J., Middlehurst, B., Marcello, M., Haines, L.R., Lisack, J., Engstler, M., Lehane, M.J., Prior, I.A., Acosta-Serrano, Á. 2020. *Trypanosoma brucei* colonizes the tsetse gut via an immature peritrophic matrix in the proventriculus. *Nature Microbiology* 5, 909-916. https://doi.org/10.1038/s41564-020-0707-z

Roth, T.F., Porter, K.R. 1964. Yolk protein uptake in the oocyte of the mosquito *Aedes aegypti* L. *Journal of Cell Biology* 20, 313-332. https://doi.org/10.1083/jcb.20.2.313

Rothnie, A., Clarke, A.R., Kuzmic, P., Cameron, A., Smith, C.J. 2011. A sequential mechanism for clathrin cage disassembly by 70-kDa heat-shock cognate protein (Hsc70) and auxilin. *Proceedings of the National Academy of Sciences of the United States of America* 108, 6927-6932. https://doi.org/10.1073/pnas.1018845108

RStudio Team. 2020. RStudio: Integrated development for R. Available at: https://www.r-project.org/conferences/useR-2011/abstracts/180111-allairejj.pdf (Accessed: 24 July 2023).

Ruijtenberg, S., van den Heuvel, S. 2016. Coordinating cell proliferation and differentiation: Antagonism between cell cycle regulators and cell type-specific gene expression. *Cell Cycle* 15, 196-212. https://doi.org/10.1080/15384101.2015.1120925

Sabharanjak, S., Sharma, P., Parton, R.G., Mayor, S. 2002. GPI-anchored proteins are delivered to recycling endosomes via a distinct cdc42-regulated, clathrin-independent pinocytic pathway. *Developmental Cell* 2, 411-423. https://doi.org/10.1016/S1534-5807(02)00145-4

Saenz-Garcia, J.L., Borges, B.S., Souza-Melo, N., Machado, L.V., Miranda, J.S., Pacheco-Lugo, L.A., Moretti, N.S., Wheleer, R., Soares Medeiros, L.C., DaRocha, W.D. 2022. Trypanin disruption affects the motility and infectivity of the protozoan *Trypanosoma cruzi*. *Frontiers in Cellular and Infection Microbiology* 11, 807236. https://doi.org/10.3389/fcimb.2021.807236

Saito, N., Okada, Y., Noda, Y., Kinoshita, Y., Kondo, S., Hirokawa, N. 1997. KIFC2 is a novel neuron-specific C-terminal type kinesin superfamily motor for dendritic transport of multivesicular body-like organelles. *Neuron* 18, 425-438. https://doi.org/10.1016/s0896-6273(00)81243-x

Santos, R., Ástvaldsson, Á., Pipaliya, S.V., Zumthor, J.P., Dacks, J.B., Svärd, S., Hehl, A.B., Faso, C. 2022. Combined nanometric and phylogenetic analysis of unique endocytic compartments in *Giardia lamblia* sheds light on the evolution of endocytosis in Metamonada. *BMC Biology* 20, 206. https://doi.org/10.1186/s12915-022-01402-3

Sato, H., Leo, N., Katakai, Y., Takano, J., Akari, H., Nakamura, S., Une, Y. 2008. Prevalence and molecular phylogenetic characterization of *Trypanosoma* (*Megatrypanum*) *minasense* in the peripheral blood of small neotropical primates after a quarantine period. *The Journal of Parasitology* 94, 1128-1138. https://doi.org/10.1645/GE-1513.1

Sato, M., Kakui, Y., Toya, M. 2021. Tell the difference between mitosis and meiosis: Interplay between chromosomes, cytoskeleton, and cell cycle regulation. *Frontiers in Cell and Developmental Biology* 9, 660322. https://doi.org/10.3389/fcell.2021.660322

Sayyad, W.A., Pollard, T.D. 2022. The number of cytokinesis nodes in mitotic fission yeast scales with cell size. *eLife* 11, e76249. https://doi.org/10.7554/eLife.76249

Schauberger, P., Walker, A., Braglia, L., Sturm, J., Garbuszus, J.M., Barbone, J.M. 2023. openxlsx: Read, write and edit xlsx files. Available at: https://cran.r-project.org/web/packages/openxlsx/openxlsx.pdf (Accessed: 24 July 2023).

Schichler, D., Spath, E.-M., Konle, A., Riegler, S., Klein, A., Seleznev, A., Jung, S., Wuppermann, T., Wetterich, N., Borges, A., Meyer-Natus, E., Havlicek, K., Cabrera, S.P., Niedermüller, K., Sajko, S., Dohn, M., Malzer, X., Riemer, E., Tumurbaatar, T., Djinovic-Carugo, K., Dong, G., Janzen, C.J., Morriswood, B. 2022. Endocytosis is required for access of surface-bound cargo to the flagellar pocket of trypanosomes [Preprint]. Available at: https://www.biorxiv.org/content/10.1101/2022.03.15.484455v1 (Accessed: 23 May 2023).

Schindelin, J., Arganda-Carreras, I., Frise, E., Kaynig, V., Longair, M., Pietzsch, T., Preibisch, S., Rueden, C., Saalfeld, S., Schmid, B., Tinevez, J.-Y., White, D.J., Hartenstein, V., Eliceiri, K., Tomancak, P., Cardona, A. 2012. Fiji: an open-source platform for biological-image analysis. *Nature Methods* 9, 676-682. https://doi.org/10.1038/nmeth.2019

Schliep, K.P. 2011. phangorn: phylogenetic analysis in R. *Bioinformatics* 27, 592-593. https://doi.org/10.1093/bioinformatics/btq706

Schubert, K.O., Föcking, M., Prehn, J.H.M., Cotter, D.R. 2012. Hypothesis review: are clathrin-mediated endocytosis and clathrin-dependent membrane and protein trafficking core pathophysiological processes in schizophrenia and bipolar disorder? *Molecular Psychiatry* 17, 669-681. https://doi.org/10.1038/mp.2011.123

Schulz-Schaeffer, J. 1980. Chromosomes during meiosis, in: Schulz-Schaeffer, J. (ed.), Cytogenetics: Plants, animals, humans. New Yok: Springer, pp. 102-127.

Schuster, S., Krüger, T., Subota, I., Thusek, S., Rotureau, B., Beilhack, A., Engstler, M. 2017. Developmental adaptations of trypanosome motility to the tsetse fly host environments unravel a multifaceted *in vivo* microswimmer system. *eLife* 6, e27656. https://doi.org/10.7554/eLife.27656

Schuster, S., Lisack, J., Subota, I., Zimmermann, H., Reuter, C., Mueller, T., Morriswood, B., Engstler, M. 2021. Unexpected plasticity in the life cycle of *Trypanosoma brucei*. *eLife* 10, e66028. https://doi.org/10.7554/eLife.66028

Scott, C.C., Vacca, F., Gruenberg, J. 2014. Endosome maturation, transport and functions. *Seminars in Cell & Developmental Biology* 31, 2-10. https://doi.org/10.1016/j.semcdb.2014.03.034

Seaman, M.N.J., Marcusson, E.G., Cereghino, J.L., Emr, S.D. 1997. Endosome to Golgi retrieval of the vacuolar protein sorting receptor, Vps10p, requires the function of the Vps29, Vps30, and Vps35 gene products. *Journal of Cell Biology* 137, 79-92. https://doi.org/10.1083/jcb.137.1.79

Seed, J.R., Sechelski, J.B. 1989. Mechanism of long slender (LS) to short stumpy (SS) transformation in the African trypanosomes. *Journal of Protozoology* 36, 572-577. https://doi.org/10.1111/j.1550-7408.1989.tb01099.x

Seed, J.R., Wenck, M.A. 2003. Role of the long slender to short stumpy transition in the life cycle of the African trypanosomes. *Kinetoplastid Biology and Disease* 2, 3. https://doi.org/10.1186/1475-9292-2-3

Seibel, P.N., Müller, T., Dandekar, T., Schultz, J., Wolf, M. 2006. 4SALE – A tool for synchronous RNA sequence and secondary structure alignment and editing. *BMC Bioinformatics* 7, 498. https://doi.org/10.1186/1471-2105-7-498

Seibel, P.N., Müller, T., Dandekar, T., Wolf, M. 2008. Synchronous visual analysis and editing of RNA sequence and secondary structure alignments using 4SALE. *BMC Research Notes* 1, 91. https://doi.org/10.1186/1756-0500-1-91

Serio, G., Margaria, V., Jensen, S., Oldani, A., Bartek, J., Bussolino, F., Lanzetti, L. 2011. Small GTPase Rab5 participates in chromosome congression and regulates localization of the centromere-associated protein CENP-F to kinetochores. *Proceedings of the National Academy of Sciences of the United States of America* 108, 17337-17342. https://doi.org/10.1073/pnas.1103516108

Serricchio, M., Bütikofer, P. 2011. *Trypanosoma brucei*: a model micro-organism to study eukaryotic phospholipid biosynthesis. *The FEBS Journal* 278, 1035-1046. https://doi.org/10.1111/j.1742-4658.2011.08012.x

Sharma, R., Peacock, L., Gluenz, E., Gull, K., Gibson, W., Carrington, M. 2008. Asymmetric cell division as a route to reduction in cell length and change in cell morphology in trypanosomes. *Protist* 159, 137-151. https://doi.org/10.1016/j.protis.2007.07.004

Sherwin, T., Gull, K. 1989. The cell division cycle of Trypanosoma brucei brucei: timing of event markers and cytoskeletal modulations. *Philosophical Transactions of the Royal Society B: Biological Sciences* 323, 573-588. https://doi.org/10.1098/rstb.1989.0037

Shih, W., Gallusser, A., Kirchhausen, T. 1995. A clathrin-binding site in the hinge of the beta 2 chain of mammalian AP-2 complexes. *Journal of Biological Chemistry* 270, 31083-31090. https://doi.org/10.1074/jbc.270.52.31083

Shimogawa, M.M., Ray, S.S., Kisalu, N., Zhang, Y., Geng, Q., Ozcan, A., Hill, K.L. 2018. Parasite motility is critical for virulence of African trypanosomes. *Scientific Reports* 8, 9122. https://doi.org/10.1038/s41598-018-27228-0

Shuster, C.B., Burgess, D.R. 2002. Targeted new membrane addition in the cleavage furrow is a late, separate event in cytokinesis. *Proceedings of the National Academy of Sciences of the United States of America* 99, 3633-3638. https://doi.org/10.1073/pnas.052342699

Siegel, T.N., Hekstra, D.R., Cross, G.A. 2008. Analysis of the *Trypanosoma brucei* cell cycle by quantitative DAPI imaging. *Molecular and Biochemical Parasitology* 160, 171-174. https://doi.org/10.1016/j.molbiopara.2008.04.004

Silva Pereira, S., de Almeida Castilho Neto, K.J.G., Duffy, C.W., Richards, P., Noyes, H., Ogugo, M., Rogério André, M., Bengaly, Z., Kemp, S., Teixeira, M.M.G., Machado, R.Z., Jackson, A.P. 2020. Variant antigen diversity in *Trypanosoma vivax* is not driven by recombination. *Nature Communications* 11, 844. https://doi.org/10.1038/s41467-020-14575-8

Silverman, J.S., Muratore, K.A., Bangs, J.D. 2013. Characterization of the late endosomal ESCRT machinery in *Trypanosoma brucei*. *Traffic* 14, 1078-1090. https://doi.org/10.1111/tra.12094

Silverman, J.S., Schwartz, K.J., Hajduk, S.L., Bangs, J.D. 2011. Late endosomal Rab7 regulates lysosomal trafficking of endocytic but not biosynthetic cargo in *Trypanosoma brucei*. *Molecular Microbiology* 82, 664-678. https://doi.org/10.1111/j.1365-2958.2011.07842.x

Sinclair-Davis, A.N., McAllaster, M.R., de Graffenried, C.L. 2017. A functional analysis of TOEFAZ1 uncovers protein domains essential for cytokinesis in *Trypanosoma brucei*. *Journal of Cell Science* 130, 3918-3932. https://doi.org/10.1242/jcs.207209

Skalický, T., Dobáková, E., Wheeler, R.J., Tesařová, M., Flegontov, P., Jirsová, D., Votýpka, J., Yurchenko, V., Ayala, F.J., Lukeš, J. 2017. Extensive flagellar remodeling during the complex life cycle of *Paratrypanosoma*, an early-branching trypanosomatid. *Proceedings of the National Academy of Sciences of the United States of America* 114, 11757-11762. https://doi.org/10.1073/pnas.1712311114

Skjeldal, F.M., Haugen, L.H., Mateus, D., Frei, D.M., Rødseth, A.V., Hu, X., Bakke, O. 2021. *De novo* formation of early endosomes during Rab5-to-Rab7a transition. *Journal of Cell Science* 134, jcs254185. https://doi.org/10.1242/jcs.254185

Skop, A.R., Bergmann, D., Mohler, W.A., White, J.G. 2001. Completion of cytokinesis in *C. elegans* requires a brefeldin A-sensitive membrane accumulation at the cleavage furrow apex. *Current Biology* 11, 735-746. https://doi.org/10.1016/S0960-9822(01)00231-7

Šlapeta, J., Morin-Adeline, V., Thompson, P., McDonell, D., Shiels, M., Gilchrist, K., Votýpka, J., Vogelnest, L. 2016. Intercontinental distribution of a new trypanosome species from Australian endemic Regent Honeyeater (*Anthochaera phrygia*). *Parasitology* 143, 1012-1025. https://doi.org/10.1017/S0031182016000329

Small, E.M., Osley, M.A. 2023. A screen for histone mutations that affect quiescence in *S. cerevisiae*. *The FEBS Journal* 290, 3539-3562. https://doi.org/10.1111/febs.16759

Sochacki, K.A., Taraska, J.W. 2019. From flat to curved clathrin: controlling a plastic ratchet. *Trends in Cell Biology* 29, 241-256. https://doi.org/10.1016/j.tcb.2018.12.002

Song, Y., Wu, Y., Xu, L., Jiang, T., Tang, C., Yin, C. 2021. Caveolae-mediated endocytosis drives robust siRNA delivery of polymeric nanoparticles to macrophages. *ACS Nano* 15, 8267-8282. https://doi.org/10.1021/acsnano.0c08596

Spitznagel, D., O'Rourke, J.F., Leddy, N., Hanrahan, O., Nolan, D.P. 2010. Identification and characterization of an unusual class I myosin involved in vesicle traffic in *Trypanosoma brucei*. *PLoS One* 5, e12282. https://doi.org/10.1371/journal.pone.0012282

Spodareva, V.V., Grybchuk-Ieremenko, A., Losev, A., Votýpka, J., Lukeš, J., Yurchenko, V., Kostygov, A.Y. 2018. Diversity and evolution of anuran trypanosomes: insights from the study of European species. *Parasites & Vectors* 11, 447. https://doi.org/10.1186/s13071-018-3023-1

Steinman, R.M., Brodie, S.E., Cohn, Z.A. 1976. Membrane flow during pinocytosis. A stereologic analysis. *Journal of Cell Biology* 68, 665-687. https://doi.org/10.1083/jcb.68.3.665

Stevens, J., Rambaut, A. 2001. Evolutionary rate differences in trypanosomes. *Infection, Genetics and Evolution* 1, 143-150. https://doi.org/10.1016/s1567-1348(01)00018-1

Stevens, J.R., Noyes, H.A., Dover, G.A., Gibson, W.C. 1999. The ancient and divergent origins of the human pathogenic trypanosomes, *Trypanosoma brucei* and *T. cruzi*. *Parasitology* 118, 107-116. https://doi.org/10.1017/s0031182098003473

Stijlemans, B., Radwanska, M., Trez, C.D., Magez, S. 2017. African trypanosomes undermine humoral responses and vaccine development: link with inflammatory responses*? Frontiers in Immunology* 8, 582. https://doi.org/10.3389/fimmu.2017.00582

Stoorvogel, W., Strous, G.J., Geuze, H.J., Oorschot, V., Schwartz, A.L. 1991. Late endosomes derive from early endosomes by maturation. *Cell* 65, 417-427. https://doi.org/10.1016/0092-8674(91)90459-c

Straus, W. 1964. Occurrence of phagosomes and phago-lysosomes in different segments of the nephron in relation to the reabsorption, transport, digestion, and extrusion of intravenously injected horseradish peroxidase. *Journal of Cell Biology* 21, 295-308. https://doi.org/10.1083/jcb.21.3.295

Swanson, J., Bushnell, A., Silverstein, S.C. 1987. Tubular lysosome morphology and distribution within macrophages depend on the integrity of cytoplasmic microtubules. *Proceedings of the National Academy of Sciences of the United States of America* 84, 1921-1925. https://doi.org/10.1073/pnas.84.7.1921

Szöőr, B., Silvester, E., Matthews, K.R. 2020. A leap into the unknown – Early events in African trypanosome transmission. *Trends in Parasitology* 36, 266-278. https://doi.org/10.1016/j.pt.2019.12.011

Teixeira, M.M.G., Borghesan, T.C., Ferreira, R.C., Santos, M.A., Takata, C.S.A., Campaner, M., Nunes, V.L.B., Milder, R.V., de Souza, W., Camargo, E.P. 2011. Phylogenetic validation of the genera *Angomonas* and *Strigomonas* of trypanosomatids harboring bacterial endosymbionts with the description of new species of trypanosomatids and of proteobacterial symbionts. *Protist* 162, 503-524. https://doi.org/10.1016/j.protis.2011.01.001

Terada, Y., Tatsuka, M., Suzuki, F., Yasuda, Y., Fujita, S., Otsu, M. 1998. AIM-1: a mammalian midbody-associated protein required for cytokinesis. *The EMBO Journal* 17, 667-676. https://doi.org/10.1093/emboj/17.3.667

Trivedi, P.C., Bartlett, J.J., Pulinilkunnil, T. 2020. Lysosomal biology and function: Modern view of cellular debris bin. *Cells* 9, 1131. https://doi.org/10.3390/cells9051131

Umaer, K., Bangs, J.D. 2020. Late ESCRT machinery mediates the recycling and rescue of invariant surface glycoprotein 65 in *Trypanosoma brucei*. *Cellular Microbiology* 22, e13244. https://doi.org/10.1111/cmi.13244

Umaer, K., Bush, P.J., Bangs, J.D. 2018. Rab11 mediates selective recycling and endocytic trafficking in *Trypanosoma brucei*. *Traffic* 19, 406-420. https://doi.org/10.1111/tra.12565

Ungewickell, E., Branton, D. 1981. Assembly units of clathrin coats. Nature 289, 420-422. https://doi.org/10.1038/289420a0

Ungewickell, E., Ungewickell, H., Holstein, S.E., Lindner, R., Prasad, K., Barouch, W., Martin, B., Greene, L.E., Eisenberg, E. 1995. Role of auxilin in uncoating clathrin-coated vesicles. *Nature* 378, 632-635. https://doi.org/10.1038/378632a0

Urbina, F.L., Gupton, S.L. 2020. SNARE-mediated exocytosis in neuronal development. *Frontiers in Molecular Neuroscience* 13, 133. https://doi.org/10.3389/fnmol.2020.00133

Van Den Abbeele, J., Claes, Y., van Bockstaele, D., Le Ray, D., Coosemans, M. 1999. *Trypanosoma brucei* spp. development in the tsetse fly: Characterization of the post-mesocyclic stages in the foregut and proboscis. *Parasitology* 118, 469-478. https://doi.org/10.1017/s0031182099004217

van der Beek, J., de Heus, C., Liv, N., Klumperman, J. 2021. Quantitative correlative microscopy reveals the ultrastructural distribution of endogenous endosomal proteins. *Journal of Cell Biology* 221, e202106044. https://doi.org/10.1083/jcb.202106044

Vassella, E., Reuner, B., Yutzy, B., Boshart, M. 1997. Differentiation of African trypanosomes is controlled by a density sensing mechanism which signals cell cycle arrest via the cAMP pathway. *Journal of Cell Science* 110, 2661-2671. https://doi.org/10.1242/jcs.110.21.2661

Vickerman, K. 1985. Developmental cycles and biology of pathogenic trypanosomes. *British Medical Bulletin* 41, 105-114. https://doi.org/10.1093/oxfordjournals.bmb.a072036

Vickerman, K. 1978. Antigenic variation in trypanosomes. *Nature* 273, 613-617. https://doi.org/10.1038/273613a0

Vickerman, K. 1969. On the surface coat and flagellar adhesion in trypanosomes. *Journal of Cell Science* 5, 163-193. https://doi.org/10.1242/jcs.5.1.163

Votýpka, J., Lukeš, J., Orboník, M. 2004. Phylogenetic Relationship of *Trypanosoma corvi* with other avian trypanosomes. *Acta Protozoologica* 43, 225–231.

Walczak, C.E., Cai, S., Khodjakov, A. 2010. Mechanisms of chromosome behaviour during mitosis. *Nature Reviews Molecular Cell Biology* 11, 91-102. https://doi.org/10.1038/nrm2832

Wall, D.A., Wilson, G., Hubbard, A.L. 1980. The galactose-specific recognition system of mammalian liver: the route of ligand internalization in rat hepatocytes. *Cell* 21, 79-93. https://doi.org/10.1016/0092-8674(80)90116-6

Wan, B., Poirié, M., Gatti, J.L. 2020. Parasitoid wasp venom vesicles (venosomes) enter *Drosophila melanogaster* lamellocytes through a flotillin/lipid raft-dependent endocytic pathway. *Virulence* 11, 1512-1521. https://doi.org/10.1080/21505594.2020.1838116

Wandinger-Ness, A., Zerial, M. 2014. Rab proteins and the compartmentalization of the endosomal system. *Cold Spring Harbor Perspectives in Biology* 6, a022616. https://doi.org/10.1101/cshperspect.a022616

Wang, N., Lee, I.J., Rask, G., Wu, J.Q. 2016. Roles of the TRAPP-II complex and the exocyst in membrane deposition during fission yeast cytokinesis. *PLoS Biology* 14, e1002437. https://doi.org/10.1371/journal.pbio.1002437

Wang, Z., Wheeler, R.J., Sunter, J.D. 2020. Lysosome assembly and disassembly changes endocytosis rate through the *Leishmania* cell cycle. *Microbiology Open* 9, e969. https://doi.org/10.1002/mbo3.969

Warren, G., Davoust, J., Cockcroft, A. 1984. Recycling of transferrin receptors in A431 cells is inhibited during mitosis. *The EMBO Journal* 3, 2217-2225.

Weisman, L.S. 2006. Organelles on the move: insights from yeast vacuole inheritance. *Nature Reviews Molecular Cell Biology* 7, 243-252. https://doi.org/10.1038/nrm1892

Wheeler, R.J. 2015. Analyzing the dynamics of cell cycle processes from fixed samples through ergodic principles. *Molecular Biology of the Cell* 26, 3898-3903. https://doi.org/10.1091/mbc.E15-03-0151

Wheeler, R.J., Gull, K., Sunter, J.D. 2019. Coordination of the cell cycle in trypanosomes. *Annual Review of Microbiology* 73, 133-154. https://doi.org/10.1146/annurev-micro-020518-115617

Wheeler, R.J., Scheumann, N., Wickstead, B., Gull, K., Vaughan, S. 2013. Cytokinesis in *Trypanosoma brucei* differs between bloodstream and tsetse trypomastigote forms: implications for microtubule-based morphogenesis and mutant analysis. *Molecular Microbiology* 90, 1339-1355. https://doi.org/10.1111/mmi.12436

Wheeler, W.M. 1891. Neuroblasts in the arthropod embryo. *Journal of Morphology* 4, 337-343. https://doi.org/10.1002/jmor.1050040305

Whitman, C.O. 1878. Memoirs: The embryology of clepsine. *Journal of Cell Science* s2-18, 215-315. https://doi.org/10.1242/jcs.s2-18.71.215

WHO. 2023. Trypanosomiasis, human African (sleeping sickness). Available at: https://www.who.int/news-room/fact-sheets/detail/trypanosomiasis-human-african-(sleeping-sickness) (Accessed: 25 May 2023).

WHO. 2012. Research priorities for Chagas disease, human African trypanosomiasis and leishmaniasis. Available at: https://apps.who.int/iris/handle/10665/77472 (Accessed: 25 May 2023).

Wickham, H., Navarro, D., Pedersen, T.L. 2023a. ggplot2: Elegant graphics for data analysis. New York: Springer.

Wickham, H., Vaughan, D., Girlich, M., Ushey, K., Posit, P. 2023b. tidyr: Tidy messy data. Available at: https://tidyr.tidyverse.org/ (Accessed: 24 July 2023).

Wirtz, E., Leal, S., Ochatt, C., Cross, G.A. 1999. A tightly regulated inducible expression system for conditional gene knock-outs and dominant-negative genetics in *Trypanosoma brucei*. *Molecular and Biochemical Parasitology* 99, 89-101. https://doi.org/10.1016/S0166-6851(99)00002-X

Wolf, M., Achtziger, M., Schultz, J., Dandekar, T., Müller, T. 2005. Homology modeling revealed more than 20,000 rRNA internal transcribed spacer 2 (ITS2) secondary structures. *RNA* 11, 1616-1623. https://doi.org/10.1261/rna.2144205

Wolf, M., Koetschan, C., Müller, T. 2014. ITS2, 18S, 16S or any other RNA – Simply aligning sequences and their individual secondary structures simultaneously by an automatic approach. *Gene* 546, 145-149. https://doi.org/10.1016/j.gene.2014.05.065

Wolf, M., Ruderisch, B., Dandekar, T., Schultz, J., Müller, T. 2008. ProfDistS: (profile-) distance based phylogeny on sequence-structure alignments. *Bioinformatics* 24, 2401-2402. https://doi.org/10.1093/bioinformatics/btn453

Woodward, R., Gull, K. 1990. Timing of nuclear and kinetoplast DNA replication and early morphological events in the cell cycle of *Trypanosoma brucei*. *Journal of Cell Science* 95, 49-57.

Yamada, E. 1955. The fine structure of the gall bladder epithelium of the mouse. *Journal of Biophysical and Biochemical Cytology* 1, 445-458.

Yazaki, E., Ishikawa, S.A., Kume, K., Kumagai, A., Kamaishi, T., Tanifuji, G., Hashimoto, T., Inagaki, Y. 2017. Global Kinetoplastea phylogeny inferred from a large-scale multigene alignment including parasitic species for better understanding transitions from a free-living to a parasitic lifestyle. *Genes & Genetic System* 92, 35-42. https://doi.org/10.1266/ggs.16-00056

Zhang, C., Cordelières, F.P. 2016. 3D Quantitative colocalization analysis, in: Miura, K. (ed.). Bioimage Data Analysis. Weinheim: Wiley-VCH, pp. 237–266.

Zhang, X., An, T., Pham, K.T.M., Lun, Z.R., Li, Z. 2019. Functional analyses of cytokinesis regulators in bloodstream stage *Trypanosoma brucei* parasites identify functions and regulations specific to the life cycle stage. *mSphere* 4, e00199-19. https://doi.org/10.1128/mSphere.00199-19

Zhou, Q., An, T., Pham, K.T.M., Hu, H., Li, Z. 2018a. The CIF1 protein is a master orchestrator of trypanosome cytokinesis that recruits several cytokinesis regulators to the cytokinesis initiation site. *Journal of Biological Chemistry* 293, 16177-16192. https://doi.org/10.1074/jbc.RA118.004888

Zhou, Q., Gu, J., Lun, Z.R., Ayala, F.J., Li, Z. 2016. Two distinct cytokinesis pathways drive trypanosome cell division initiation from opposite cell ends. *Proceedings of the National Academy of Sciences of the United States of America* 113, 3287-3292. https://doi.org/10.1073/pnas.1601596113

Zhou, Q., Hu, H., Li, Z. 2014. New insights into the molecular mechanisms of mitosis and cytokinesis in trypanosomes. *International Review of Cell and Molecular Biology* 308, 127-166. https://doi.org/10.1016/B978-0-12-800097-7.00004-X

Zhou, Q., Lee, K.J., Kurasawa, Y., Hu, H., An, T., Li, Z. 2018b. Faithful chromosome segregation in *Trypanosoma brucei* requires a cohort of divergent spindle-associated proteins with distinct functions. *Nucleic Acids Research* 46, 8216-8231. https://doi.org/10.1093/nar/gky557

Zimmermann, H., Subota, I., Batram, C., Kramer, S., Janzen, C.J., Jones, N.G., Engstler, M. 2017. A quorum sensing-independent path to stumpy development in *Trypanosoma brucei*. *PLoS Pathogens* 13, e1006324. https://doi.org/10.1371/journal.ppat.1006324

Zlotek-Zlotkiewicz, E., Monnier, S., Cappello, G., Le Berre, M., Piel, M. 2015. Optical volume and mass measurements show that mammalian cells swell during mitosis. *Journal of Cell Biology* 211, 765-774. https://doi.org/10.1083/jcb.201505056

Appendices

Supplementary material – Chapter 1

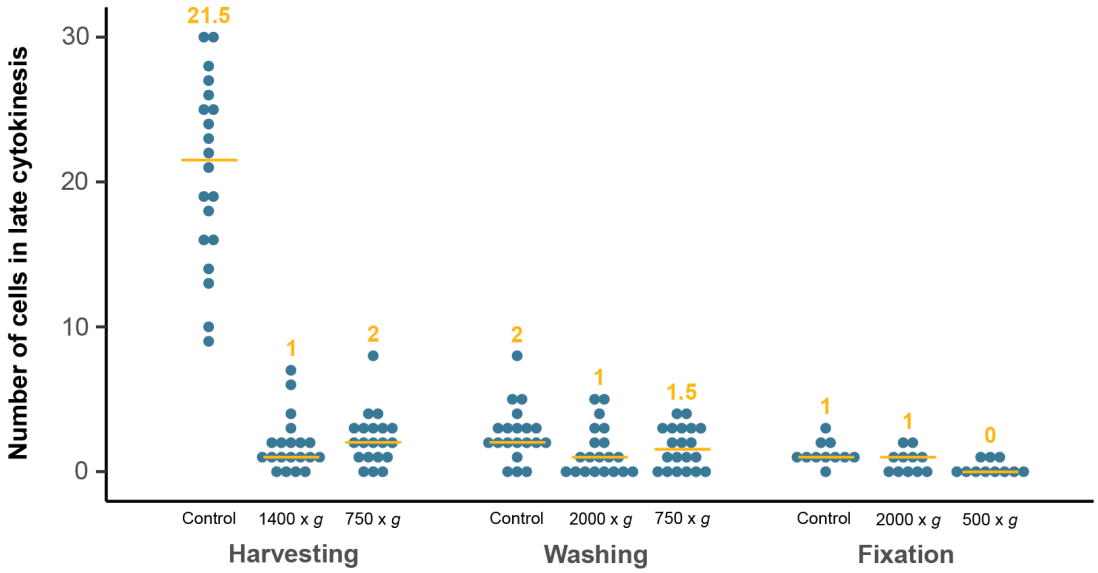

Figure S1.1. The centrifugal forces imposed on trypanosomes during harvesting, washing, and fixation protocols decrease the number of cells in late cytokinesis. The dot plot shows the number of cells in late cytokinesis. Each dot represents the counts of one assay, yellow bars represent the median, and yellow numbers are the median value of the counts. The differential counting of cell stages (single cells *vs.* late cytokinesis stages) was performed using a Neubauer chamber, and a total of 150 stages were counted per assay. A minimum of 10 replicates were performed.

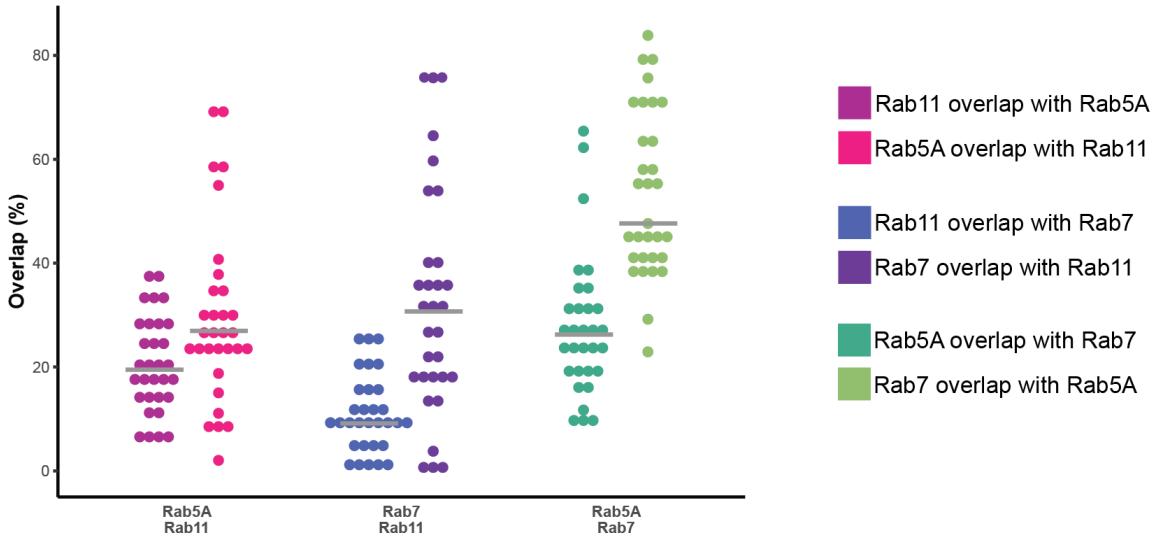

Figure S1.2. Dot plot showing Manders' colocalization coefficients (overlap) between the different TbRab markers. Gray bars represent the median (N = 31, 2 replicates).

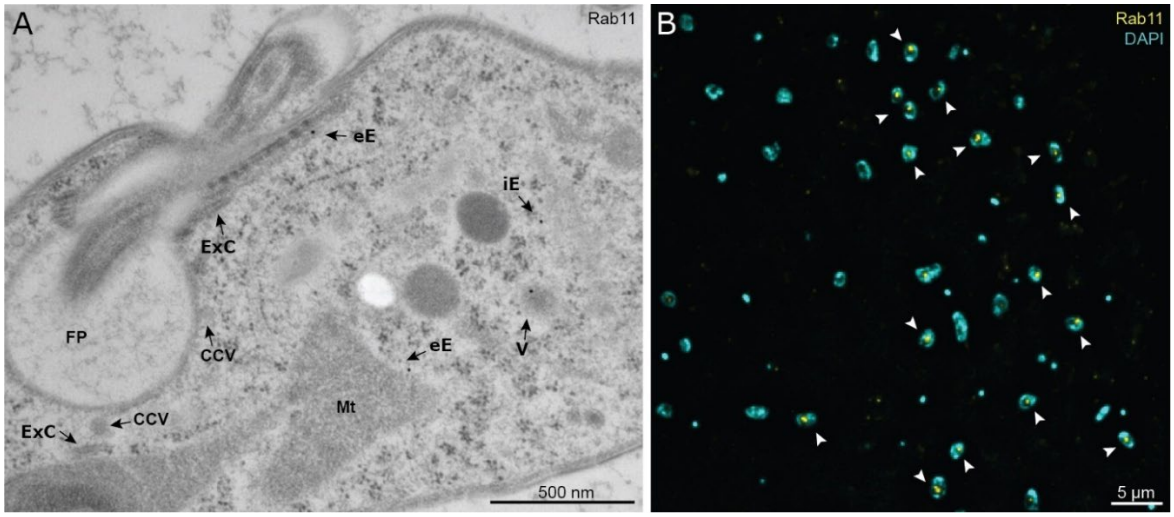

Figure S1.3. Attempts of super-resolution microscopy methods using TbRab11. (A) Transmission electron microscopy showing the best result of immunogold assays performed in ultrathin sections (60 nm) of high-pressure frozen cells. In the exemplary image, it is possible to identify four gold particles (12 nm) marking elongated endosomes (eE), an irregular-shaped endosome (iE), and a vesicular-like endosome (V). Other known TbRab11-positive structures, as exocytic carriers (ExC), are seen in the picture but are not labeled. It is also possible to identify other structures: the flagellar pocket (FP), clathrin-coated vesicles (CCV), and mitochondria (Mt). (B) TbRab11 signal (arrowheads) is observed in the nucleus of *T. brucei* cells. The exemplary image is the result of immunofluorescence attempts performed on thin sections (100 nm) of high-pressure frozen cells embedded in LR-White. The signal localization was considered ectopic and the correlation between light and electron microscopy (CLEM) was not performed.

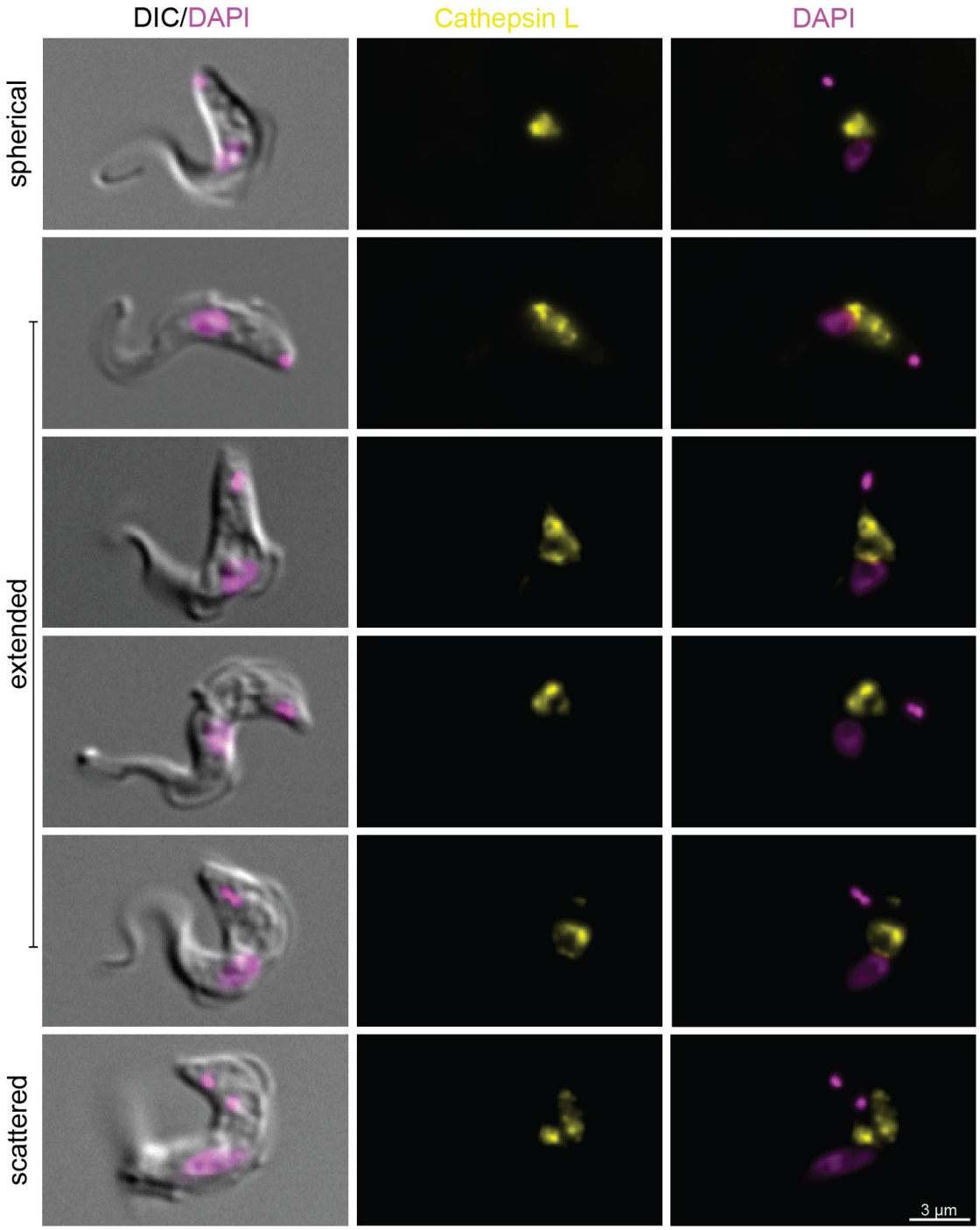

Figure S1.4. Cathepsin L-labeled cells show the morphological plasticity of the lysosomes. *T. brucei* lysosomes are grouped according to their morphology into: spherical, extended (spherical or elongated signal presenting one or more protrusions), and scattered (two or more punctate signals with our without protrusions spreading in the posterior region of the cell). All exemplary images presented have the same magnification.

Supplementary material – Chapter 2

Supplementary data to the published paper can be found online at https://doi.org/10.1016/j.ejop.2021.125824.

Abbreviations

°C	Celsius degrees
µg	Micrograms
µL	Microliters
µM	Micromolar
Ø	Diameter
AP-2	Adaptor protein 2
Arp2/3	Actin-related protein 2/3 complex
ATPase	Adenosine triphosphatase
BARP	brucei alanine rich protein
BORI	Borealin related interactor
BSA	Bovine serum albumin
CCD	Charge-coupled device sensor
CIF1	Cytokinesis initiation factor 1 (also known as TOEFAZ1)
CCP/CCPs	Clathrin-coated pit/Clathrin-coated pits
CCV/CCVs	Clathrin-coated vesicle/Clathrin-coated vesicles
CCV I	Class I clathrin-coated vesicle
CCV II	Class II clathrin-coated vesicle
cE	Circular endosomal cisternae
CLC	Clathrin light chain
CLEM	Correlative light and electron microscopy
CMLE	Classic maximum likelihood estimation
CPC	Chromosomal passenger complex
CRW	Comparative RNA web
ddH_2O	Double-distilled water
DIC	Differential interference contrast
DNA	Deoxyribonucleic acid
ECVs	Endosomal carrier vesicles
eE	Elongated endosomal cisternae
EE	Early Endosomes
Ent1	Epsin-1
EPS15	Epidermal growth factor receptor substrate 15
EP1	Isoform of EP procyclin
EP1::GFP	*Trypanosoma brucei brucei* MITat1.2 1390 with EP1 tagged with GFP

ER	Endoplasmic reticulum
ERES	Endoplasmic reticulum exit site
ESCRT	Endosomal sorting complex required for transport
ExC/EXC	Exocytic carrier
FA	Formaldehyde
F-BAR	Fes/CIP4 Homology-Bin-Amphiphysin-Rvs
FCHO 1/2	F-BAR domain only protein 1 and 2 complex
FCS	Fetal calf serum
FP	Flagellar pocket
g	Relative centrifugal force (expressed in units of gravity)
g	Grams
G	Golgi apparatus
G0	Quiescent phase of the cell cycle
G1	Gap 1 phase of the cell cycle
G2	Gap 2 phase of the cell cycle
GA	Glutaraldehyde
GAPDH/gGAPDH	Glycosomal glyceraldehyde phosphate dehydrogenase/Glycosomal glyceraldehyde phosphate dehydrogenase gene
GDP	Guanosine diphosphate
GFP	Green fluorescent protein
GPI	Glycosylphosphatidylinositol
GP63	GP63 metalloprotease
GTP	Guanosine triphosphate
GTPase	Guanosine triphosphatase
h	Hour
Hsc70	Heat shock cognate 70 protein
iE	Endosomal cisternae with irregular shape
ILVs	Intraluminal vesicles
ITS2	Internal transcribed spacer 2
IMDM	Iscove’s modified Dulbecco’s medium
INCENP	Inner centromere protein
K	Kinetoplast
L	Lysosome
Las17	Proline-rich protein LAS17 (WASp-interacting protein)
LB1/LB2	Labeling buffers (used to dilute antibodies during immunogold protocols)

LE	Late endosome
M	Molarity of a solution (expresses the concentration in number of moles of solute per liter of solution)
M	Mitotic phase of the cell cycle (used with this meaning on page 16)
mM	Millimolar
min	Minutes
mL	Milliliters
ML	Maximum likelihood
mm	Millimeters
MVBs	Multivesicular bodies
N	Nucleus
NJ	Neighbor joining
nm	Nanometers
PBS	Phosphate-buffered saline
PSF	Point spread function
Rab5	Ras-related protein Rab5
Rab7	Ras-related protein Rab7
Rab11	Ras-related protein Rab11
rDNA	Ribosomal DNA sequences coding for rRNA
RE	Recycling endosome
RNA	Ribonucleic acid
RNAi	RNA interference
rRNA	Ribosomal RNA
ROI	Region of interest
RT	Room temperature
s	Seconds
S	Synthesis phase of the cell cycle in which DNA replication takes place
sCMOS	Scientific complementary metal-oxide-semiconductor sensor
SEM	Scanning electron microscopy
SIF	Stumpy induction factor
SIM	Structured illumination microscopy
Sla1	Actin cytoskeleton-regulatory complex protein SLA1
Sla2	Actin assembly protein SLA2
SNR	Signal-to-noise ratio
TbAUK1	*T. brucei* aurora kinase 1

TbCALM	*T. brucei* clathrin assembly lymphoid myeloid leukemia protein
TbCAP	*T. brucei* clathrin-associating proteins
TbCatL	*T. brucei* cathepsin L
TbCPC1	*T. brucei* centromere protein C 1
TbCPC2	*T. brucei* centromere protein C 2
TbEpsinR	*T. brucei* epsin-related protein
TbHsc70	*T. brucei* heat-shock protein 70
TbMyo1	*T. brucei* myosin class 1
TbPLK	*T. brucei* polo-like kinase
TbRab5A	*T. brucei* Ras-related protein Rab5A
TbRab7	*T. brucei* Ras-related protein Rab7
TbRab11	*T. brucei* Ras-related protein Rab11
TbTOR	*T. brucei* target of rapamycin kinase
TbVps	*T. brucei* vacuolar protein sorting
TDB	Trypanosome dilution buffer
TEM	Transmission electron microscopy
TfR	Transferrin receptor
TGN	*Trans*-Golgi network
TOEFAZ1	Tip of the extending FAZ 1 (also known as CIF1)
TS	*Trans*-sialidase
U	Units
VSG/VSGs	Variant surface glycoprotein/Variant surface glycoproteins
VSG_{biotin}	Biotinylated VSG
YFP/eYFP	Yellow fluorescent protein/Enhanced yellow fluorescent protein
YFP::CLC	*Trypanosoma brucei brucei* MITat1.2 1390 with clathrin light chain tagged with eYFP

Publication list

Rackevei, A.S., **Borges, A.**, Engstler, M., Dandekar, T., Wolf, M. 2022. About the analysis of 18S rDNA sequence data from trypanosomes in barcoding and phylogenetics: tracing a continuation error occurring in the literature. *Biology (Basel)* 11, 1612. https://doi.org/10.3390/biology11111612.

Borges, A.R.*, Link, F.*, Engstler, M., Jones, N.G. 2021. The glycosylphosphatidylinositol anchor: a linchpin for cell surface versatility of trypanosomatids. *Frontiers in Cell and Developmental Biology* 9, 720536. https://doi.org/10.3389/fcell.2021.720536.

Borges, A.R., Engstler, M., Wolf, M. 2021. 18S rRNA gene sequence-structure phylogeny of the Trypanosomatida (Kinetoplastea, Euglenozoa) with special reference to *Trypanosoma*. *European Journal of Protistology* 81, 125824. https://doi.org/10.1016/j.ejop.2021.125824.

Link, F.*, **Borges, A.R.***, Jones, N.G., Engstler, M. 2021. To the surface and back: Exo- and endocytic pathways in *Trypanosoma brucei*. *Frontiers in Cell and Developmental Biology* 9, 720521. https://doi.org/10.3389/fcell.2021.720521.

Link, F., **Borges, A.**, Karo, O., Jungblut, M., Müller, T., Meyer-Natus, E., Sachs, S., Jones, N.G., Krüger, T., Morphew, M., Sauer, M., Stigloher, C., McIntosh, J.R., Engstler, M. 2023. Continuous endosomes form functional subdomains and orchestrate rapid membrane trafficking in trypanosomes [Preprint]. Available at: https://www.biorxiv.org/content/10.1101/2023.07.20.549860v1 (Accessed: 24 July 2023).

* These authors have contributed equally to these works

Acknowledgements

I would like to express my gratitude to CAPES for awarding me the PhD scholarship and providing the funds for my studies. I extend my thanks to my primary supervisor, Prof. Dr. Markus Engstler, for accepting me into his research group, and would also like to acknowledge the other members of my thesis advisory committee, Dr. Brooke Morriswood, Prof. Dr. Philip Kollmannsberger, and Prof. Dr. Derek Nolan, for their support and encouragement over the years. Additionally, I want to express my gratitude to Dr. Matthias Wolf for sharing his passion about phylogeny with me and teaching me a new method.

I am deeply grateful to Dr. Nicola Jones for her invaluable help, support, and friendship. The same holds true for Dr. Brooke Morriswood, whose support proved vital during particularly challenging moments. I extend my appreciation to both of them for engaging in fruitful discussions, providing mentorship, and proofreading my thesis. I would also like to express my gratitude to Prof. Dr. Susanne Kramer for her attentive listening and valuable advice whenever I needed it.

I extend my sincere thanks to Fabian Link for his partnership in this project, providing essential antibodies for this work, and proofreading this thesis. To my student, Helena Ferrer Gámez, I thank her for her dedication to the mini project she was given, for being a constant source of happiness and motivation, and, most importantly, for having given me the opportunity to exchange knowledge. Teaching is a calling I received a long time ago, and having a student during this PhD journey was fulfilling.

I express my sincere gratitude to the exceptional staff of the department, who are responsible for creating and maintaining a productive environment. I thank Dr. Tim Krüger for his guidance and assistance with microscopy. When I first arrived, I had never even touched a fluorescence microscope, but with his help, I leave with ample knowledge and experience. Thanks to Lidia, Elina, and Silke for always providing me with essential materials, and to Uli and Manu for efficiently handling all documentation, saving me

precious time. Finally, to Kathrin, Reinhild, and Elisabeth, besides your hard work, you have given me something I deeply cherish: your friendship and affection. I already miss you.

Speaking of affection, I am reminded of my dear friends who have been a constant source of support. Jaime, Nico, Maíra, Bárbara and Dani, thank you for proofreading this thesis, but even more for your friendship that warms my heart in good and bad times. To Laura Hauf, Thomas, Stephan, Kevin, Laura Hartleb, Elisa, and the alumni Majeed (my Prince), Erick (my Dr. Love), and Claudia, I want to express my gratitude for creating a nurturing work environment. It was essential to my journey, and I treasure you for that. I am also grateful to my other friends who have contributed to making Germany feel like home, especially Ju Bibiano, Ju Schneider, Cami, Pauline, Jonas, Consti, and Aline, I am grateful for your emotional support. And I cannot forget about my long-term friends, Cícero, Daly, Tharcy, Thierre, Lucas, Henrique, Nath, Eve, Camilinha, Grilo, Diego, Sara, Aninha, and Érika, who have always been close enough to reach out and remind me of my place in this world. You are all indispensable to me.

To my beloved husband, Rico, who entered my life to show me the real meaning of every single thing, I cannot even find words to express my gratitude for your support, love, and patience, especially during the past few months. To my family, for whom I dedicate everything I do, I have done this for you too! *Obrigada por acreditarem em mim em todos os momentos, principalmente naqueles em que eu mesma havia perdido a fé. Persisti, tive coragem e venci. Tudo isso graças a vocês, que me inspiram, me acolhem e me conectam com a minha essência. Obrigada por serem o chão em que eu piso e o vento que me faz voar. Amo vocês.*

Statement of contributions – Chapter 1

Helena Ferrer Gámez contributed to the cell cycle analysis and conducted the centrifugation experiments. Elisabeth Meyer-Natus performed freeze substitution and ultramicrotomy on all electron microscopy samples, and provided assistance with the electron microscopy techniques. Fabian Link generated the antibodies against TbRabs.

Statement of individual author contributions to figures/tables of manuscripts included in the dissertation

Manuscript 1: **Borges, A.R.,** Link, F., Engstler, M., Jones, N.G. 2021. The Glycosylphosphatidylinositol Anchor: A Linchpin for Cell Surface Versatility of Trypanosomatids. *Frontiers in Cell and Developmental Biology* 9, 720536. https://doi.org/10.3389/fcell.2021.720536.					
Figure	**Author Initials,** Responsibility decreasing from left to right				
1	FL	AB	NJ	ME	
2	FL	AB	NJ	ME	
3	FL	AB	NJ	ME	
4	AB	FL	NJ	ME	
Table	**Author Initials,** Responsibility decreasing from left to right				
1	FL	AB	NJ	ME	
2	FL	AB	NJ	ME	

Explanations (if applicable):

Manuscript 2: **Borges, A.R.,** Engstler, M., Wolf, M. 2021. 18S rRNA gene sequence-structure phylogeny of the Trypanosomatida (Kinetoplastea, Euglenozoa) with special reference to *Trypanosoma*. *European Journal of Protistology* 81, 125824. https://doi.org/10.1016/j.ejop.2021.125824.					
Figure	**Author Initials,** Responsibility decreasing from left to right				
1	MW	AB	ME		
2	MW	AB	ME		
3	MW	AB	ME		

Explanations (if applicable):.

Manuscript 3: Link, F., **Borges, A.R**., Jones, N.G., Engstler, M. 2021. To the Surface and Back: Exo- and Endocytic Pathways in *Trypanosoma brucei*. *Frontiers in Cell and Developmental Biology* 9, 720521. https://doi.org/10.3389/fcell.2021.720521					
Figure	**Author Initials,** Responsibility decreasing from left to right				
1	AB	ME	FL	NJ	
2	AB	FL	NJ	ME	
3	ME	AB	FL	NJ	

Explanations (if applicable):

I also confirm my primary supervisor's acceptance.

Alyssa Bergmann Borges _____

Doctoral Researcher's Name Date Place Signature

Statement of individual author contributions and of legal second publication rights to manuscripts included in the dissertation

Manuscript 1: **Borges, A.R**., Link, F., Engstler, M., Jones, N.G. 2021. The Glycosylphosphatidylinositol Anchor: A Linchpin for Cell Surface Versatility of Trypanosomatids. *Frontiers in Cell and Developmental Biology* 9, 720536. https://doi.org/10.3389/fcell.2021.720536					
Participated in	**Author Initials,** Responsibility decreasing from left to right				
Study Design Methods Development					
Data Collection	AB FL	NJ	ME		
Data Analysis and Interpretation					
Manuscript Writing Writing of Introduction Writing of Materials & Methods Writing of Discussion Writing of First Draft	AB FL	NJ	ME		

Explanations (if applicable):

Manuscript 2: **Borges, A.R.,** Engstler, M., Wolf, M. 2021. 18S rRNA gene sequence-structure phylogeny of the Trypanosomatida (Kinetoplastea, Euglenozoa) with special reference to *Trypanosoma*. *European Journal of Protistology* 81, 125824. https://doi.org/10.1016/j.ejop.2021.125824					
Participated in	**Author Initials,** Responsibility decreasing from left to right				
Study Design Methods Development	MW	AB	ME		
Data Collection	MW	AB	ME		
Data Analysis and Interpretation	AB	MW	ME		
Manuscript Writing Writing of Introduction Writing of Materials & Methods Writing of Discussion Writing of First Draft	AB	MW	ME		

Explanations (if applicable):

Manuscript 3: Link, F., **Borges, A.R**., Jones, N.G., Engstler, M. 2021. To the Surface and Back: Exo- and Endocytic Pathways in *Trypanosoma brucei*. *Frontiers in Cell and Developmental Biology* 9, 720521. https://doi.org/10.3389/fcell.2021.720521					
Participated in	**Author Initials,** Responsibility decreasing from left to right				
Study Design Methods Development					
Data Collection	AB FL	NJ	ME		
Data Analysis and Interpretation					
Manuscript Writing Writing of Introduction Writing of Materials & Methods Writing of Discussion Writing of First Draft	AB FL	NJ ME			

Explanations (if applicable):

If applicable, the doctoral researcher confirms that she/he has obtained permission from both the publishers (copyright) and the co-authors for legal second publication.

The doctoral researcher and the primary supervisor confirm the correctness of the above mentioned assessment.

Alyssa Bergmann Borges _____

Doctoral Researcher's Name Date Place Signature

Markus Engstler _____

Primary Supervisor's Name Date Place Signature

Curriculum vitae

(Information omitted)

Affidavit

I hereby confirm that my thesis entitled “The endo-lysosomal system of *Trypanosoma brucei*: insights from a protist cell model” is the result of my own work. I did not receive any help or support from commercial consultants. All sources and/or materials applied are listed ad specified in the thesis.

Furthermore, I confirm that this thesis has not yet been submitted as part of another examination process neither in identical nor in similar form.

Place, Date Signature

Eidesstattliche Erklärung

Hiermit erkläre ich an Eides statt, die Dissertation „Das Endo-lysosomale System von *Trypanosoma brucei*: Erkenntnisse aus einem Protisten-Zellmodell“ eigenständig, d.h. insbesondere selbstständig und ohne Hilfsmittel eines kommerziellen Promotionsberaters, angefertigt und keine anderen als die von mir angegebenen Quellen und Hilfsmittel verwendet zu haben.

Ich erkläre außerdem, dass die Dissertation weder in gleicher noch in ähnlicher Form bereits in einem anderen Prüfungsverfahren vorgelegen hat.

Ort, Datum Unterschrift